0 0 0 4 8 0 4 3 3 3

UC-37
UC-38

LBL-6611

I. LOW FREQUENCY NOISE IN METAL FILMS AT THE SUPERCONDUCTING TRANSITION
II. RESISTANCE OF SUPERCONDUCTOR - NORMAL METAL - SUPERCONDUCTOR SANDWICHES AND THE QUASIPARTICLE RELAXATION TIME

RECEIVED
LAWRENCE
BERKELEY LABORATORY

FEB 1 1978

LIBRARY AND
DOCUMENTS SECTION

Thomas Y. Hsiang
(Ph. D. thesis)

July 1977

Prepared for the U. S. Energy Research and
Development Administration under Contract W-7405-ENG-48

For Reference

Not to be taken from this room

LAWRENCE BERKELEY LABORATORY
UNIVERSITY OF CALIFORNIA
BERKELEY

LBL-6611

DISCLAIMER

This document was prepared as an account of work sponsored by the United States Government. While this document is believed to contain correct information, neither the United States Government nor any agency thereof, nor the Regents of the University of California, nor any of their employees, makes any warranty, express or implied, or assumes any legal responsibility for the accuracy, completeness, or usefulness of any information, apparatus, product, or process disclosed, or represents that its use would not infringe privately owned rights. Reference herein to any specific commercial product, process, or service by its trade name, trademark, manufacturer, or otherwise, does not necessarily constitute or imply its endorsement, recommendation, or favoring by the United States Government or any agency thereof, or the Regents of the University of California. The views and opinions of authors expressed herein do not necessarily state or reflect those of the United States Government or any agency thereof or the Regents of the University of California.

0 0 0 0 4 8 0 4 5 6 6

I. LOW FREQUENCY NOISE IN METAL FILMS AT THE SUPERCONDUCTING TRANSITION

II. RESISTANCE OF SUPERCONDUCTOR - NORMAL METAL - SUPERCONDUCTOR SANDWICHES AND THE QUASIPARTICLE RELAXATION TIME

Thomas Y. Hsiang

(Ph.D Thesis)

August 1977

0 0 0 0 4 8 0 4 5 6 7

CONTENTS

ABSTRACT v

PART I: LOW FREQUENCY NOISE IN METAL FILMS AT THE SUPERCONDUCTING TRANSITION

I. INTRODUCTION 2

II. THEORY

A. Richardson's Theory and Its Interpretation 4

B. Application of Richardson's Theory and the Semi-Empircal Model 11

C. Correlation Functions 17

III. EXPERIMENTAL PROCEDURES

A. Film Preparation and the Cryostat 20

B. Measurement Techniques. 22

C. Spurious Noise Sources. 23

IV. EXPERIMENTAL RESULTS

A. Thermal Coupling of Type A and Type B Samples 26

B. Noise Power Spectra for Tin 30

C. Spatial Correlation of the Noise. 35

D. Effect of Magnetic Field on Type A Samples. 38

E. Experimental Results for Lead 40

V. DISCUSSION AND CONCLUSION

A. Thermal Noise or Flux-flow Noise? 43

B. Conclusive Remarks. 44

C. Boundary Conditions - Solution to the Mystery of 1/f? 47

PART II: RESISTANCE OF SUPERCONDUCTOR - NORMAL METAL - SUPERCONDUCTOR SANDWICHES AND THE QUASIPARTICLE RELAXATION TIME

VI. INTRODUCTION. 57

VII. THEORY

A. Excess of Quasiparticles and the Electric Field 59

B. Andreév Reflection. 68

C. Transport Properties of Quasiparticles at the SN Boundary and the Resistance of SNS Junctions. 74

D. Comments on Waldram's Formulation 94

E. The Relaxation Times. 97

F. Time-Dependent-Ginzburg-Landau Theory 103

VIII. EXPERIMENTAL PROCEDURES

A. The Preparation of Specimens. 109

B. The SQUID Voltmeter and Measurement Techniques. 117

C. The Cryostat. 120

IX. EXPERIMENTAL RESULTS

A. Junction Properties 124

B. Junction Resistance and the Quasiparticle Relaxation Time 128

C. Rappaport's Data. 142

X. DISCUSSIONS AND CONCLUSIONS

A. Comparison of the Experimental Data with Waldram's Theory. 147

B. Related Experiments by Other Authors. 153

C. Comparison of the Values of $\tau_3(0)$ Obtained by Theory and Other Experiments, and the Effect of Impurity . . 158

D. Conclusions 160

Acknowledgement 163

References 164

0 0 0 0 4 8 0 4 5 6 8

I. LOW FREQUENCY NOISE IN METAL FILMS AT THE SUPERCONDUCTING TRANSITION

AND

II. RESISTANCE OF SUPERCONDUCTOR - NORMAL METAL - SUPERCONDUCTOR JUNCTIONS

Thomas Y. Hsiang

ABSTRACT

In the first part of this thesis, we report measurements of the noise power spectra $S_V(f)$ of tin and lead films at the superconducting transition in the frequency range of 0.1 Hz to 5k Hz. Two types of samples were made. Type A were evaporated directly onto glass substrate, while Type B were evaporated onto glass or sapphire substrate with a 50Å aluminum underlay. The results were consistent with a thermal diffusion model which attributes the noise to the intrinsic temperature fluctuation in the metal film driven with a random energy flux source. In both types of metal films, the noise power was found to be proportional to $\overline{V}^2\ \beta^2/\Omega$, where $\overline{V}$ was the mean voltage across the sample, β was the temperature coefficient of resistance which could be changed by either biasing the metal film at different temperatures on the superconducting transition or by the application of a magnetic film, and Ω was the volume of the sample. Correlation of noises in two regions of the metal film a distance d apart was detected at frequencies $\leqslant D/\pi d^2$. The noise

power spectra of type B samples were always rather flatter than 1/f at lower frequencies, with the degree of flatness different for lead or tin. The degree of spatial correlation of the noise in type B samples was also reduced. These changes are ascribed to the enhancement of thermal contact between the films and the substrate by the aluminum underlay. Separate experiments confirmed that the underlay decreased the thermal boundary resistance between the film and the substrate. A possible explanation of the noises using quantitative boundary conditions and implications of this work for device applications are discussed.

In the second part of this thesis, we report theoretical and experimental investigation on the resistance of superconductor-normal metal-superconductor sandwiches near T_c. The increase in SNS resistance is attributed to the penetration of normal electric current in the superconductor. We prove from first principle that electric field can exist inside the superconductor when quasiparticles are not equally populated on the two branches of the excitation spectrum, and such is the case in a current biased SNS junction. A set of Boltzman equations are used to calculate the relaxation of quasiparticles in the superconductor. It is found that the electric field inside S decays according to a diffusion law. The diffusion length is determined by the quasiparticle "branch-crossing" relaxation time. The R(T) of the SNS junction thus provides a measurment of this relaxation time.

Experimentally we used a dc SQUID voltmeter to measure the SNS resistance. The branch-crossing relaxation times were measured to be $1 - 1.5 \times 10^{-11}\ \Delta(0)/\Delta(T)$ sec/ for lead amd $2\text{-}3 \times 10^{-10}\ \Delta(0)/\Delta(T)$ sec.

0 0 0 0 4 8 0 4 5 6 9

for tin. Comparison of these values with that determined by theoretical calculations and other experiments will be made. Impurity-doping of tin was found to decrease this relaxation time. This effect is possibly due to the electron-transverse phonon coupling mediated by the impurity scattering.

0 0 0 0 4 8 0 4 5 7 0

PART I

LOW FREQUENCY NOISE IN METAL FILMS AT THE SUPERCONDUCTING TRANSITION

I. INTRODUCTION

A model involving equilibrium temperature fluctuations has been used by Voss and Clarke[1,2] to quantitatively predict the 1/f voltage noise observed in metal films at room temperature. Their model is closely related to an earlier theory by J. M. Richardson.[3] The temperature fluctuations generate resistance fluctuations if the temperature coefficient of resistance, $\beta = (1/R)dR/dT$, is non-zero. In the presence of a steady current the resistance fluctuations in turn give rise to voltage fluctuations. In this thesis, measurements of 1/f noise in tin and lead films at the superconducting transition are reported. These measurements provide strong additional evidence to support the thermal fluctuation model.

There are few reported measurements of low frequency noise at the superconducting transition when the applied magnetic field and current are sufficiently low that the transition temperature is not significantly suppressed from its zero field value. Maul, Strandberg, and Kyhl[4] found excess noise at the superconducting transition of tin films, but did not demonstrate explicitly that the power spectrum was 1/f at low frequencies. They analysed their results using a model in which equilibrium temperature fluctuations of the film gave rise to resistance fluctuations. They assumed that the temperature of the film was uniform at any instant of time, and that the substrate was a constant temperature reservoir. In this model the decay of a fluctuation was exponential, characterized by a single relaxation time, and the power spectrum was a Lorentzian. The voltage power spectrum was shown experimentally to be proportional to

$(dR/dT)^2 I^2$, where I was the current flowing in the film. Katz and Rose[5] showed that the low frequency noise at the transition of tin films had a 1/f power spectrum, but they did not propose a mechanism for this behavior.

There have been extensive measurements of low frequency noise generated by flux flow in superconducting films and foils[6-16]. Most of these measurements were made in the presence of high magnetic fields and/or currents and at temperatures well below the zero field transition temperature. The samples were therefore in an intermediate state (Type I superconductors) or a mixed state (Type II superconductors) in which flux motion was induced by the current. In the measurements reported here, the low frequency noise is dominated by the thermal fluctuation mechanism. I will compare the results expected from the flux flow and thermal mechanisms in Section V.A.

I will start by reviewing the theory relevant to these experiments. The general theory will be formulated and interpreted. After describing the experimental procedures and results, some discussions and speculations will appear in Chapter V.

II. THEORY

A. Richardson's Theory and its Interpretation

J. M. Richardson[3] was the first to thoroughly calculate the noise of a fluctuating quantity resulting from a fluctuating concentration of heat or particles. His approach is perhaps the most general one existing. I shall therefore start the theoretical discussion with a method closely related to his.

The quantity of relevance in this experiment is the average temperature of the metal film under investigation, $\overline{T}(t)$. $\overline{T}(t)$ can be written in terms of the local temperature $T(\vec{r},t)$ as

$$\overline{T}(t) = \int F(\vec{r})\ T(\vec{r},t)\ d\vec{r} \quad , \tag{2-1}$$

where $T(\vec{r},t)$ is the temperature of $d\vec{r}$ at time t. The form of $F(\vec{r})$ defines the averaging range and form. In the particular case of a rectangular film of dimensions ℓ_1, ℓ_2 and ℓ_3. $F(\vec{r})$ is defined as

$$F(\vec{r}) = \begin{cases} \frac{1}{\Omega} & \text{for } 0 < x < \ell_1 \ , \ 0 < y < \ell_2 \ , \ 0 < z < \ell_3 \ , \\ 0 & \text{otherwise} \ , \end{cases} \tag{2-2}$$

and $\Omega = \ell_1\ \ell_2\ \ell_3$. The validity of choosing this form of $F(\vec{r})$ will be discussed later.

It should be noted that here the use of "local temperature" is for convenience. Energy is the fluctuating quantity and temperature is defined in thermodynamics as an average quantity. Here $T(\vec{r},t)$ is understood as the local energy density divided by the heat capacity.

$T(\vec{r},t)$ is governed by the diffusion equation:

$$\frac{\partial}{\partial t} T(\vec{r},t) - D\nabla^2 T(\vec{r},t) - g(\vec{r},t) \tag{2.3}$$

where D, the diffusivity, equals to K/C, the thermal conductivity divided by heat capacity, and $g(\vec{r},t)$ is a random source function representing the scattering processes the heat carriers experience.

We may apply the spatial Fourier transform to both $T(\vec{r},t)$ and $F(\vec{r})$;

$$T(\vec{r},t) = \sum_{\vec{k}} T_{\vec{k}}(t)\, e^{i\vec{k}\cdot\vec{r}} \quad , \quad T_{\vec{k}}(t) = \frac{1}{\Omega}\int T(\vec{r},t) e^{-i\vec{k}\cdot\vec{r}}\, d\vec{r} \quad , \tag{2.4}$$

$$F(\vec{r}) = \sum_{\vec{k}} F_{\vec{k}}\, e^{i\vec{k}\cdot\vec{r}} \quad , \qquad F_{\vec{k}} = \frac{1}{\Omega}\int F(\vec{r})\, e^{-i\vec{k}\cdot\vec{r}}\, d\vec{r} \quad . \tag{2.5}$$

(2.3) becomes

$$\overline{T}(t) = \Omega \sum_{\vec{k}} F^*(\vec{k})\, T_{\vec{k}}(t) \quad , \tag{2.6}$$

and the diffusion equation can be expressed as

$$\frac{\partial}{\partial t} T_{\vec{k}}(t) + D\, k^2\, T_{\vec{k}}\,(t) - g_{\vec{k}}(t) \quad , \tag{2.7}$$

where $g_{\vec{k}}(t)$ is defined by

$$g(\vec{r},t) = \sum_{\vec{k}} g_{\vec{k}}(t) e^{i\vec{k}\cdot\vec{r}} \ , \quad g_{\vec{k}}(t) = \frac{1}{\Omega}\int g(\vec{r},t) e^{-i\vec{k}\cdot\vec{r}} dr. \tag{2.8}$$

When time Fourier transform is applied,

$$T_{\vec{k}}(t) \ = \int T_{\vec{k}}(\omega)\ e^{i\omega t}\ d\omega, \quad g_{\vec{k}}(t) \ = \int g_{\vec{k}}(\omega) e^{i\omega t} d\omega \ , \tag{2.9}$$

we get, from (2.7),

$$T_{\vec{k}}(\omega) = g_{\vec{k}}(\omega)/(Dk^2 + i\omega), \tag{2.10}$$

and the spectral ensemble average is

$$\langle T_{\vec{k}}(\omega)\ T_{\vec{k}}^*(\omega)\rangle \ = \ \frac{\langle g_{\vec{k}}(\omega)\ g_{\vec{k}}(\omega)\rangle}{D^2k^4 + \omega^2} \quad . \tag{2.11}$$

The spectral distribution of $\overline{T}$ is obtained by substituting (2.10) and (2.11) into (2.6)

$$\langle \overline{T}(\omega)\overline{T}^*(\omega)\rangle = \Omega^2 \sum_{\vec{k}} F_{\vec{k}} F_{\vec{k}}^* \langle T_{\vec{k}}(\omega)\ T_{\vec{k}}^*(\omega)\rangle$$

$$= \Omega^2 \sum_{\vec{k}} |F_{\vec{k}}|^2 \frac{\langle g_{\vec{k}}(\omega)\ g_{\vec{k}}^*(\omega)\rangle}{D^2k^4 + \omega^2} \tag{2.12}$$

$$= \Omega^2 \sum_{\vec{k}} |F_{\vec{k}}|^2 \frac{b_{\vec{k}}\ \Delta f}{D^2k^4 + \omega^2} \quad .$$

The last equality was obtained by dropping the frequency dependence of $g_{\vec{k}}(\omega)$. This is possible because for frequency less than the inverse of the scattering time, $g(\vec{r},t)$ is totally random in time. Since we are interested in the low frequency behaviour of $\overline{T}$, it is justified to take $\langle g_{\vec{k}}(\omega) g_{\vec{k}}^*(\omega)\rangle$ as independent of frequency. In particular, since g is totally random, $\langle g_{\vec{k}}(\omega)\ g_{\vec{k}}^*(\omega)\rangle$ is proportional to the bandwidth Δf. Although it is impossible to calculate $g(\vec{r},t)$, we can obtain the value of $b_{\vec{k}}$ as follows:

From (2.8) and (2.9), we get

$$\langle T_{\vec{k}}(t)\ T_{\vec{k}}^*(t)\rangle = \sum_{\omega} \langle T_k(\omega)\ T_k^*(\omega)\rangle$$

$$= \sum_{\omega} \frac{b_{\vec{k}}\,\Delta f}{D^2k^4 + \omega^2} \quad \frac{1}{2\pi} \int \frac{b_{\vec{k}}\,d\omega}{D^2k^4 + \omega^2}$$

$$= \frac{b_{\vec{k}}}{4Dk^2}$$

$\langle T_{\vec{k}}(t)\ T_{\vec{k}}^*(t)\rangle$ can also be calculated from thermodynamic theory of fluctuations. Under the restriction that the average value of $T(\vec{r},t)$ is independent of $\vec{r}$ and that the system is in thermal equilibrium, a deviation of T from the average value will give rise to a deviation ΔS in entropy S from the equilibrium value S_o:

$$\Delta S = -\frac{1}{2}\ S'' \int T^2(\vec{r},t)\ d\vec{r} \quad , \tag{2.14}$$

where $S'' = \left.\frac{d^2S}{dT^2}\right|_{T = \overline{T}}$.

In the Fourier transformed form, (2.14) becomes

$$\Delta S = -\frac{S''\Omega}{2} \sum_{\vec{k}} T_{\vec{k}}(t)\ T_{\vec{k}}^*(t) \tag{2.15}$$

S is related to the probability distribution function W(S) by $S = k_B \times \ln(W(s))$. Substituting $S = S_o + \Delta S$,

$$W(s) \propto e^{\Delta S/k_B} \quad . \tag{2.16}$$

The probability distribution for $T_{\vec{k}}(t)$ is then proportional to $e^{-(s''/2k_BT)\sum_{\vec{k}} T_k(t)\, T_k^*(t)}$. This is the usual Maxwellian distribution for each component of $T_{\vec{k}}(t)$. Hence

$$\langle T_{\vec{k}}(t)\, T_{\vec{k}}^*(t) \rangle = \frac{2k_BT}{S''} \quad , \tag{2.17}$$

[the extra factor of 2 results from the two sine and cosine components for $T_{\vec{k}}(t)$]. We then have, from (2.13),

$$b_{\vec{k}} = \frac{8\, D\, k_B\, T}{S''}\, k^2 \quad , \tag{2.18}$$

and the spectrum of $\overline{T}$ becomes

$$S_T(\omega) \equiv \frac{\langle \overline{T}(\omega)\overline{T}^*(\omega) \rangle}{\Delta f} \quad \frac{8\, D\, k_B\, T}{(2\pi)^3\, S''} \int \frac{k^2 |F(\vec{k})|^2}{\omega^2 + D^2 k^4}\, d\vec{k} \quad . \tag{2.19}$$

Richardson's results are totally general and apply to any quantity governed by the diffusion equation. Two assumptions were used in the calculation: that the system is in thermal equilibrium and that large fluctuations from equilibrium is improbable. [The latter assumption is implicit in (2.16)]. His final result of b_k proportional to k^2 can be physically understood as follows.

If $g(\vec{r},t)$ is a totally random quantity in both time and space, one expects $\langle g(\vec{r},t)\ g(\vec{r}',t')\rangle \propto \delta(\vec{r}-\vec{r}')\ \delta(t-t')$, which would give $\langle g(\vec{k})g^*(\vec{k})\rangle$ = constant. However, if we introduce a $f(\vec{r},t)$ such that $g(\vec{r},t) = \vec{\nabla}\cdot\vec{f}\ (\vec{r},t)$, then $\langle g(\vec{k})g^*(\vec{k})\rangle = k_2\langle \vec{f}(\vec{k})\cdot\vec{f}^*(\vec{k})\rangle$. If $\langle \vec{f}(\vec{k})\ \cdot\ \vec{f}^*(\vec{k})\rangle$ is constant, we get back Richardson's results, Eq. (2.18). We can rewrite (2.3) as

$$\frac{\partial}{\partial t}\ T(\vec{r},t) - D\nabla^2 T(\vec{r},t) = \vec{\nabla}\cdot\vec{f}\ (\vec{r},t) \qquad (2.20)$$

and here $\vec{f}(\vec{r},t)$ is a random source function uncorrelated in time and space. From the continuity equation for energy $\frac{\partial}{\partial t}\ T(\vec{r},t) - \vec{\nabla}\vec{J}_T(\vec{r},t) = 0$. Where $\vec{J}_T$ is the energy flux, it is apparent that $\vec{f}(\vec{r},t)$ corresponds to a random energy flux driving term. The physical meaning of Eq. (2.20) is that the time rate of energy change in $d\vec{r}$ is just equal to the flux being driven in and out of by $\vec{f}(\vec{r},t)$. A scalar driving term on the other hand, would imply a random appearance (or disappearance) of energy in $d\vec{r}$. Eq.(2.20) thus tells us that energy can be randomly distributed through

scattering but there can be no energy sources or sinks. In a closed system, Eq. (2.20) is a restatement that energy must be conserved.

B. Application of Richardson's Theory and the Semi-Empirical Model

Richardson's results can be readily applied to calculate the average temperature fluctuation in a metal strip. $F(\vec{k})$ is given by the Fourier transform of (2.2)

$$F(\vec{k}) \propto \frac{\sin(k_x \ell_1/2)}{k_x \ell_1} \quad \frac{\sin(k_y \ell_2/2)}{k_y \ell_2} \quad \frac{\sin(k_z \ell_3/2)}{k_z \ell_3/2} \quad . \tag{2.21}$$

Substituting (2.21) into (2.19), $S_T(f)$ can be calculated.

A typical spectrum of $S_T(f)$ with $\ell_1 >> \ell_2 >> \ell_3$ is shown in Fig. 1, where $f_i = D/4\pi\ell_i^2$. In various regions, the spectrum has the approximate form

$$S_T(f) \propto \begin{cases} \text{constant} & f_1 >> f \quad , \\ \ell n\ (1/f) & f_2 >> f >> f_1 \quad , \\ 1/f^{0.5} & f_3 >> f >> f_2 \quad , \\ 1/f^{1.5} & f >> f_3 \quad . \end{cases} \tag{2.22}$$

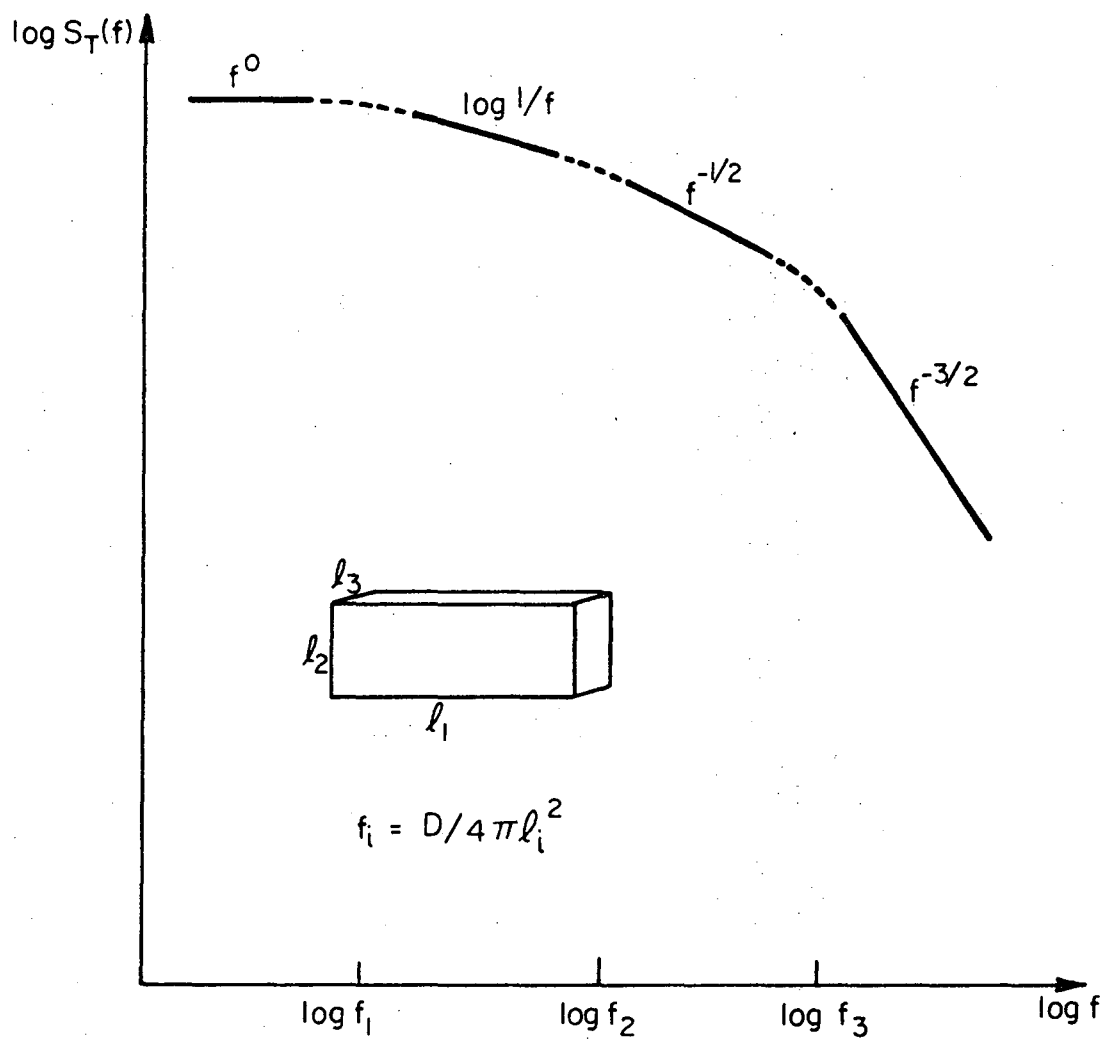

XBL 777-5771

Fig. 1 Noise temperature spectrum for a box-shaped volume.

There is no section of the spectrum where a 1/f region stands out. In real experiments, a 1/f region is always observed. Richardson's original paper proposed that a special choice of $F(\vec{k})$may yield a 1/f spectrum. As will be discussed in the next section, the voltage noise measured in metal films actually reflects $S_T(f)$ at low frequencies with $F(\vec{k})$ specified by (2.21). How is this discrepancy resolved? Clarke and Voss[1] noted that an experimental system of metal film and insulating substrate is very different from an ideal 3-dimensional diffusive system. The diffusivities of the two are different, and there is a thermal boundary resistance between them[17]. They therefore adopted a semi-empirical approach: one assumes that the noise originates from temperature fluctuation, and there is an explicit 1/f region in the spectrum. Their model spectrum is shown in Fig. 2.

The spectrum, analytically, is given by

$$S_T(f) \propto \begin{cases} \text{constant} & f < f_1 \ , \\ 1/f & f_1 < f < f_2 \ , \\ 1/f^{1.5} & f_2 < f \ . \end{cases} \tag{2.23}$$

Together with the normalization condition

$$\int S_T(f)df = \frac{k_B T^2}{C_v \Omega} \tag{2.24}$$

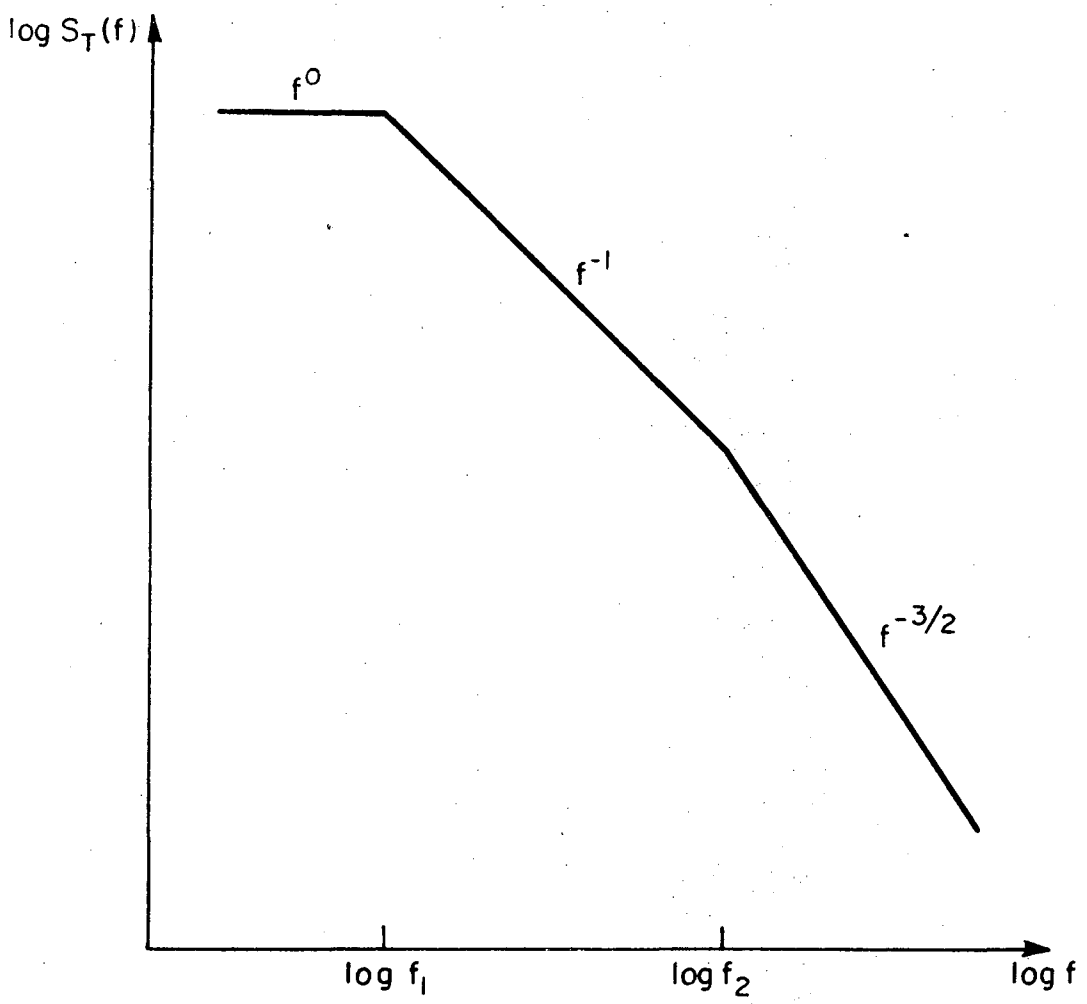

XBL777-5772

Fig. 2 Semi-empirical noise power spectrum.

one gets, for $f_1 < f < f_2$

$$S_T(f) = \frac{k_B T^2}{C_V \Omega} \frac{1}{(3 + 2 \ln \frac{\ell_2}{\ell_1})} \frac{1}{f} \quad . \tag{2.25}$$

Even though the noise has been seen below the lower truncation frequency f_1, the normalization is weakly dependent on the values of f_1 and f_2. $S_T(f)$ is not changed significantly should the truncation frequencies be very different.

For metal films at room temperature, $C_V \simeq 3Nk_B$. Where N is the density of atoms. The geometric factor $1/(3 + 2 \ln \frac{\ell_2}{\ell_1})$ is roughly 0.1 for most measured films. The voltage noise is given by

$$S_V(f) = \overline{V}^2 \left(\frac{1}{R} \frac{dR}{dT}\right)^2 \times S_T(f) \equiv \overline{V}^2 \beta^2 S_T(f) \quad , \tag{2.26}$$

where β, the temperature coefficient of resistance, is on the order of 10^{-3} for most pure metals, and $\overline{V}$ is the average voltage across the film. If we take $\beta \simeq 3 \times 10^{-3}$ (for Sn, Ag, Cu), we get $S_V(f) = \overline{V}^2 \times 3 \times 10^{-2}/N\Omega f$. This is in good agreement with the experimental results of Clarke and Voss.

The dependence of S_V on $N\Omega$ indicates that S_V is a volume effect and does not depend on whether the metal is a good or poor conductor.

Equations (2.25) and (2.26) will be compared with results of this experiment. It was not possible to test in detail the dependence of (2.25) on β, Ω, and $\overline{V}$ by studying the room-temperature samples. However, at superconducting transition, the metal films have high β, which depends on temperature, and the $S_V(f)$ dependence on various parameters may be checked.

The fact that the superconducting transition is smeared out in temperature is a consequence of fluctuations in the order parameter. A recent review of the microscopic fluctuation theories and of their experimental verification has been given by Tinkham.[16] These fluctuations occur on a time scale that is extremely short compared with the times of interest in the present work. We are concerned only with the resultant average shape of the transition curve, and the relatively slow thermal fluctuations that take place due to the exchange of energy between the superconductor and its substrate.

In order to apply Eq. (2.25) to our results, we require a value for the heat capacity of the film C_V. As the temperature of the film is lowered through the superconducting transition there is an increase in the electronic heat capacity that we assume to be smeared out in a way that reflects the shape of the resistive transition. Thus, as energy is exchanged between the film and the substrate, the heat capacity of the film fluctuates.

However, assume that the electronic heat capacity near T_c can be written in the form $C_e = C_{en} + (C_{es} - C_{en})(T_n - T)/\delta T$, where C_{en} and C_{es} are the heat capacities just above and below the transition at temperatures

T_n and T_s. From Ref. 16 we find $C_{es} - C_{en} = 1.43\ C_{en}$. Writing $T = \overline{T} + \Theta(t)$, where $\overline{T}$ is the average temperature, and where the mean square value of the fluctuating quantity $\Theta(t)$ is $k_B T^2/C$, we find $C_e(t) = \overline{C}_e\ [1 - 1.43\ (C_{en}/\overline{C}_e)\Theta(t)/\delta T]$. The rms correction to C_e is thus of order $\langle (\Delta T)^2 \rangle^{1/2}/\delta T$.

For our samples, $\langle (\Delta T)^2 \rangle^{1/2} \sim 10^{-7}$ and $\delta T \sim 3$ mK, so that the correction is of order 10^{-4}, and negligible compared with other errors in the measurements. Since most of our measurements were made with the films near the midpoint of the transition, we shall take as the heat capacity the sum of the phonon heat capacity at T_c and the average of the superconducting and normal electronic heat capacities just below and just above the transition.

C. Correlation Functions

An alternative approach of calculating $S_T(\omega)$ is by the use of correlation functions. Since this was extensively discussed by Clarke and Voss,[2] I shall only briefly quote the important results.

The spatial-time correlation function of (2.20) was calculated by Chandrasekhar[18]. In a one-dimensional system, it is

$$C_T\ (\vec{s},\tau) \equiv \langle T(\vec{x}+\vec{s}\ ,\ t+\tau)\ T(\vec{x},t)\rangle$$

$$= [k_B T^2/C_V \Omega (4\pi D\tau)^{\frac{1}{2}}]\ \exp(-s^2/4D\tau) \quad . \tag{2.27}$$

Here, the dc part of $T(\vec{x},t)$ is ignored. A more useful form of C_T, which also gives physical insight into the noise spectrum, is the frequency dependent correlation function, $C_T(\vec{s},\omega) \equiv \langle T(\vec{x}+\vec{s},\omega)\, T^*(\vec{x},\omega)\rangle$. In 1-, 2-, and 3-dimensional systems, it is

$$C_T^{(1)}(\vec{s},\omega) = \frac{k_B T^2 \cos[(\pi/4) + |\vec{s}|/\lambda]}{2\pi\, C_V \Omega\, D^{\frac{1}{2}}\, W^{\frac{1}{2}}} \exp(-|\vec{s}|/\lambda) \quad , \tag{2.28}$$

$$C_T^{(2)}(\vec{s},\omega) = \frac{k_B T^2}{2\pi D C_V \Omega} \ker\,(\sqrt{2}|\vec{s}|/\lambda) \quad , \tag{2.29}$$

$$C_T^{(3)}(\vec{s},w) = \frac{k_B T^2}{4\pi^2\, D C_V \Omega |\vec{s}|} \cos\,(|\vec{s}|/\lambda) \exp\,(-|\vec{s}|/\lambda) \tag{2.30}$$

where $\lambda \equiv (2D/\omega)^{\frac{1}{2}}$, is the frequency-dependent correlation length and is a measure of the spatial correlations of a fluctuation at frequency ω.

From the definitions of $C_T(\vec{s},\omega)$ and $S_T(\omega)$, it is apparent that

$$S_T(\omega) = \Omega^{-2} \int_\Omega d\vec{x} \int d\vec{x}'\; C_T(\vec{x}-\vec{x}',\omega) \quad , \tag{2.31}$$

because S_T is defined as the intensity spectrum of the <u>average</u> temperature in Ω. At low frequencies, the whole volume is correlated, that is, $\lambda(\omega) >> \ell i$. In this limit, the spatial dependence of $C_T(\vec{s},\omega)$ drops out, and $S_T(\omega) \simeq C_T(o,\omega)$. $S_T(\omega)$ then is proportional to constant, $\ell n\frac{1}{\omega}$, and $\omega^{-0.5}$ for the 3-, 2-, 1-dimensional system respectively. In the high frequencies, where $\lambda(\omega) << \ell_i$, $S_T(\omega)$ in all dimensions is proportional to$\omega^{-1.5}$. Figure 1 describes $S_T(\omega)$ in any dimensional case, with the region below f_1 absent for the 2-dimensional case, and the region below f_2 absent for the 1-dimensional case.

The above considerations have an important consequence in that it makes it possible to use electrical methods for probing temperature fluctuations in metal films. At low enough frequencies (typically < 10k H_z), $\lambda(\omega)$ becomes longer than ℓ_2 and ℓ_3 of the metal films used in this experiment. Therefore the temperature is correlated through the crosssection of the current flow in the experiment (which is along the ℓ_1 direction). A temperature fluctuation that changes R of the film but does not change $\overline{T}(t)$ can only happen at higher frequencies. We can then claim (2.26) is applicable, and the voltage fluctuation truly represents the temperature fluctuation.

III. EXPERIMENTAL PROCEDURES

A. Film Preparation and Cryostat

Tin and lead films, typically 0.1 μm thick, were evaporated at about 5×10^{-5} torr onto glass slides or single crystal c-cut sapphire plates at room temperature. These will be referred to as type A samples. Other samples (type B) were prepared with a 5-nm aluminum film deposited on the substrate prior to the tin or lead evaporation. A period of about one minute elapsed between the completion of the aluminum deposition and the beginning of the tin or lead evaporation, so that the aluminum was largely oxidized. Type A and B films have comparable resistivity ratio (~5 for tin and ~30 for lead), T_C (~3.8K for tin and ~7.2K for lead), and transition widths (~3mK for tin and ~30mK for lead).

The films were cut with a diamond point into a strip geometry. A few examples are shown in Fig. 3, with separate current and voltage leads. Films with cut edges tend to have sharper transition than those with the tapered edge left by evaporation through a mask.[19] Manganin leads were attached to the films with cold-pressed indium. The reverse side of the substrate was greased with Apiezon N grease, and the substrate clamped to a copper plate.

The cryostat is similar to the one described in Section VIIB without the SQUID attachments. The copper plate on which the sample is mounted has a 68-Ω Allen Bradley carbon resistor and a non-inductively wound heater glued to its reverse side for monitoring and controlling temperature. The plate was supported by a stainless steel rod, and the whole assembly mounted in a vacuum can. The can was immersed in liquid helium

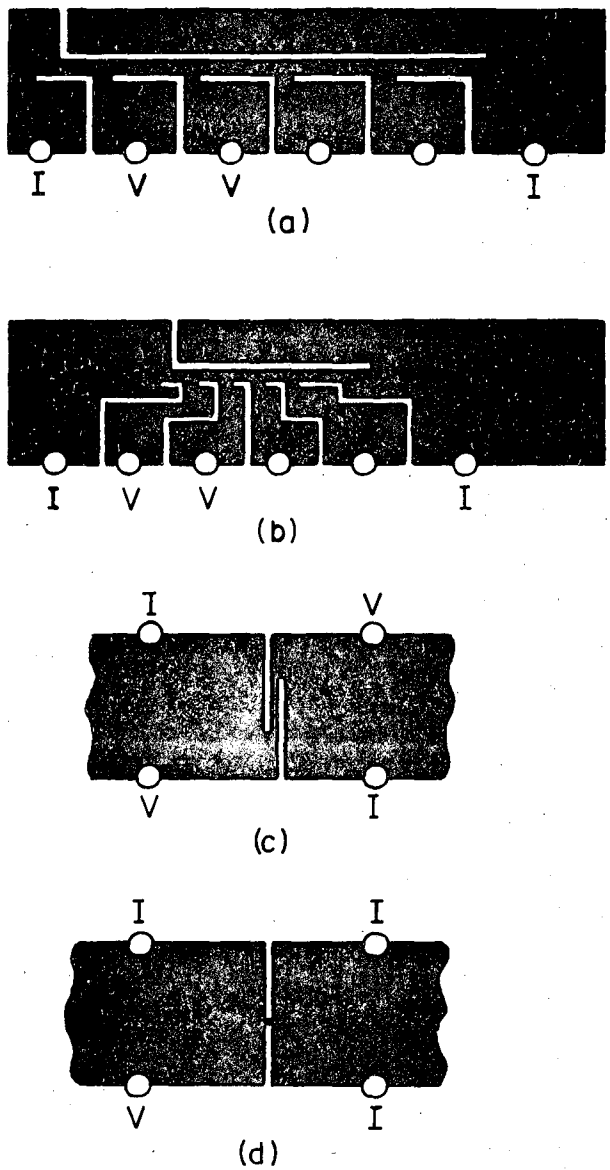

XBL 777-5773

Fig. 3 Specimen configurations: (a) long specimen used also for correlation measurements; (b) short specimen used also for correlation measurements; (c) short specimen; (d) very short specimen.

whose temperature was stabilized to ± 100 μK by a mechanical manostat. The temperature of the copper plate, whose thermal time constant at 4K is about 75 sec, could be raised above the bath temperature with the heater. At first, Rochlin bridge[62] was used to electronically control the temperature of the copper plate with an ac resistance bridge and feedback circuit. Later it was found the Rochlin bridge generates an untolerable amount of temperature noise in the sample. Dc heating was then used. Which, with the mechanical manostat and the long thermal time constant, was capable of stabilizing the temperature of the sample to more than 10 minutes, enough to make measurements possible.

The vacuum can, in which the sample was mounted, was supported by a stainless steel tube extended from the top of the dewar. Electrical leads were made into the can with an epoxy feedthrough. The pump line was blackened from room temperature radiation with a copper spacer. A superconducting solenoid was wound around the can and provided persistent magnetic field in some experiments. The cryostat was surrounded by two μ-metal cylinders which reduced the ambient magnetic field to about 10 m G. The complete cryostat was placed in a shielded room that effectively eliminated rf pick-ups.

B. Measurement Techniques

A steady current was supplied to the sample from a mercury battery, pre-drained to very steady voltage level, in series with a large wire-wound resistor, always at least 1000 times larger than the sample resistance. Four-probe measurements were always made to insure that

no contact noise would be seen. The fluctuating voltage across the sample was amplified by a capacitively coupled transformer of turns ratio 100:1 (PAR-190 below 100 H_z and Triad JZ-5 above 100 H_z) dc coupled to a battery operated PAR-113 preamplifier inside the shielded room. The overall gain of the system was calibrated with an ac signal of variable frequency and a white noise source for each sample resistance. A typical gain for input resistance of 20 Ω is shown in Fig. 4. The output from the amplifier was filtered and Fourier analyzed with either the tune amplifier in PAR HR-8 lock-in detector with a Q of 25, or by a POP-11 computer using a Fast Fourier Transform algorism. Pre-amplifier noise was subtracted from each measured spectrum.

C. Spurious Noise Sources

There are several sources of extraneous noise:

(i) 60-Hz pickup. A 60-Hz signal was observed in most measurements as an easily recognizable peak in the spectrum that could be subtracted out.

(ii) Current supply noise. The noise in the dc current supplied to the sample was investigated by taking a noise spectrum with the sample in the normal state: The noise was indistinguishable from that obtained with the current turned off. This noise source was thus insignificant.

(iii) Nonequilibirum fluctuations in the temperature of the substrate. Slow drifts in the temperature of the helium bath and the heater current induced low-frequency fluctuations in the temperature of the copper plate. We investigated these fluctuations by measuring the 1/f noise in a film whose area was about 100 times greater than that

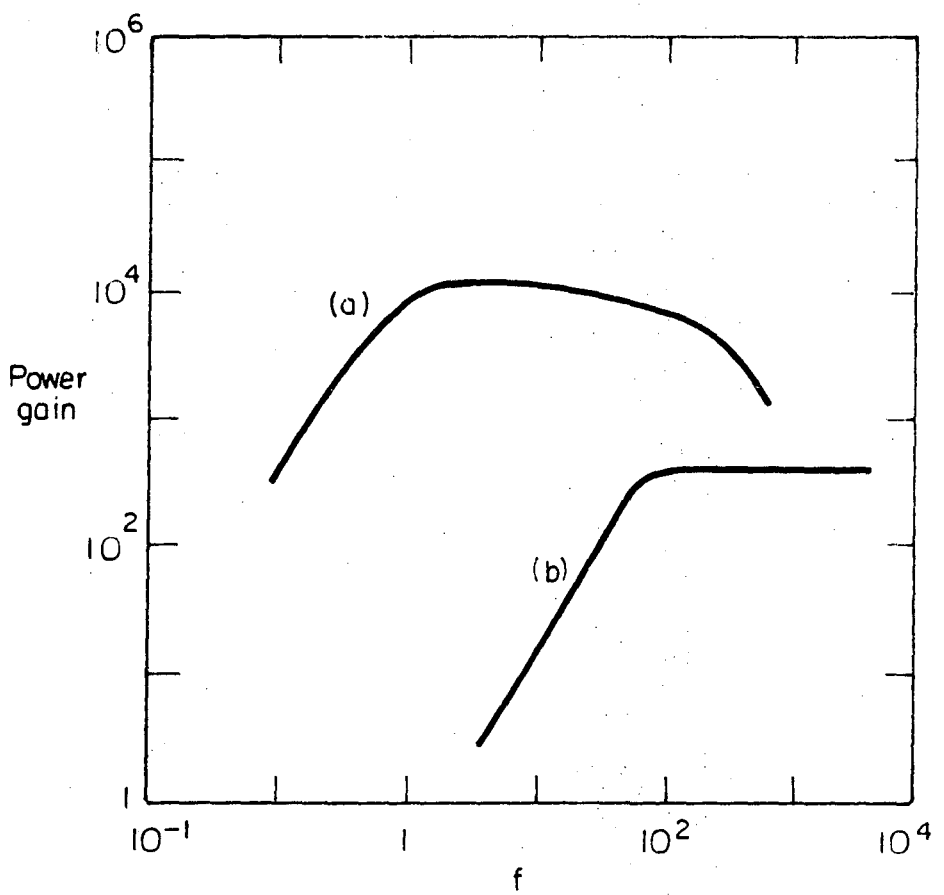

XBL 777-5774

Fig. 4 Power gain for (a) PAR 190 + PAR 113, (b) Triad JZ-5 + PAR 113 for input impedance of 20 Ω. DC filter of 1.6×10^{-2} Farad is also included.

of our typical size samples. Above about 0.1 Hz, $S_V(f)/\overline{V}^2$ was about 100 times smaller for the larger sample than for the typical sample, as predicted by Eq. (2.25). If the noise had originated from fluctuations in the temperature of the copper plate, the measured spectrum would have been independent of sample volume. AS the frequency was lowered below 0.1 Hz, the power spectra of the two films approached each other, and their slope steepened. (With our measuring technique, a linear change of voltage with time produces a $1/f^2$ power spectrum.)

We concluded that temperature fluctuations in the substrate were significant at or below 0.1 Hz, while at or above 0.1 Hz, the measured noise for our typical sample size was dominated by intrinsic equilibrium fluctuations in the film. We generally regarded our measured spectra to be reliable down to about 1 Hz.

(iv) Microphonic noise. Vibration of the cryostat could induce a substantial amount of noise. The effects were minimized by rigidly mounting the sample and can, and by taking care not to disturb the cryostat during measurements.

(v) Preamplifier noise. At frequencies above .1 Hz preamplifier noise was usually the dominant background noise source. The noise was measured by switching off the dc bias supply or by having the sample in the normal or superconducting state with the bias current switched on. The preamplifier noise spectrum was measured immediately after the power spectrum of each sample was measured, and subtracted out. The preamplifier power spectrum was typically 1-5 orders of magnitude below the sample power spectrum. For a combined sample and lead resistance of 22 Ω, the noise was typically 5×10^{-18} V^2 Hz^{-1} referred to the input of the transformer.

IV. EXPERIMENTAL RESULTS

A. Thermal Coupling of Type-A and Type-B Films

Before describing the measured noise spectra, it is convenient to discuss the thermal coupling between the films and the substrates with and without an aluminum underlay. The original motivation for preparing type B samples was as follows. In an attempt to investigate the effect of the substrate properties on the noise spectrum, Type A tin samples were prepared on single crystal sapphire plates whose thermal diffusivity was several orders of magnitude higher than that of glass. It was found that the film was very poorly anchored to the sapphire, and could easily be removed. In order to improve the bonding of the film to the substrate a 50Å layer of aluminum was predeposited. This layer greatly enhanced the bonding. I shall briefly describe two methods by which the effect of the underlay on the thermal contact of the films to the substrate was qualitatively investigated.

At sufficiently high bias currents all of our samples became unstable due to self-heating effects, and could not be maintained at the superconducting transition. Low frequency instabilities set in when βP becomes comparable with the thermal conductance between the film and the substrate[20], where P is the power dissipated in the film. For type A tin samples of size 2.5mm x 15μm x 1000Å and with $\beta \sim 150K^{-1}$ thermal instability occurred with a glass substrate at a power dissipation of order 1μW. This power is at least an order of magnitude greater than the power dissipated in any of the noise measurements, during which the samples had no tendency to become unstable. Type A lead samples

on glass substrates of comparable size and with $\beta \sim 30K^{-1}$ became thermally unstable at a power level of around 4μW. Since $\beta_{sn} \sim 5\beta_{pb}$, these results tend to suggest that the thermal coupling of tin and lead films to glass substrate is of the same order. Type A tin samples on sapphire substrates were subject to thermal runaway at relatively low power dissipation ($\ll$1μW), indicating a poor thermal contact with sapphire. For type B samples of the same size, thermal instability occurred at typically 10μW for tin films and 4μW for lead films for both glass and sapphire substrates. It appears that the aluminum underlay greatly enhances the thermal contact of tin to glass and sapphire, but has relatively little effect on lead deposited on glass.

Another measure of the effective thermal conductance between film and substrate was obtained as follows. With the temperature in the transition range, the voltage across the film generated by a given bias current was measured. The value of the current was then changed, and the voltage remeasured when the sample had again reached a steady state. The change in the temperature of the film was deduced from the change in its resistance. An effective thermal conductivity (K_e) was calculated from the change in temperature resulting from a given change in power dissipation. For tin samples of size 2.5mm x 15μm x 1000Å on glass substrates, for type A, $K_e \approx 1.5\mu WK^{-1}$ ($\sim 40\mu WK^{-1}$ for $1mm^2$), while for type B, $K_e \approx 12\mu WK^{-1}$. For lead films of size 25mm x 20μm x 1200Å on glass substrates, for type A, $K_e \approx 6\mu WK^{-1}$ ($\sim 120\mu WK^{-1}$ for $1mm^2$) while for type B, $K_e \approx 12\mu WK^{-1}$. These results confirm that the aluminum underlay greatly enhances the thermal contact between tin films and a glass

substrate, but has relatively little effect on lead films. It is far from clear what "effective" thermal conductively is measured by this technique. When power is dissipated in the film, a temperature gradient is established in the substrate in the vicinity of the film. Consequently, the measured thermal conductivity cannot be interpreted as the ratio of the power dissipation to the temperature difference between the film and a constant temperature substrate.

It was believed that the aluminum underlay enhances the thermal contact by improving the bonding of these films to the substrate. Other people here found that aluminum[21] adheres strongly to glass whereas tin[22] does not. As mentioned in the previous chapter, the aluminum film is certainly partially oxidized, and it is known that an oxide layer can greatly enhance the bonding of a metal film to glass[22,23]. As evidence for this hypothesis, Fig. 5 shows scanning electron micrographs of A and B tin films on the same glass substrate. In Fig. 5(A), the type A film shows considerable clumping of the tin, while in Fig. 5(B), the tin grains are much more uniformly nucleated. It is therefore likely that the effective contact area between film and substrate is substantially higher in type B samples than in type A.

An interesting experiment was done on aluminum to test the enhancement in the bonding of metal film to glass by an oxide underly. 1000Å aluminum films were evaporated on glass slides. In one case, the film was continuously deposited on glass. In the second case, a 50Å layer was deposited and allowed to oxidize at a pressure of 5×10^{-5} Torr before the remaining aluminum was evaporated. The second kind of film,

0 0 0 0 4 8 0 4 5 8 3

(A)

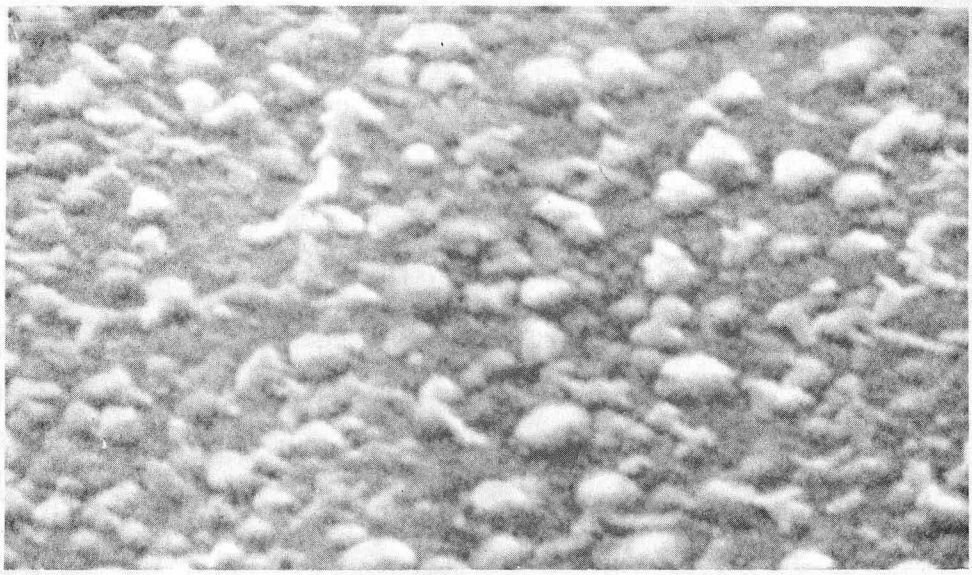

1 μm

(B)

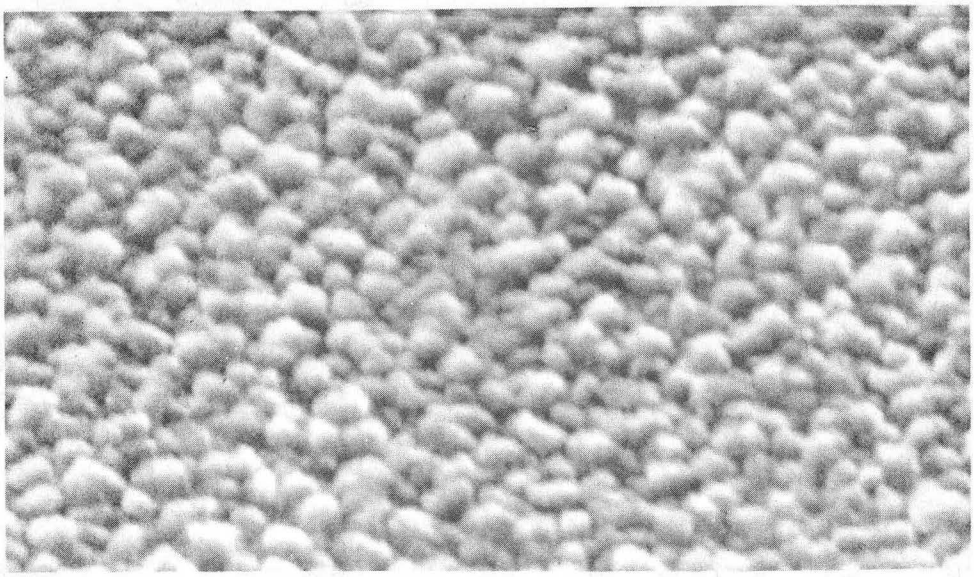

XBB 7511 8462

Fig. 5 Scanning electron micrograph of tin films on a glass substrate: (a) Type A, (b) Type B.

judged from tape-lift technique and scratching, was found to be much more strongly attached to the substrate. Similar results for tin and tin oxides were found by other authors.[24]

The fact that the transmission probability of phonon from a film to its substrate depends strongly on the nature of the films probably also plays a role in the reduction of the thermal contact resistance by the aluminum underlay. The fraction[25] of ballistic phonons transmitted from an aluminum film to a glass substrate is about 0.8, while the fraction for a tin film is only about 0.1. These values are calculated[25] on the assumption that the films are ideally bonded to the substrate. Thus one expects the boundary resistance between aluminum film and a glass substrate to be substantially lower than that between a tin film and a glass substrate.

Despite the highly qualitative nature of our experiments, it is apparent that the underlay makes a marked improvement in the thermal contact between tin films and glass or sapphire substrates, but has little effect in the case of lead films. In the next sections, we will see that the change in the thermal contact can have a marked effect on the noise spectrum.

B. Noise Power Spectra for Tin

A typical power spectrum for a type A tin sample on a glass substrate is shown in Fig. 6(a) with a dc current bias of 50μA. The sample resistance in the normal state was about 20Ω. The dashed line indicates the spectrum obtained from Eq. (2.4) using the following parameters: $\Omega = 3.8 \times 10^{-9}$ cm^3,

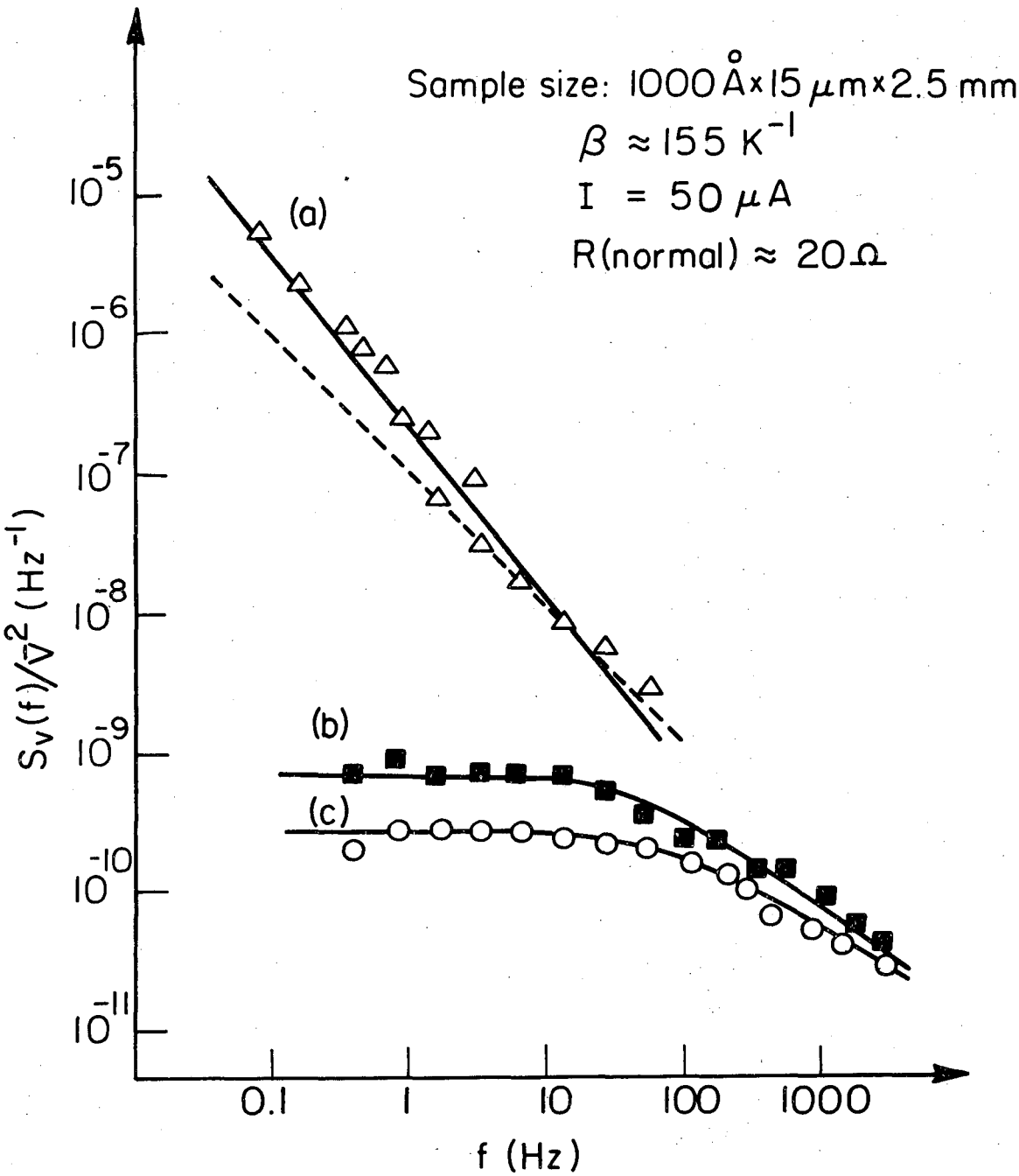

XBL 749-7145B

Fig. 6 Typical noise power spectra for tin films: (a) Type A on glass, (b) Type B on sapphire, (c) and (d) Type B on glass. Dashed line is calculated from Eq. (2.25).

$\beta = 155K^{-1}$, and an average $C_V = 1.44 \times 10^{-3}\ JK^{-1}cm^{-3}$.[26] Although the slope of the measured curve is a little steeper than -1, the general agreement between the two curves is good.

The dependence of $S_V(f)$ on Ω, β, and $\overline{V}$ was investigated. In Fig. 7(a) S_V is plotted vs. Ω^{-1} for six samples of different volumes, each biased to give the same value of $\overline{V}$. Five of these samples (solid circles) were 1000Å thick, and each was biased at a point on the transition to give a comparable value of β, about $155K^{-1}$. The sixth sample [a triangle in Fig. 3(a)] had a thickness of 6000Å and its superconducting transition was broadened to give $\beta = 62K^{-1}$ at the mid-point. In Fig. 7(a), the value of $S_V(f)$ has been multiplied by a factor of 6.25 to account for the lower β. The fact that $S_V(f)$ scales with Ω^{-1} for variations in both the area and the thickness of the films provides strong evidence that the 1/f noise is a bulk effect. If the noise were a surface effect, $S_V(f)/\overline{V}^2$ would scale inversely as the area of the films, but would presumably be independent of the thickness of the films.

In Fig. 7(b), $S_V(f)$ is plotted vs. $(dR/dT)^2$ for one sample at constant bias current. Each value of dR/dT was obtained by maintaining the sample at a slightly different temperature on the transition curve. No corrections were made for the variation in T^2/C_V: This error is insignificant compared with the measurement errors. In Fig. 7(c), $S_V(f) \propto \overline{V}^2$ indicates that self-heating effects did not contribute measurably to the noise spectra.

In each figure, a line of unity slope was fitted. Bearing in mind the uncertainties in the measurements, the measured dependence of

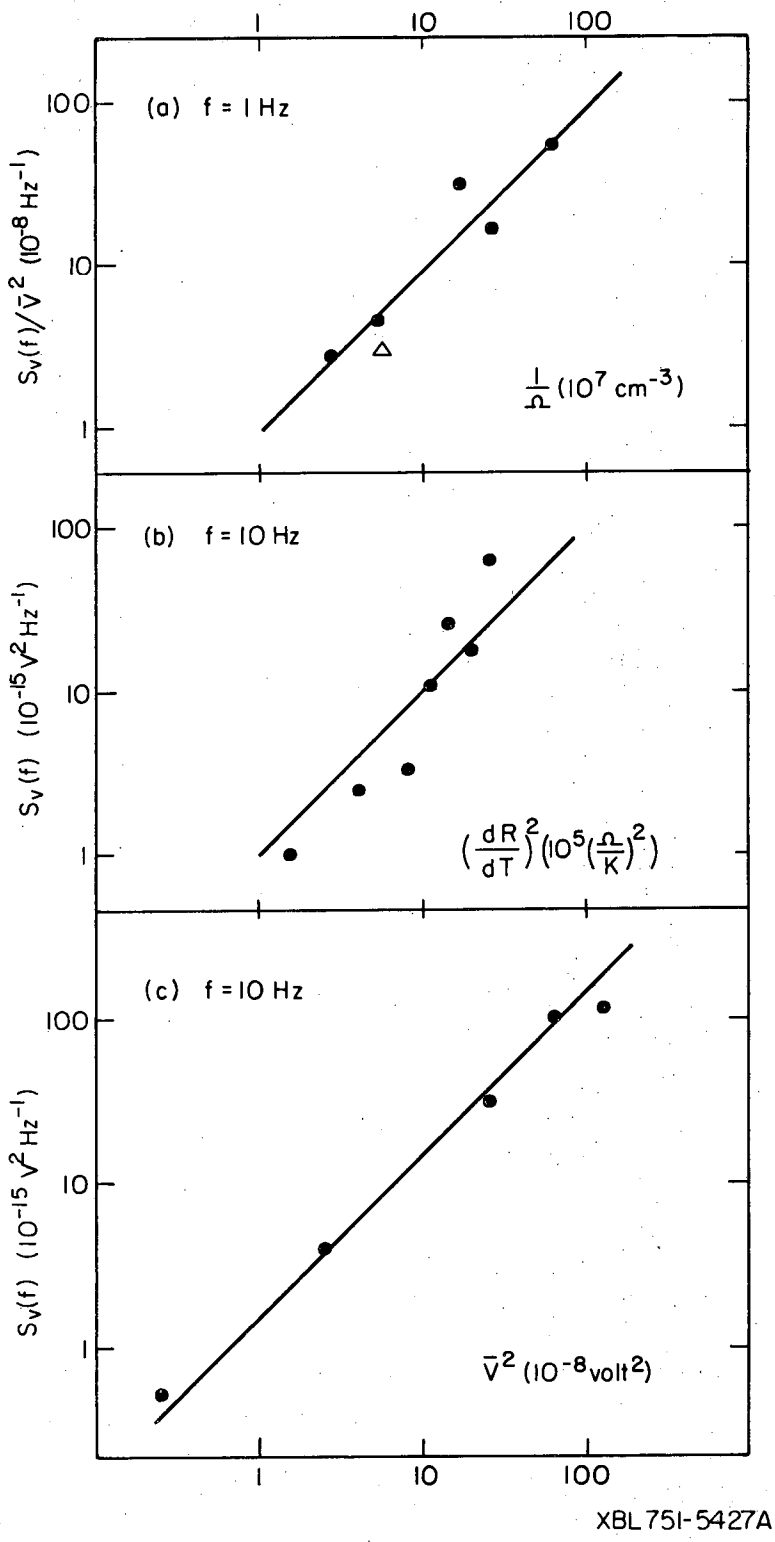

Fig. 7 (a) $S_V(1)/\bar{V}^2$ vs. Ω^{-1} (solid circles, 0.1 -μm films; triangle, 0.6 μm film); (b) $S_V(10)$ vs. $(dR/dT)^2$; (c) $S_V(10)$ vs. $\bar{V}^2$. A line of slope unity has been fitted in each figure.

$S_V(f)/\overline{V}^2$ on Ω^{-1}, and on $dR/dT^{\ 2}$ and $\overline{V}^2$ is regarded to be in satisfactory agreement with the predictions of Eq. (2.25).

The power spectra was next measured on type B tin samples. Typical noise power spectra for a sapphire substrate ($D \sim 10^5 cm^2 sec^{-1}$) and a glass substrate ($D \sim 3 cm^2 sec^{-1}$) are shown in Figs. 6(b) and (c). The spectra flatten below about 30Hz, and have a slope of less than -1 at higher frequencies. Since A and B samples had almost identical volumes, resistivities, transition temperatures, and transition widths, it is highly likely that the enormous difference between their noise spectra arises from the different thermal coupling of the films to the substrates. The flattening of the spectra at low frequencies indicates that the heat flow is much closer to ideal 3-dimensional diffusive systems in B samples than in A samples. A fluctuation at one point on the film has a higher probability of decaying into the substrate (rather than along the film) in a type B sample. It is interesting to note that the type B samples have very similar spectra on both glass and sapphire substrates, suggesting that the thermal boundary resistance, rather than the diffusivity of the substrate, is the dominant factor in determining the heat flow out of the film.

For one type B sample on a glass substrate the power spectrum shown in Fig. 6(d) was obtained. The spectrum is intermediate between the spectra (a) for type A samples and the more typical type B spectra, (b) and (c). Thus the low frequency end at the power spectrum is less depressed than that of the other type B samples, and the slope is about -0.35. Apparently the thermal conductance between the film and the substrate was less enhanced by the aluminum underlay than was usual.

It was initially speculated that the knee in Figs. 6(b) and (c) at 30 Hz corresponded to the frequency f_1. However, when the spectra of type B samples in which the length was varied from 0.6mm to 5mm were measured, no systematic variation in the knee frequency was found. It is possible that the knee frequency corresponds to the inverse of the relaxation time of the film and part of the substrate; this time, about 10ms, is independent of the length of the sample. It should be noted that this time is much greater than the time defined by the ratio of the heat capacity of the film ($\sim 5 \times 10^{-12} JK^{-1}$ for 2.5mm x 15μm x 1000Å) to $K_e(\sim 10 \mu WK^{-1})$, which is on the order of 1μs. This result suggests that part of the substrate adjacent to the film is involved in the thermal relaxation process, and that the heat capacity of this part of the substrate contributes to the relaxation time.

C. Spatial Correlation of the Noise

As a further test of the thermal diffusion mechanism, I studied the spatial correlation of the 1/f noise. The experimental configuration is shown inset in Fig. 8. The correlation of the noise generated in two regions of the same film separated by a distance d was measured. The two noise voltages $V_1(t)$ and $V_2(t)$ were separately amplified with PAR-190 transformers and PAR-113 preamplifiers, and the spectrum of their sum or difference measured in the usual way. If $S_+(t)$ is the spectrum of $[V_1(t) + V_2(t)]$ and $S_-(f)$ is the spectrum of $[V_1(t) - V_2(t)]$ the fractional correlation between the strips, C(f), is given by

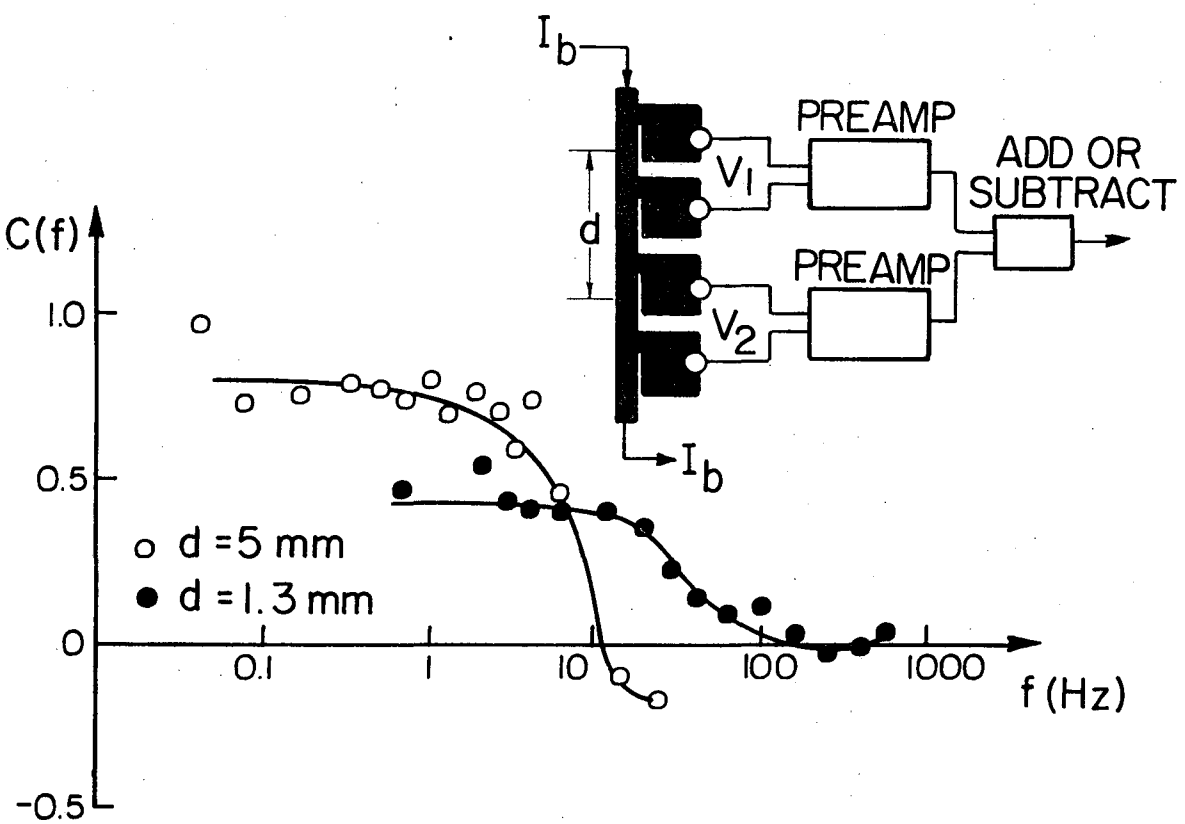

XBL751-5428A

Fig. 8 C(f) vs. f for Type-A tin films on glass (open circles) and Type B tin films on glass (solid circles). Inset is experimental configuration.

$$C(f) = [S_+(f) - S_-(f)]/[S_+(f) + S_-(f)]. \tag{4.1}$$

When V_1 and V_2 are independent, $S_+ = S_-$ and $C(f) = 0$. When $V_1 = V_2$, S_- vanishes, and $C(f) = 1$. The measured correlation for d = 5mm is shown as open circles in Fig. 8. At high frequencies, $\lambda(f) < d$, and $C(f) \to 0$, while at low frequencies $\lambda(f) > d$, and $C(f) \to$ constant. The change from correlated to uncorrelated behaviour occurs when $\lambda(f) \sim d$. Because of the thermally inhomogeneous nature of the system, I will use an <u>effective</u> diffusivity, D_e, that represents an appropriate average from the film and the substrate. The observed changeover from correlated to uncorrelated noise at about 8Hz corresponds to $D_e \approx 6\text{cm}^2\ \text{sec}^{-1}$. From the measured electrical resistance of the film, its estimated heat capacity, and the Wiedemann-Franz law[27].

$$D = \frac{K}{C_V} = \frac{\sigma T}{C_V} \times 2.45 \times 10^{-8}\ \text{watt} \cdot \text{ohm/K}^2 \tag{4.2}$$

D is estimated to be approximately 50 cm^2/sec. Given the complexity of the metal-on-glass system, it is difficult to quantitatively relate D_e to the diffusivity of the film. One would expect the relatively low diffusivity of the substrate ($D \sim 3\text{cm}^2\ \text{sec}^{-1}$) to lower the effective

diffusivity measured by the correlation experiment, and the low value of D_e is perhaps not too surprising.

Correlation measurements were performed on type B samples using the same configuration as for type A samples. With d = 5mm, no convincing correlation was observed in any of several samples tested. With d = 1.3mm and a glass substrate, the correlation shown as solid circles in Fig. 8 was observed. The degree of correlation at low frequencies is less than that for type A samples. This smaller correlation and the lack of correlation for d = 5mm are consistent with the idea that type B samples are much closer to ideal 3-dimensional diffusive systems than type A: A fluctuation in the film in a type A sample tends to decay along the film, whereas in a type B sample, it has a much greater probability of decaying into the substrate, thereby reducing the correlation along the film. This result may be seen by comparing 1-D and 3-D correlation functions, Eqs. (2.28) and (2.30). The presence of $1/|\underset{\sim}{s}|$ in $C_T^{(3)}(\underset{\sim}{s}, \omega)$ indicates that the correlation between two regions is smaller in a 3-dimensional system than in a 1-dimensional system.

For both 1-dimensional and 3-dimensional systems, C(f) is expected to roll off when $\lambda(f) \sim d$. The value of D_e that we deduce, about 4 $cm^2 sec^{-1}$, is not siginificantly different from the value for type A samples.

D. Effect of Magnetic Field on Type A Samples

With a magnetic field H applied perpendicularly to the plane of the film, $S_V(f)$ and its dependence on β, T_c were investigated. In the inset of Fig. 9 T_c and β (measured at the mid-point of transition) are plotted

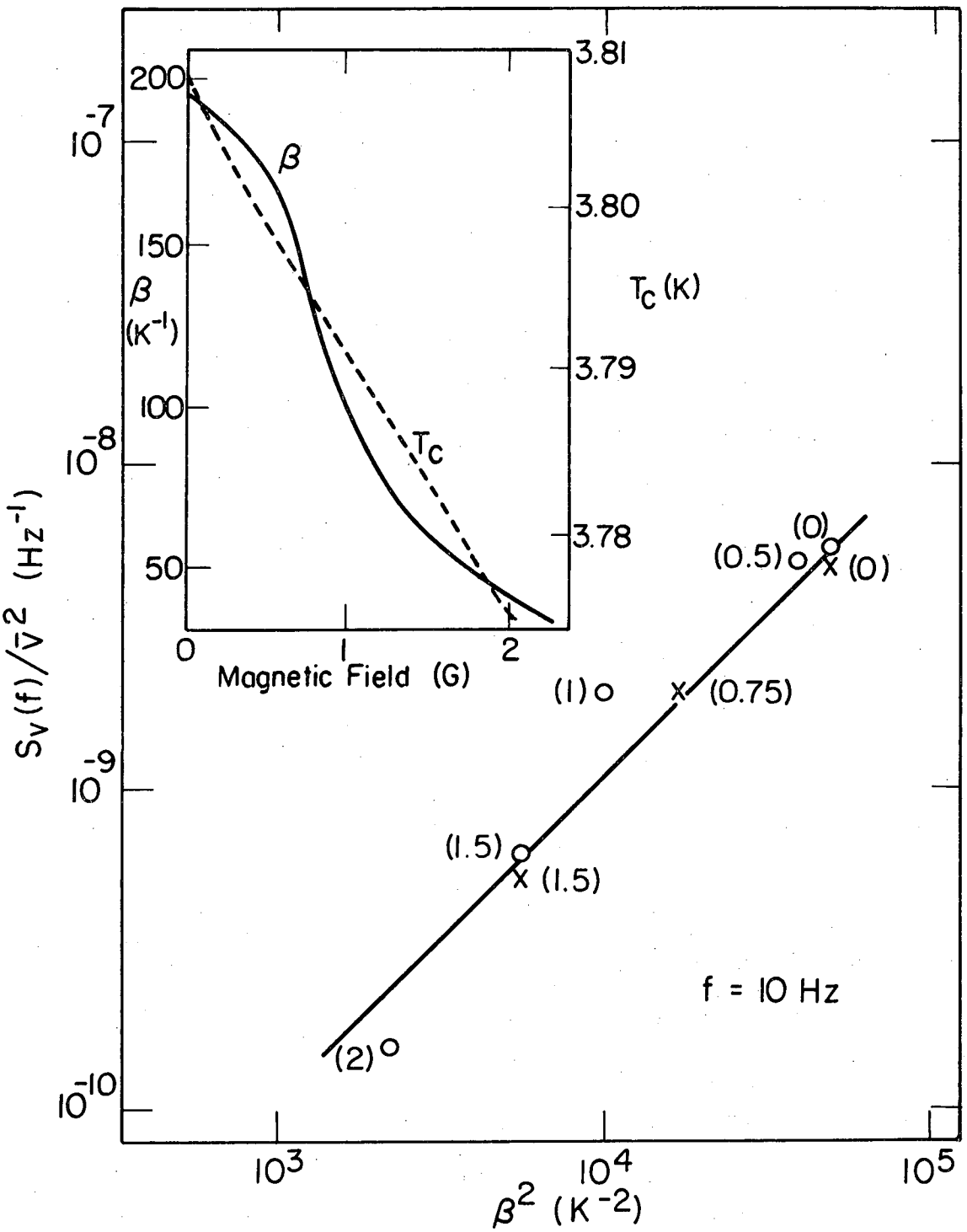

XBL 7511-7616

Fig. 9 $S_V(10)/\bar{V}^2$ vs. β^2 for Type A samples for several values of magnetic field (in parenthesis in G). Inset shows variation of β and T_c with magnetic field.

vs. H. A field of a few gauss was enough to reduce β by an order of magnitude. The noise power spectra were 1/f for all values of magnetic field investigated.

In Fig. 9 $S_V(10)/V^{-2}$ is plotted vs. β^2. Open circles and crosses are for bias current of 150 μA and 50 μA respectively. The value of magnetic field for each measurement is written in parenthesis. This value is determined by a Develco flux-gate magnetometer at room temperature, and is perhaps accurate within 20%. The points scatter about a fitted line of slope unity.

The general dependence of $S_V(f) \propto \beta(H)$ and that $S_V(f)$ decreases as H increases are strong pieces of evidence for believing that the 1/f noise originates from temperature fluctuation and not from flux flow mechanism (see Section V.A).

E. Experimental Results for Lead

A typical noise power spectrum for a type A lead film with a normal resistance of 4Ω and a dc current bias of 500μA is shown in Fig. 10(a). The slope of the spectrum is -1.1. The dashed line is calculated from Eq. (2.25) using $\Omega = 6.0 \times 10^{-9}$ cm^3, $\beta = 32K^{-1}$, and $C_V = 5.7 \times 10^{-2}$ JK^{-1} cm^{-3}.[26] At 1Hz the theoretical power spectrum exceeds the measured power spectrum by a factor of about 5. Samples evaporated on a sapphire substrate (with no underlay) had similar power spectra. $S_V(f)$ was again found to be proportional to $\overline{V}^2$ and $(dR/dT)^2$. The power spectrum of a sample whose volume was 9 times greater than that of Fig. 11(a) was approximately a factor of 10 smaller in magnitude, as expected if $S_V(f) \propto \Omega^{-1}$.

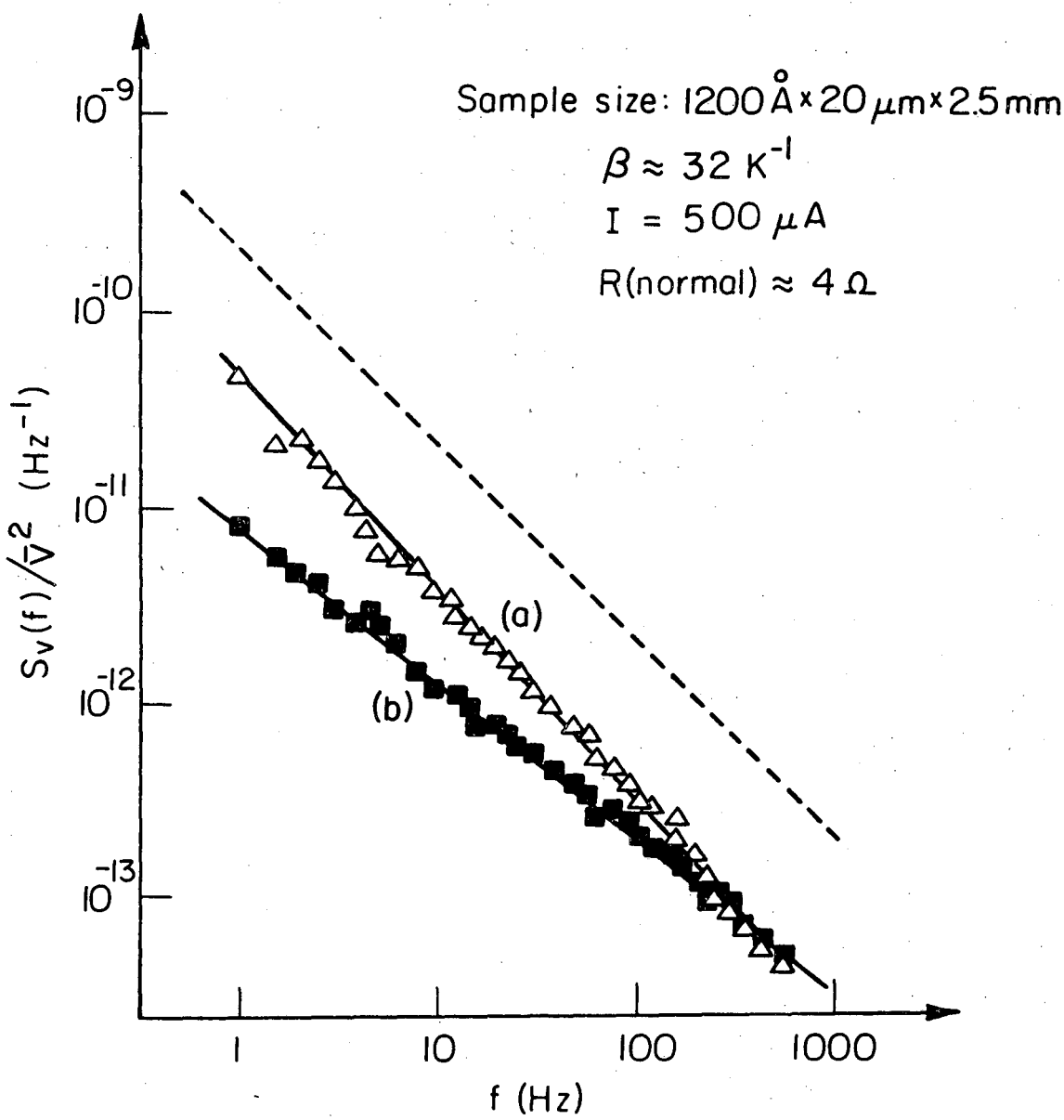

XBL7511-7615

Fig. 10 Typical noise power spectrum for lead films: (a) Type A on glass; (b) Type B on glass. Dashed line is calculated from Eq. (2.25)

A typical spectrum for a type B lead sample on a glass substrate is shown in Fig. 10(b). Similar results were obtained using a sapphire substrate. The slope is about -0.8, somewhat smaller than in Fig. 10(a). The spectrum is reminiscent of that obtained for the anomalous type B tin sample, Fig. 6(d). The fact that the flattening of the spectrum at low frequencies is much less dramatic than that usually observed for tin, suggests that the aluminum underlay has much less effect on the thermal contact for lead than for tin.

V. DISCUSSIONS AND CONCLUSIONS

A. Thermal Noise or Flux-Flow Noise?

I will show below that the low frequency noise observed is inconsistent with what may be expected from a flux-flow mechanism. The idea of flux-flow noise[6], qualitatively, is that when a magnetic field (or a high current) is applied to a superconductor, the superconductor is eventually driven into either a mixed state (type II) or intermediate state (type I). There will then be regions where the metal is locally normal and forms a "flux bundle". This flux, when driven by a current, generates an emf $\vec{E} = -\frac{1}{c}\vec{v} \times \vec{H}_2$. When voltage probes are placed along the superconductor strip, "flux bundles" cross the probes and will generate voltage pulses that average to $\overline{V}$. If the pulses were short and equal in magnitude, one has a voltage noise similar to shot noise in diodes, except the latter is a current noise while flux-flow noise exhibits itself as a voltage noise.

The flux bundles are usually not sharp and not equal. Various models were proposed[6] and noise power spectra calculated. The spectra are in general not 1/f-like and always have a flat region at low frequencies. We can make a calculation of the maximum flux-flow noise in our samples: according to Reference 6, the maximum noise (zero frequency noise) is $2\phi V_f$, where ϕ is the flux contained in each "bundle", and V_f is the voltage across the sample due to flux-flow. The maximum area of the bundle is ℓ_2^2(ℓ_2, the strip width, is typically 15μm), and the maximum ambient field, together with the self-field of the current, is 0.1 G. Thus $\phi \approx 2 \times 10^{-7}$ G - cm^2. Let us further suppose that the average

voltage across the film is entirely due to flux-flow: A maximum value for a typical sample would be 1mV. Thus an upper limit on the zero frequency noise power is $4 \times 10^{-18}\ V^2\ Hz^{-1}$, a value typically 5 orders of magnitude smaller than the observed noise at 1 Hz. In fact, for a sample biased at a voltage of half the normal state voltage, V_f is a very small portion of $\overline{V}$ (See Fig. 6 of Ref. 6). Thus the flux-flow noise is considerably less than our estimate of $4 \times 10^{-18}\ V^2\ Hz^{-1}$.

Furthermore, the observed noise decreases as the applied magnetic field is increased (Fig. 9), whereas for a constant bias voltage, the flux flow noise would increase. Finally, flux-flow noise is maximum when the film resistance is about 1/10 of the normal state resistance, while our observed noise is proportional to β^2, and is maximum at the mid-point of the transition.

It is thus concluded, the observed noise is quite inconsistent with that expected from flux-flow.

B. Conclusive Remarks

The experimental results presented in this thesis provide strong support for the thermal diffusion theory of 1/f noise. It has been shown that for tin films the noise voltage power spectrum $S_V(f)$ is proportional to $\overline{V}^2$, β^2, and Ω^{-1} as predicted by Eq. (2.25). In particular, $S_V(f)$ is inversely porportional to the film thickness, indicating that the noise is a bulk rather than a surface effect. The flattening of $S_V(f)$ at low frequencies when the film is in good thermal contact with the substrate strongly supports a thermal diffusion model.

The spatial correlation of the noise at low frequencies observed in both type A and type B samples provides further clear evidence for a thermal diffusion process. Finally, the prediction of the semi-empirical formula Eq. (2.25) is in excellent agreement with the measured magnitude of the noise. It is particularly noteworthy that although β^2T^2/C_V increases by about 9 orders of magnitude when a tin film is cooled from room temperature to the mid-point of its superconducting transition, Eq. (2.25) predicts the magnitude of the noise at each temperature to within a factor of 2 or 3.[1,2] In Fig. 11 we plot measured values of $S_V(10)$ for type A tin samples versus the values of $S_V(10)$ predicted by Eq. (2.25) for the measurements plotted in Figs. 7 and 9. Although there is considerable scatter of the data, there is a good fit to a line of slope unity over four decades.

The small amount of data collected on lead films also supports the thermal diffusion model. The correct dependences of $S_V(f)$ on $\overline{V}^2$, β^2, and Ω^{-1} were observed. The type A films have 1/f -like spectra that are within a factor of about 5 of the prediction of Eq. (2.25). However, it should be noted that had it been possible to obtain data at a somewhat higher frequency, the agreement between the experimental data and the semi-empirical model would have been improved. Clearly, if the observed slope $S_V(f)$ differs from -1, there will be good numerical agreement between the measured and calculated spectra only over a limited frequency range. (In the same way, the good fit to the theory obtained for the power spectra of the type A tin films may be regarded as somewhat fortuitous: The fit would have been poorer at a substantially higher

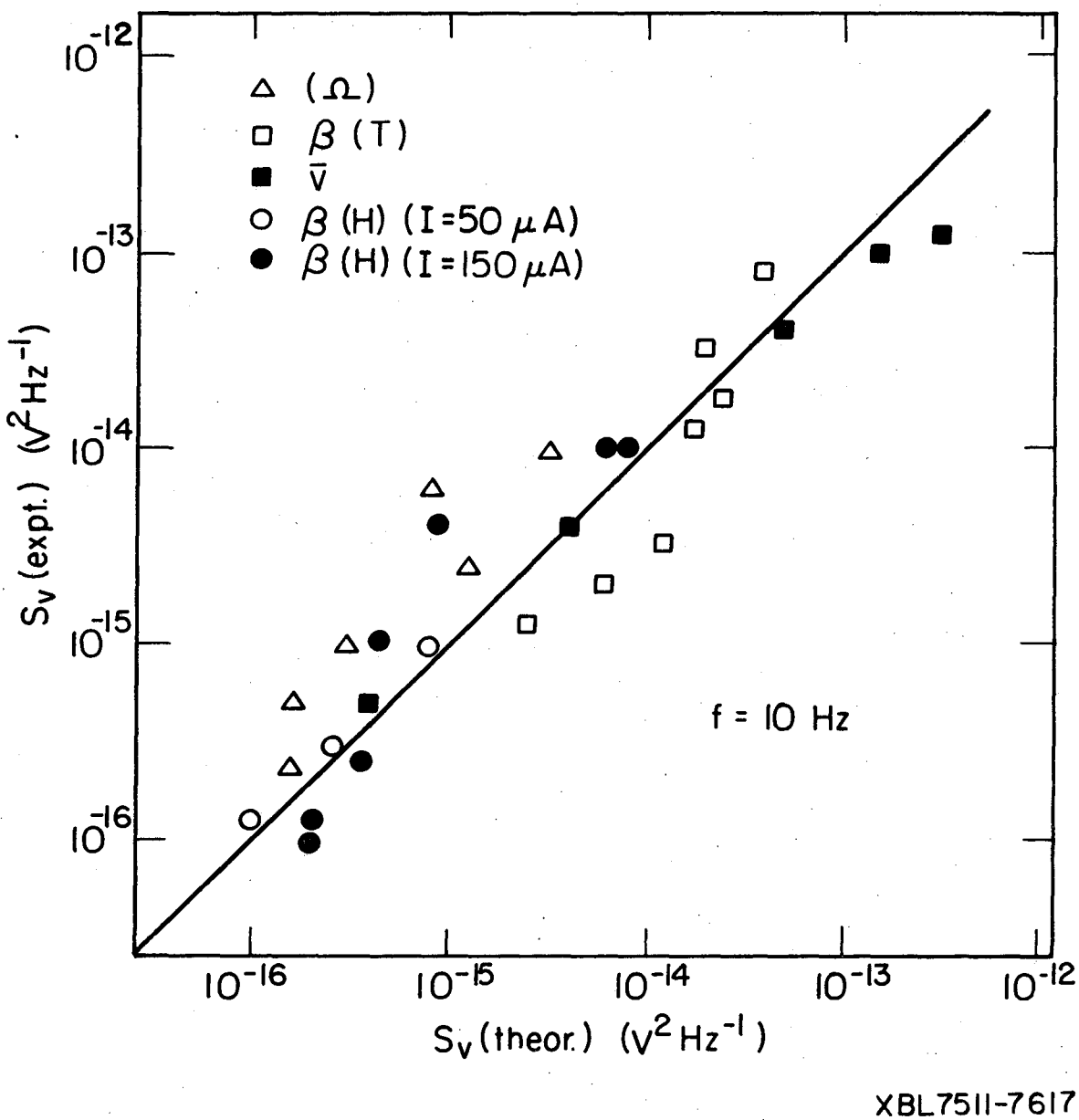

Fig. 11 Comparison of measured $S_V(10)$ from Figs. 6, 7 and 9 with $S_V(10)$ calculated from Eq. (2.25) for Type A tin samples.

or lower frequency.) For type B lead samples, the slope of $S_V(f)$ was reduced to about -0.8. Although this was a significantly lower slope than that of the type A samples (about -1.1), the changes was much less marked than for most of the tin samples, presumably because of the relatively small change in the thermal boundary resistance.

These results had immediate application in the noise considerations of devices utilizing superconductive thin films. The understanding of the role of the various parameters in determining the magnitude of the 1/f noise has made possible the construction of a superconducting bolometer[29] with unprecedented low noise equivalent power. The technique of constructing type B samples may also be of interest to experiments on non-equilibrium superconductivity where self-heating of the films is of concern.[28]

C. Boundary Conditions - Solution to the Mystery of 1/f?

The major remaining problem is the microscopic origin of the 1/f noise in type A samples. One would like to construct a model that specifically exhibits an extended region of 1/f noise. The thermal diffusion theory theory outlined in Sections II-A and II-B, which is applicable to uniform diffusive system, fails to produce such (Fig. 1). Voss and Clarke[1] proposed that if it was possible to have a generating term in Eq. (2.3) of such form

$$\langle g(\vec{r},t)\, g(\vec{r}\,',t\,')\rangle \propto \delta(\vec{r}-\vec{r}\,')\, \delta(t-t\,') \quad , \qquad (5.1)$$

which generates noise termed as "correlated noise" because

$$\langle T(\vec{r},t)\ T(\vec{r}',t)\rangle \ \propto 1/|\vec{r}-\vec{r}'|, \tag{5.2}$$

unlike the case of $g = \vec{\nabla} \cdot \vec{f}$, where

$$\langle T(\vec{r},t)\ T(\vec{r}',t')\rangle \ \propto \delta(\vec{r}-\vec{r}')\,\delta(t-t') \quad , \tag{5.3}$$

then, by carrying out similar calculations as in Section II.B, the noise spectrum is found to be 1/f - like in the region between f_1 and f_2. An example of this is shown in Fig. 12, where in various limits, $S_V(f)$ takes on the form

$$S_V(f) \propto \begin{cases} f^{-0.5} & f \ll f_1 \ , \\ f^{-1} & f_1 \ll f \ll f_2 \ , \\ f^{-1.5} & f_2 \ll f \ll f_2 \ , \\ f^{-2} & f_3 \ll f \quad . \end{cases} \tag{5.4}$$

As was discussed in Section II.A, generating terms such as (5.1) would violate conservation of energy in a <u>closed</u> system, because it represents local energy "source" and "sinks". However, is it possible that in the case of the experimental system of glass and metal films, the interface between the two may serve as such an energy pole? D. N. Langenberg[28] made an interesting suggestion that phonons may be "trapped"

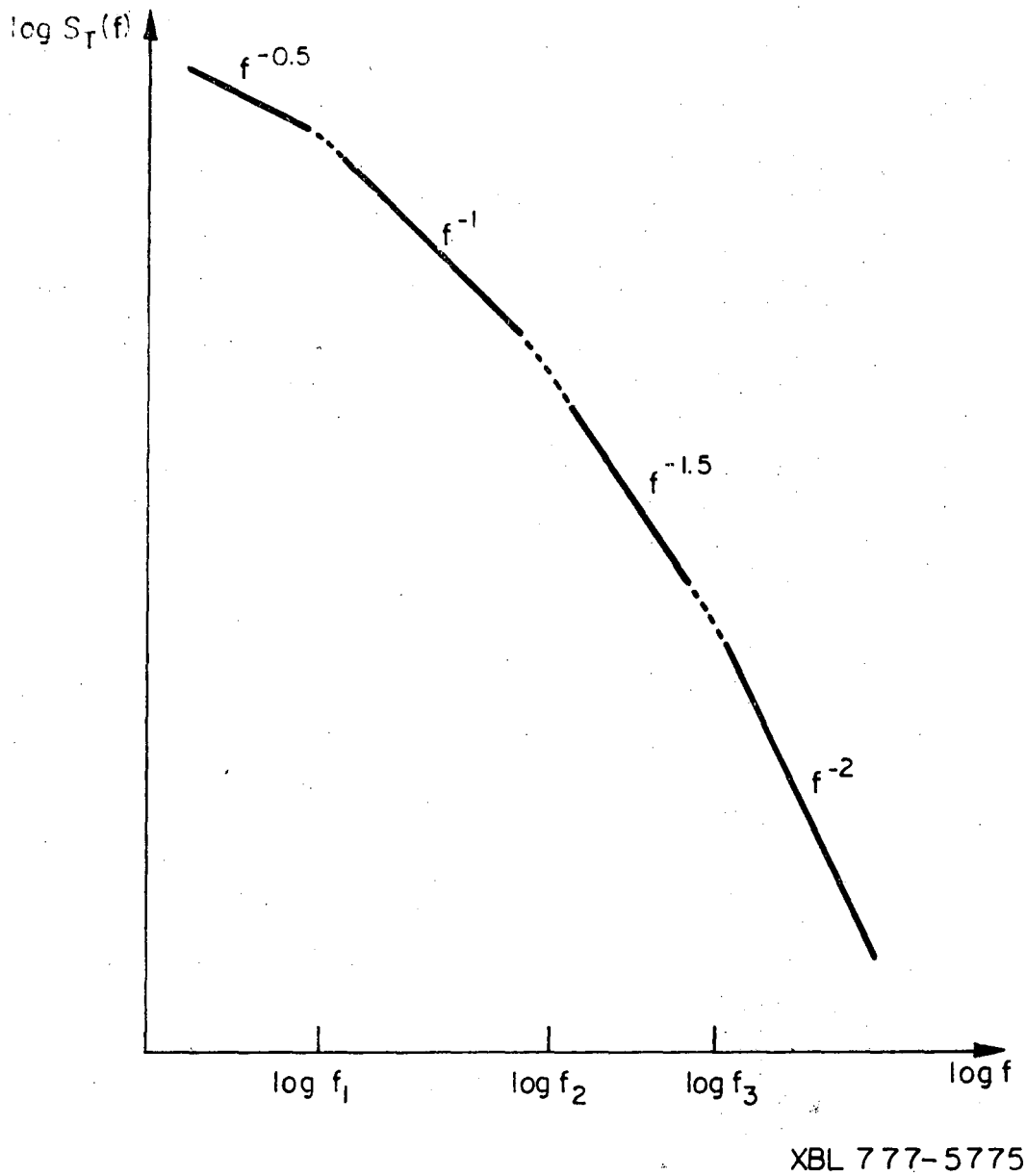

Fig. 12 Model noise spectrum for uncorrelated generation term in the diffusion equation.

at the boundary. Such a trap will release its energy randomly and provides a local large variation in temperature not governed by the Boltzmann factor in Eq. (2.16). In this case, generation terms like (5.1) are certainly a possibility. It is interesting to note that in our type B samples, such possible effect is greatly reduced. The aluminum oxide has a thickness of ~50Å, about the same as the phonon wavelength of tin at 4K. It may be that this oxide fills the "pockets" between film and glass where trapping mechanisms may exist.

S. H. Liu[30] recently proposed to use this idea as boundary conditions to supplement the calculation in Section II.B. His idea was to set boundary conditions in the z-direction (along the thickness ℓ_3 of the film and perpendicular to the substrate). They are

$$\frac{\partial}{\partial z} T \Big|_{z=\ell_3} = 0 \quad ,$$

and

$$K \frac{\partial}{\partial z} T \Big|_{z=0} = G(x,y,t) \quad . \tag{5.5}$$

The first boundary condition states that no heat can escape from the surface of the metal film. The second condition states that heat is randomly exchanged between the substrate and the metal film. Proceeding with these equations, he calculated the noise spectrum which exactly looks like Fig. 12 except the region $f \ll f_1$ is missing. It thus seems

that if (5.5) dominates the noise source, one would indeed get a 1/f noise explicitly. But this approach, which perhaps contains some elements that the simple theory for infinite, uniform medium cannot account for, does not describe the complete picture for the following reasons:

i) The effect of boundary resistance is conspicuously absent. In the limit of a perfect coupling between substrate and film, one expects to get back to the 3-dimensional diffusive system, i.e, the second equation of (5.5) should be lifted. It is not clear how this transittion would occur.

ii) The diffusion of heat inside the substrate is not considered.

This author believes that perhaps, in substitution of (5.5), one should use,

$$\frac{\partial}{\partial z} T \Big|_{z=\ell_3} = 0 \,,$$

$$\text{and} \qquad K \frac{\partial}{\partial z} T \Big|_{z=0} = \kappa (T - T_s) \Big|_{z=0} \tag{5.6}$$

In the second equation, T_s is the temperature of the substrate at the boundary, and κ is the boundary thermal conductance. In the weak coupling case, T and T_s can fluctuate independently in their respective medium, and (5.5) is perhaps justifiable. However, in the strong coupling case ($\kappa >> K/\ell_3$). T and T_s are not independent, and the system approaches closer to an ideal infinite system as κ gets larger.

How (5.6) would be applied to calculate the low frequency noise is not trivial. But a simple case can readily be calculated in the experiments of M. B. Ketchen[31]. He measured the noise in a suspended superconducting film. The geometry of his experiment is shown inset in Fig. 13. The tin film is clamped with two thick tabs at two ends, leaving a length of ℓ_0 in the middle. Lead was evaporated on the film except a middle region of length ℓ_1. For this system, the boundary conditions are

$$T\Big|_{x=0,\ \ell_0} = 0 \quad ,$$

$$\frac{\partial T}{\partial y}\Big|_{y=0,\ell_2} = 0 \quad , \tag{5.7}$$

and

$$\frac{\partial T}{\partial z}\Big|_{z=0,\ell_3} = 0 \quad .$$

Therefore in all three directions, the Fourier space of $\vec{k}$ take on quantized values:

$$k_i = \frac{n_i \pi}{\ell_i} \quad , \tag{5.8}$$

with ℓ_0 replacing ℓ_1 in the x direction and $n_i = 0,1,2,3....$ Only sine waves can exit in y and z direction and cosine waves in x direction, to satisfy (5.7). When substituted into Eq. (2.19), we obtain

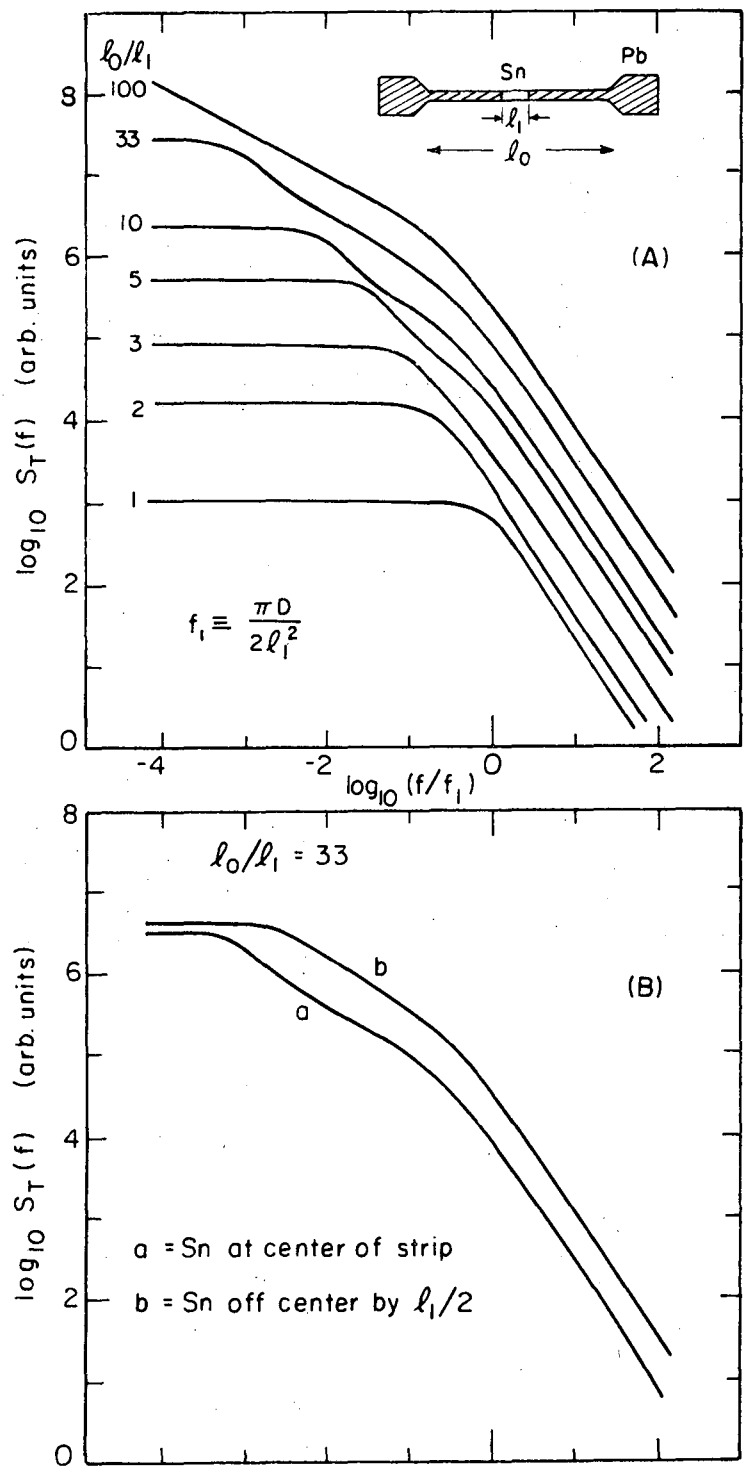

Fig. 13 1-D noise spectra. Inset in (A) is the experimental configuration.

$$S_T(\omega) \propto \sum_{n \text{ odd}} \frac{1}{\omega^2 + D^2 \frac{n\pi}{\ell o}^4} \left(\sin \frac{1}{2} \frac{n\pi}{\ell_o} \ell_1\right)^2 . \tag{5.9}$$

Where the k_y and k_z can only have value 0 because any other terms corresponding to nonzero n_y and n_z would integrate out to zero. Only odd n_x remains because $\sin \frac{n\pi}{\ell_o} x$ would also integrate to zero for even n's.

Equation (5.9) is calculated with the computer and plotted in Fig. 13(A) for several rations of ℓ_o/ℓ_1. The values of ℓ_o/ℓ_1 = 0, 1, 3, 5, 10 correspond to what M. B. Ketchen has used. The following features agree excellently with his experimental results:

i) The spectrum always becomes flat at frequencies lower than f_o.

ii) The slope of the spectrum between f_o and f_1 varies from -1.5 to -0.5 with increasing value of ℓ_o/ℓ_1.

iii) The change of spectrum slope near f_1 is not as obvious as the one near f_o.

iv) There is a slight wiggle in the spectrum above f_o. (This is especially conspicuous for ℓ_o/ℓ_1 = 10,33).

The last effect is due to the fact that we only took the odd n terms in (5.9). If the even terms are also taken into the iteration, the wiggle is smoothed out. Fig. 13(B) shows the spectra for ℓ_o/ℓ_1 = 33 with and without the even n terms. The case of even terms being also present corresponds to moving the central Sn region a distance $\ell_1/2$ away from the center of the film. It is also seen that the low frequency "knee" is shifted to a higher frequency. It would be interesting to experimentally verify this effect.

The next step is to do the calculation with (5.6) as boundary conditions. One needs to solve the two coupled equations for T and T_s for any general value of κ. There has yet been no concrete progress in this calculation.

It seems that using the boundary conditions has lead us a big step forward in the right direction. This author hopes one day, with clear understanding of the mysteries of the f and G and κ and T_s, the puzzle of 1/f noise will be totally unraveled. For the theorists who might be interested in this problem, the author suggests that he starts from the basics of how microscopically the electrons and phonons and their scattering would give rise to a macroscopic temperature fluctuation generating term g. This is perhaps the most important of all the unknowns in this problem.

PART II

RESISTANCE OF SUPERCONDUCTOR - NORMAL METAL - SUPERCONDUCTOR JUNCTIONS

VI. INTRODUCTION

The current-voltage characteristics of the superconductor-normal metal-superconductor sandwitch (SNS) have been investigated by many authors[39,52-54,64,65] because of the richness of the information one could obtain from such measurements. The critical current and the low temperature resistance of the SNS junction are directly related to the electron-phonon interaction strength of the normal metal,[52,63,64,65] from which the electron-phonon interaction parameter N(0)V, and hence the critical temperature T_c, of the normal metal can be deduced.

In the second part of this thesis, we concentrate on the problem of the SNS resistance at high temperatures (0.5 T_c to T_c). The increase in the SNS resistance near T_c above the resistance of the normal metal is attributed to a penetration of the normal electron current in the superconductor. The fraction of the bias current applied to a SNS junction that penetrates the SN interface as a normal current (instead of a supercurrent) increases as temperature is raised. The normal electron current travels dissipatively in the superconductor for an average length determined by the electron relaxation time, giving rise to the extra SNS resistance at higher temperatures.

In Chapter VII we present the theoretical calculation of the SN boundary problem. We will discuss the microscopic basis for the existence of an electric field in the superconductor and its relation to the normal electric current. A set of Boltzman equations will be used to calculate the behaviour of the quasiparticle distribution functions near the SN boundary. Instead of matching these distribution

functions directly at the boundary, we will use an approximation scheme in which the quasiparticles are assumed to be thermalized on both sides of the boundary. The normal electric currents on the two sides of the boundary are linked with the help of the Andreév transmission coefficient.[36]

In Chapter VIII we discuss the experimental procedures and apparatus. The experimental results are presented in Chapter IX. The conclusions and a comparison of the electron relaxation times obtained in this work and that obtained both theoretically and experimentally by other authors are included in Chapter X.

VII. THEORY

A. Excess of Quasiparticles and the Electric Field

In this section, I will present the microscopic basis for the problem of excess boundary resistance in a SN interface. The argument was originally proposed by Waldram.[32] What I intend to show is that an electric field can exist inside a superconductor when quasi-particles are not equally populated on the $k_>$ ($k > k_F$) and $k_<$ ($k < k_F$) branches of the excitation spectrum. This situation occurs when an electric current is passed through the SN interface.

In the original B.C.S. theory[33], the pairing assumption was used to obtain a reduced Hamiltonian for the electrons in a metal:

$$H = \sum_k 2\,\varepsilon_k\, b_k^{\dagger}\, b_k + \sum_{kk'} V_{k'k}\, b_{k'}^{\dagger}\, b_k \quad , \tag{7.1}$$

where ε_k is the energy of the electrons with momentum k when unperturbed by the electron-phonon interaction $V_{k'k}$ · $b_k^{\dagger}$ (b_k) is the pair creation (annihilation) operator and is related to the electron creation (annihilation) operators $C_{ks}^{\dagger}$ (C_{ks}) by $b_k^{\dagger} = C_{k\uparrow}^{\dagger}\, C_{-k\downarrow}^{\dagger}$ and $b_k = C_{k\uparrow}\, C_{-k\downarrow}$.

Assuming the ground state ψ_o at zero temperature is

$$|\psi_o\rangle = \prod_k \left(\sqrt{1 - V_{k2}} + V_k\, b_k^{\dagger}\right) |\mathrm{vac}\rangle \tag{7.2}$$

where v_k is treated as a variational parameter with the constraint that the total number of electrons must be kept constant

$$N_o = 2 \sum_k < \psi_o \mid b_k^\dagger b_k \mid \psi_o > \quad , \tag{7.3}$$

and the total energy is minimized, one gets

$$\delta < \psi_o \mid H - \mu N_o \mid \psi_o > = 0 \quad , \tag{7.4}$$

where μ, a variational parameter, is the chemical potential.

Equation (7.4) gives the familiar results

$$v_k^2 = \frac{1}{2} \left(1 - \frac{\varepsilon_k - \mu}{E_k}\right) \quad , \tag{7.5}$$

$$E_k = [(\varepsilon_k - \mu)^2 + \Delta_k^2]^{1/2} \quad , \tag{7.6}$$

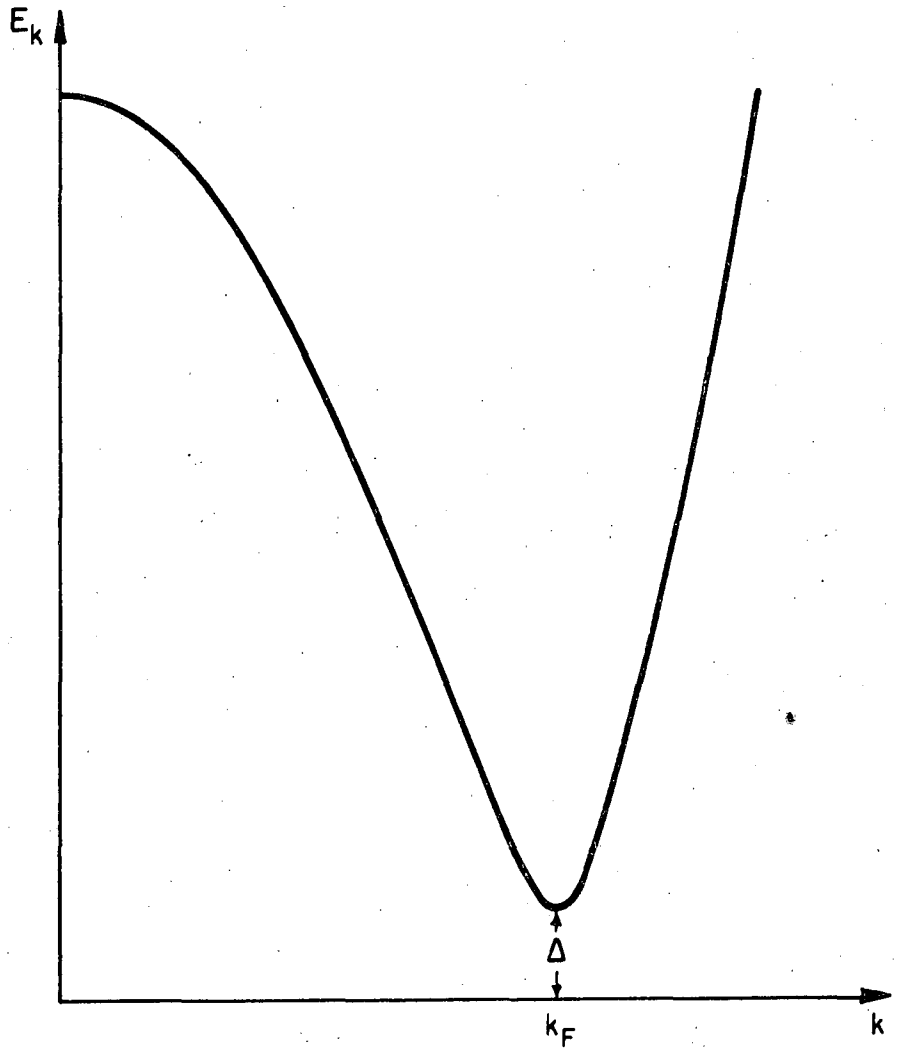

XBL777-5777

Fig. 14 Quasiparticle energy dispersion curve.

and Δ_k satisfies

$$\Delta_k = - \sum_{k'} V_{kk'} \frac{\Delta_{k'}}{2E_{k'}} \quad . \tag{7.7}$$

Together with (7.3), Δ and μ can both be obtained. E_k is interpreted as the excitation energy of the quasiparticles and has a dispersion relation shown in Fig. 14. The spectrum has two branches, $k_>$ $(k > k_F)$ and $k_<$ $(k < k_F)$ branches. For symmetric gap parameter, the two branches are closely symmetric near k_F. At finite temperature, the B.C.S. formulation is essentially the same, except that Eq. (7.3) should be replaced by

$$N_o = 2 \sum_k < \psi_o \mid b_k^\dagger b_k \mid \psi_o > (1 - f_k) + \sum_k f_k \tag{7.8}$$

to take into account the thermally excited quasiparticles. Here f_k is the quasiparticle distribution function.

In this formulation, the chemical potential μ, as in the case of normal metal, is just the Fermi energy ε_f for a system possessing electron-hole symmetry. When an electric potential, ϕ, is applied, μ is $\varepsilon_f - e\phi$.

We now inquire how the properties of superconductivity emerge and what happens when quasiparticles are not in thermal equilibrium.

Ginzburg and Landau[34] first proposed that the existence of an order parameter $\Psi(\vec{r})$ in the superconductor, which behaves like a single particle wave function, may explain the properties of superconductivity. The transport properties are, as in ordinary quantum mechanics, given by

$$\vec{J}_s = -\frac{e\hbar}{4mi}\left[\Psi^*\vec{\nabla}\Psi - \Psi\vec{\nabla}\Psi^*\right] - \frac{e^2}{m}\Psi\Psi^*\vec{A} \quad , \tag{7.9}$$

and

$$i\hbar\frac{\partial\Psi}{\partial t} = -2e\,\phi\,\Psi \quad , \tag{7.10}$$

which may be rewritten in terms of phase θ of Ψ as

$$-\Lambda\vec{J}_s = \frac{\hbar}{2e}\vec{\nabla}\theta + \vec{A} \quad , \tag{7.11}$$

and

$$\hbar\dot{\theta} = +2e\,\phi, \tag{7.12}$$

where $\Lambda \equiv m/|\Psi|^2 e^2$. With the B.C.S. theory, Ψ may be identified as the gap parameter $\Delta(\vec{r})$, which is defined by $\Delta(\vec{r}) = V < \psi(\vec{r})\ \psi(\vec{r})>$, where $\psi(\vec{r})$ is the spatial Fourier transform of the electron annihilation operator. From the reduced Hamiltonian in Eq. (7.1), we can calculate the equation of motion for $\Delta(\vec{r})$:

$$\frac{d\Delta}{dt} = \frac{i}{\hbar}\,[H,\ \Delta] \quad . \tag{7.13}$$

This leads to the B.C.S. result of

$$\frac{d\Delta}{dt} = -\ 2\ \frac{i\mu}{\hbar}\ \Delta \tag{7.14}$$

We would then expect (7.10) and (7.12) to be replaced by

$$i\hbar\ \frac{\partial\Psi}{\partial t} = 2\mu\Psi \quad , \tag{7.15}$$

and

$$\hbar\ \dot{\theta} = -\ 2\mu \quad . \tag{7.16}$$

If μ is not constant inside the superconductor, the gradient of the phase θ will change in time and establish a supercurrent pattern according to Eqs. (7.9) and (7.16) until μ is constant. If $\mu = \varepsilon_f - e\phi$, there can be no electric field (gradient of ϕ) inside a superconductor in a steady state. This is the origin of the name "superconductivity".

However, by inspecting Eq. (7.5), we see that μ is defined as the energy at which $v_k^2 = \frac{1}{2}$, or the energy at which the probability a paired state is occupied as $\frac{1}{2}$. Is there a situation where this energy is not just ε_f? To answer this, let us call this energy ε_c, the "central band energy" of the condensate and express μ in the presence of electric potential as $\mu = \varepsilon_c - e\phi$.

ε_c is determined by the normalization condition Eq. (7.8). For any general distributions f of quasiparticles, Eq. (7.8) also holds true. Writing the normalization in the integral form:

$$N_o = 2N(0) \int_0^\infty d\,\varepsilon_k\, v_k^2 \left(1-f\,(E_k)\right) + N(0) \int_0^\infty f\,(\varepsilon_k)\, d\,\varepsilon_k$$

$$= 2N(0) \int_0^\infty d\,\varepsilon_k\, v_k^2 + N(0) \int_0^\infty (1-2\,v_k^2)\, f\,(\varepsilon_k)\, d\,\varepsilon_k \qquad (7.17)$$

where N(0) is the density of state at the Fermi level. Choosing a convenient origins at ε_c, and defining $\varepsilon \equiv \varepsilon_k - \varepsilon_c$, one obtains from Eq. (7.17)

$$N_o = N(o) \int_{-\varepsilon_c}^{\infty} v_k^2 \, d\varepsilon + N(o) \int_{-\infty}^{\infty} (1 - 2v_k^2) \, f \, (E_k) \, d\varepsilon \quad , \tag{7.18}$$

where the lower integration limit in the second term is conveniently extended to $-\infty$. If $f\,(E_k)$ is symmetrical around $\varepsilon = 0$, then the second term in Eq. (7.18) is zero because $1 - 2\,v_k^2$ is an odd function of ε. We get $\varepsilon_c = \varepsilon_f$. An example for this case is if f(E) is the Fermi function $f_o(E)$.

Equation (7.18) may also be written as

$$N(o)\,(\varepsilon_c - \varepsilon_f) + N(o) \int_{-\infty}^{\infty} (1 - 2v_k^2) \left(f(E) - f_o(E)\right) \, d\varepsilon = 0.$$

or

$$\varepsilon_c = \varepsilon_f - \int_{-\infty}^{\infty} (1 - 2\,v_k^2) \left(f\,(E) - f_o\,(E)\right) \, d\,\varepsilon \equiv \varepsilon_f - Q^* \quad . \tag{7.19}$$

$f\,(E) - f_o(E)$ is the deviation of quasiparticle distribution from equilibrium value, and Q^* is a measurement of the asymmetry of f(E) about $\varepsilon = 0$. Q^* is positive if there is an excess of $k_>$ excitations over $k_<$ excitations. We now have $\mu = \varepsilon_c - e\phi = \varepsilon_f - Q^* - e\phi$. From a

previous argument, in a steady state, $\vec{\nabla}\mu = 0$ inside a superconductor and therefore

$$\vec{E} \equiv -e\,\vec{\nabla}\,\phi = -\vec{\nabla}\,\varepsilon_c = \vec{\nabla}\,Q^* \quad . \tag{7.20}$$

Equation (7.20) is of central importance in solving the SN problem. An example of non-zero Q* is the SN boundary biased with electric current. More details will be given in the next section, here it suffices to say that in this case, a normal electric current is driven into the superconductor, and this current, carried by the quasiparticles instead of by the condensate, is not equally carried by the two branches of excitations (while in normal metal, a current flow is characterized by a uniform displacement of the Fermi suface, and thus the $k_>$ excitations have the same number as the $k_<$ excitations). This normal current generates a Q* in S and a measurable electric potential difference which manifests itself as an excess boundary resistance.

Another closely related example is the SIN (superconductor-insulator-normal metal) junctions investigated by Clarke and Paterson[35]: When electrons are injected from N into S through the junction, non-zero Q* will be established in the superconductor. While both these examples require the flow of an electric current in the superconductor, a third example involves thermal current: If a superconductor has a temperature gradient, the thermal current, again carried by quasiparticles, also

supports a non-zero Q* even though no net charge is transported by the quasiparticles. This "thermo-electric effect" of superconductors will be further discussed in Chapter X as a possible future experiment.

B. Andreév Reflection

Before calculating the resistance of the SNS junctions, for convenience we first discuss how a quasiparticle responds when it hits the SN interface. Figure 15 shows the variation of the energy gap as a function of x at the SN boundary. Δ is zero deep in N, and approaches Δ_∞ deep in S. Near the boundary (x=0), there is an induced gap in N, and Δ in S is suppressed. Extensive effort has been devoted by theorists to calculate this "proximity effect" and how Δ should depend on x.[69]

Excitation spectra in both S and N are also shown in Fig. 15. Andreév[36] was the first person to consider the problem of what happens when an electron A in the normal metal propagates toward the boundary. His calculation showed that if electron A has energy smaller than Δ_∞, it will be reflected at the point where its energy is equal to Δ, and emerge on the opposite branch of the excitation spectrum as a "hole" B with the same energy as A in the normal metal. An electron pair will be injected into S and will proceed non-dissipatively. This process will not result in any additional electrical boundary resistance, although thermal current will be halted at the boundary, giving rise to an extra boundary thermal resistance.

An electron A' with energy greater than Δ_∞ will be "partially" reflected as a hole B'; instead of having an electron pair injected

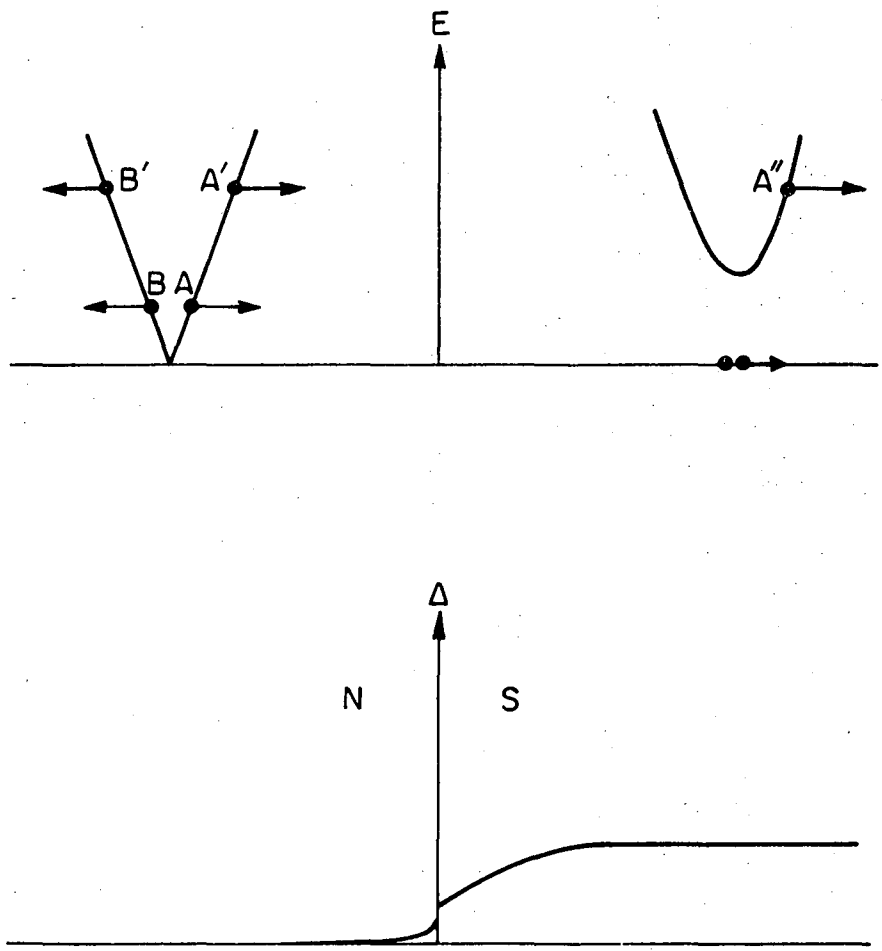

XBL 777-5778

Fig. 15 Andreév transmission and reflection for super- and sub-gap quasiparticles. Lower diagram shows the spatial variation of Δ.

into S, a normal electron A" will appear in S with the same energy as A'. The probability of A' converting into A" is defined as the transmission coefficient T(E).

We now see why there is a non-zero Q* in S near the boundary when an electric current is applied: In a normal metal, the current is equally carried by electrons ($k_>$ quasiparticles) and holes ($k_<$ quasiparticles). Deep in S, the current is carried exclusively by the condensate and there are no excess quasiparticles except those that are thermally excited. At the boundary, electrons are injected into S, but there is not a counter flow of holes to balance out the electrons. A Q* is thus established and the electric field will appear inside the superconductor. The time Q* takes to relax determines how deep the excessive quasiparticles will travel in S, which in turn determines the magnitude of the electric potential (and thereby, the boundary resistance) one measures.

Andreév calculated T(E) for a step gap potential, i.e., $\Delta = 0$ in N, and $\Delta = \Delta_\infty$ in S. His result[36] is

$$T(E) = \begin{cases} 2 \dfrac{(E^2-\Delta_\infty{}^2)^{1/2}}{E + (E^2-\Delta_\infty{}^2)^{1/2}} & \text{for } E > \Delta_\infty \\ 0 & \text{for } E < \Delta_\infty \end{cases} \tag{7.21}$$

The exact form of T(E) for a realistic distribution of Δ is quite difficult to calculate. Bar Sagi[37] has recently calculated T(E) for $\Delta = 0$ in N and $\Delta = \frac{1}{2}\Delta_\infty [1 + \tanh (x/\xi)]$ in S, where $\xi = \hbar v_f/\pi\Delta_\infty$ is the coherence length in S. The discontinuity of Δ at $x = 0$ is $\Delta_\infty/2$. He found that although T(E) is more strongly dependent on E, it is not very different from the Andreév results, Eq. (7.21). One can understand why this is the case by considering a problem generated by the Schrödinger equation: Suppose an electron with energy E and momentum k sees a potential barrier $\Delta(x)$ with three different forms;

$$\Delta_1 = \frac{\Delta_\infty}{1 + e^{-x/\xi}} \quad ,$$

$$\Delta_2 = \begin{cases} 0 & (x < 0) \\ \Delta_\infty & (x > 0) \end{cases} , \tag{7.22}$$

abd

$$\Delta_3 = \begin{cases} 0 & (x < 0) \\ \dfrac{\Delta_\infty}{1+e^{-x/\xi}} & (x > 0) \end{cases} ,$$

These three Δ's are shown inset in Fig. 16. One can calculate the transmission coefficient T(E) for each case. The first two cases can be found solved in textbooks.[38] The third case was solved by this author with some tedious algebraic effort:

$$T_1(E) = 1 - \frac{\sinh^2 \left\{ [(E/\Delta_\infty)^{1/2} - (E/\Delta_\infty - 1)^{1/2}] \, \pi/c \right\}}{\sinh^2 \left\{ [(E/\Delta_\infty)^{1/2} + (E/\Delta_\infty - 1)^{1/2}] \, \pi/c \right\}} ,$$

$$T_2(E) = \frac{4 \, [(E/\Delta_\infty) - 1]^{1/2} \, (E/\Delta_\infty)^{1/2}}{\left\{ (E/\Delta_\infty)^{1/2} + [(E/\Delta_\infty) - 1]^{1/2} \right\}^2} ,$$

$$T_3(E) = 1 - \frac{[1-(1-\Delta_\infty/E)^{1/2}] \, [C^2\Delta_\infty/E + 4(1-\Delta_\infty/E)] + [1-(1-\Delta_\infty/E)^{1/2}] \, [(1-\Delta_\infty/E)^{1/2} \, (\Delta_\infty/E)] + \Delta_\infty/E}{[1+(1-\Delta_\infty/E)^{1/2}] \, [C^2\Delta_\infty/E + 4(1-\Delta_\infty/E)] + [1+(1-\Delta_\infty/E)^{1/2}] \, [(1-\Delta_\infty/E)^{1/2} \, (\Delta_\infty/E)] + \Delta_\infty/E}$$

These three functions are plotted in Fig. 16, using the value of $C \equiv \hbar/\xi \, (2m\Delta_\infty)^{1/2} = 0.034$, which is suitable for Pb at low temperatures. We see that T_2 and T_3 are nearly the same, but T_1 is almost a step function across $E/\Delta_\infty = 1$. $T_1(E)$ is just the typical WKB result: For a potential barrier that is adequately smoothed out, the penetration probability of an electron is nearly unity if the electron energy is just higher than the maximum potential.

The Andreév equations for quasiparticles are just a pair of electron-hole equations similar to the Schrödinger equation. Therefore, Bar Sagi's results are not surprising. Since at a realistic SN boundary, $\Delta(x)$ is perhaps very close to $\Delta_3(x)$ or the Bar Sagi's $\Delta(x)$, the transmission coefficient of quasiparticles would then be very close to

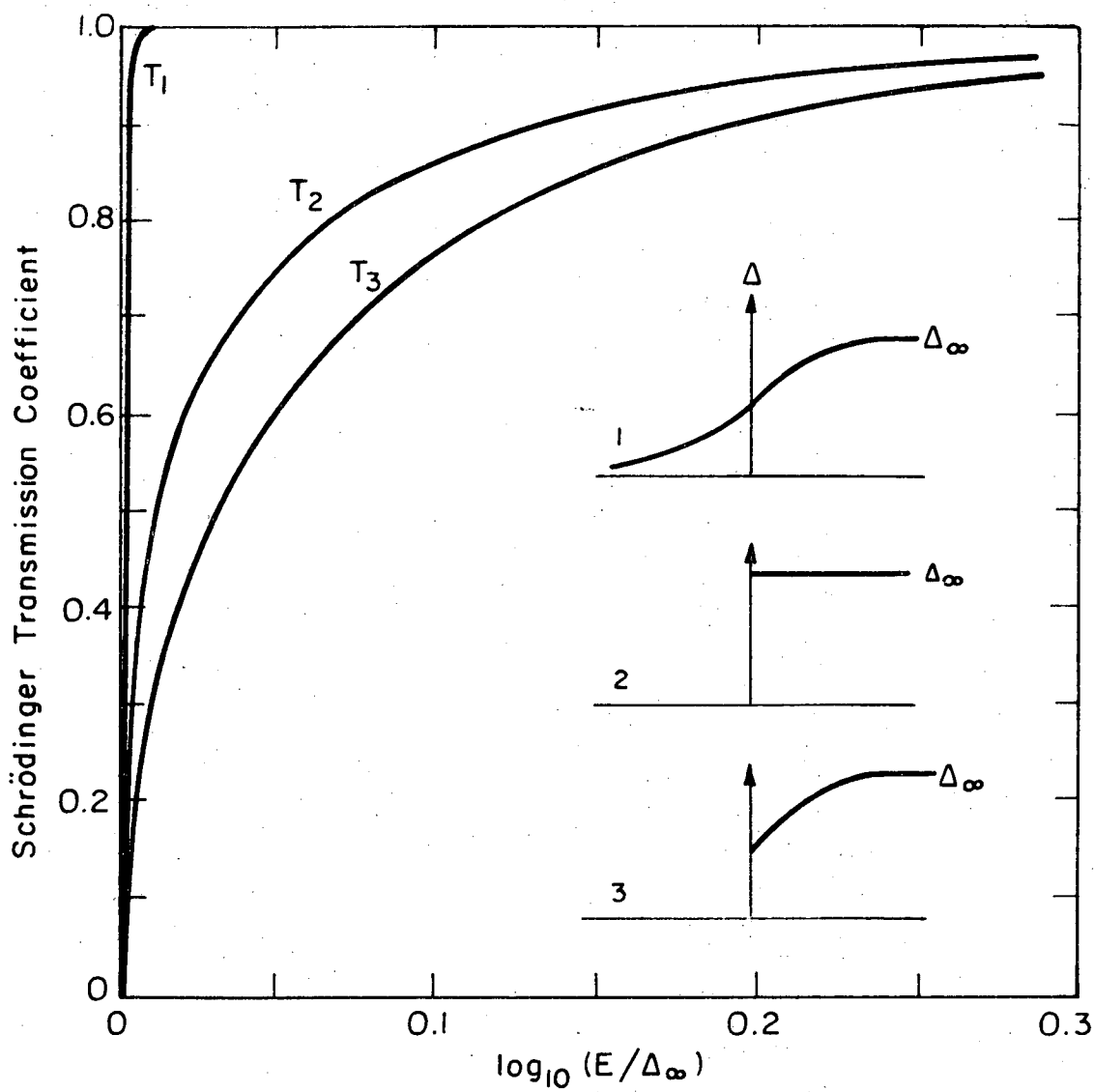

XBL 777-5779

Fig. 16 Schrödinger transmission coefficient for three potential barriers shown in the inset.

Andreév's result, Eq. (7.21). We will then use the latter for our subsequent calculations.

C. Transport Properties of Quasiparticles at the SN Boundary and the Resistance of SNS Junctions

The boundary resistance problem was first attacked by Pippard, Shepherd and Tindall[39] and later by Waldram[32]. Their method is to use the Boltzman equation for the normal excitations near the SN boundary. The decay of the normal excitations was calculated to give the boundary resistance. However, the first authors assumed that there is no electric field in the superconductor, and that the excessive boundary resistance manifests itself as a potential discontinuity at the boundary. They did not distinguish the various processes by which the quasiparticles relax. Waldram brought out the essential physics of the problem, but his approach may also be criticized for its failure to adopt the correct equations, and its incorrect treatment of the quasiparticle distribution functions. In this section, I will reformulate the problem. The final results will be used in comparison with experimental data in later sections.

Let us start by considering a one-dimensional case of four branches of the excitation spectrum in S, shown in Fig. 17. Branches 1 and 4 are "electron" branches, 2 and 3 are "hole" branches. (The use of "electrons" and "holes" are for convenience in terminology, since quasiparticles have charges of expectation value $e(1 - 2\, v_k^2)$, which is negative — "electron - like" — when $k > k_f$, and positive — "hole - like" — when $k < k_f$). The directions of motion for the quasiparticles are also shown in Fig. 17. The departure from equilibrium for a particular

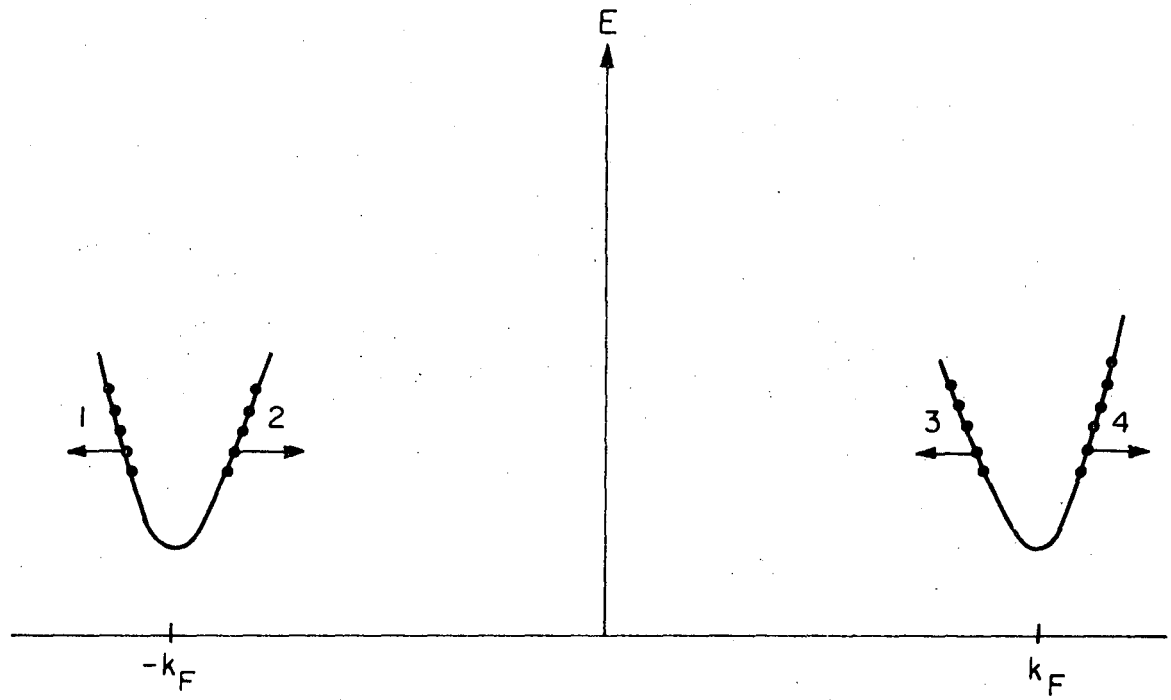

XBL 777-5780

Fig. 17 Quasiparticle branches and propagation direction on the 1-dimensional Fermi surface.

excitation energy E is now characterized by four functions, g_1, g_2, g_3, g_4. To set up the Boltzman equations, a convenient energy origin at μ will be used. μ is constant in S even in the presence of an electric field, and consequently, a quasiparticle moving through the system will stay at a constant energy E, measured with respect to μ. Similarly in N, we choose the energy origin at $\varepsilon_f - e\phi$. This choice of origin will eliminate the field dependent term in the Boltzman equations and fix the Fermi factor for the quasiparticle distributions. Also with this frame, the normal metal resistance is set aside, and only the boundary resistance will be calculated.

The Boltzman equation is

$$\frac{dg}{dt} = \left(\frac{\partial g}{\partial t}\right)_{\text{coll.}} \tag{7.24}$$

When expanded, the equations for branches 1 and 2 are

$$-v_s \frac{\partial g_1}{\partial x} = -\frac{g_1 - 1/2\,(g_1+g_4)}{\tau_1} - \frac{g_1 - g_{1Q}}{\tau_2} - \frac{g_1 - 1/2(g_{1Q} + g_{2Q})}{\tau_3} - \frac{g_1}{\tau_4} ,$$

$$v_s \frac{\partial g_2}{\partial x} = -\frac{g_2 - 1/2\,(g_2+g_3)}{\tau_1} - \frac{g_2 - g_{2Q}}{\tau_2} - \frac{g_2 - 1/2\,(g_{1Q} + g_{2Q})}{\tau_3} - \frac{g_2}{\tau_4} .$$

Each of these terms will be discussed below:

(1) The left hand side contains only one term, with $v_s = v_f|\varepsilon|/E$, the group velocity of the quasiparticle at energy E. The time-dependent term is zero because we are considering a steady state equation. The electric field term ($v_f\ \partial f/\partial E\ \partial\phi/\partial x$) does not appear because of our choice of origin for E.

(2) The first term on the right hand side of the equations is the elastic collision term. In a one-dimensional problem, elastic collisions will only mix branches 1 and 4, g_1 will consequently relax to $1/2(g_1 + g_4)$. In the "relaxation approximation", the collision integral is written as the form shown in Eq. (2.25). Branch 1 will not mix with branches 2 and 3 because the coherence factor for a quasiparticle to change state $u_k\ u_k' - v_k v_k'$ (where $u_k \equiv \sqrt{1 - v_k^2}$) is zero for $1 \rightarrow 2$ or $1 \rightarrow 3$ scattering unless the scattering is inelastic or if there is a gap anisotropy. In these cases, g_1 will "branch-cross". The branch-crossing relaxation is included below.

(3) The other three terms all contain inelastic scattering processes, i.e., electron-phonon scattering. Section 7E will deal with the calculation of each time in these terms: their magnitudes and dependences on temperature. Among them, τ_2 is the "thermalization" time. The process involved is the scattering that changes the energy, but not the "character" of the quasiparticles. This process redistributes the quasiparticles on each branch so that they are "thermalized". g_1 will then relax to its thermalized value g_{1Q}. g_1 and g_{1Q} satisfy quasiparticle conservation:

$$\int_{\Delta}^{\infty} g_1 \, N(E) \, dE = \int_{\Delta}^{\infty} g_{1Q} \, N(E) \, dE \quad , \tag{7.26}$$

where N(E) is the density of states.

(4) τ_3 is the "branch-crossing" relaxation time. This process converts an electron to a hole and vice versa. For superconductors without gap anisotropy only inelastic processes can participate. The τ_3 processes will thus relax the two branches to equal population and thermalization: g_1 will be relaxed to 1/2 $(g_{1Q} + g_{2Q})$ with this process. The possibility of elastic scattering mixing the branches when gap anisotropy is present will be discussed in Section VII.E.

(5) The last term is the "recombination" relaxation. The quasi-particles can recombine into the condensate to eliminate the excess quasi-particles and g_1 will relax to zero with the process. τ_2, τ_3 and τ_4 all derive from electron-phonon scattering, and have roughly the same order of magnitude at some intermediate temperature. However, all inelastic processes involve emission of phonons. The phonons will travel through the superconductor before escaping the system. They will generate quasiparticles from the condensate while travelling and repopulate the branches to effectively increase the relaxation of quasi-particles. The repopulation will equally occur on the two branches and enhances τ_4, while not effecting τ_3. If the enhancement is large, we can ignore the terms in Eq. (7.25) involving τ_4 in favor of those involving τ_3.

In the normal metal, Eq. (7.25) still holds, with v_s replaced by v_f and $\tau_3 = \tau_4 = \infty$. In both S and N, two similar equations can be set up for the 3- and 4- branches. Since these two branches contribute to the electric field in a similar way to the 1- and 2- branches, ("electron" excess on the k_f branches will suppress ε_c from ε_f the same way "electron" excess on the $-k_f$ branches), and, as we will see later, they contribute in an opposite sense to the electric current as the 1- and 2- branches ["electron" excess on the k_f branches carry current $-(g_3 + g_4)$, but "electron" excess on the $-k_F$ branches carry current $(g_1 + g_2)$], I will use a convenient symmetry relation $g_1 = - g_3$ and $g_2 = -g_4$ to eliminate two of the four equations. Physically, this symmetry satisfies the requirement that ε_c is suppressed uniformly on the Fermi surface, through the relation $g_1 - g_2 = g_4 - g_3$. It also divides the current flow evenly on the k_F and $-k_F$ branches, because $g_1 + g_2 = -(g_4 + g_3)$. The second property is not necessarily a real case, but the solution of the four equations without the symmetry relations will yield the same results as we will obtain below. These symmetry relations simplify the mathematics considerably.

Adding and subtracting the two parts of Eq. (7.25), and defining $\underline{q} = g_1 - g_2$, $j = g_1 + g_2$, we get

$$\nu \frac{\partial \underline{q}}{\partial x} = \frac{j}{\ell} + \frac{j - j_Q}{\ell_2} + \frac{j - j_Q}{\ell_3} + \frac{j}{\ell_4} \quad , \tag{7.27}$$

and

$$\nu \frac{\partial \dot{q}}{\partial x} = \frac{q - q_Q}{\ell_2} + \frac{q}{\ell_3} + \frac{q}{\ell_4} \quad . \tag{7.28}$$

where ℓ, the mean free path of a quasiparticle at energy E is approximately $\ell_1 = v_f \tau_1$, in our experiments, because τ_1 is much shorter than any other time. ν is defined as $|\varepsilon|/E$ and $\ell_i \equiv v_f \tau_i$. Multiplying the equations with $E/|\varepsilon|$ and integrating over energy, we get

$$\frac{dQ^*}{dx} = J \frac{1}{\ell} \quad , \tag{7.29}$$

$$\frac{dJ^*}{dx} = Q \left(\frac{1}{\ell_3} + \frac{1}{\ell_4}\right) , \tag{7.30}$$

where

$$Q^* \equiv \int_\Delta^\infty q \, dE \quad ,$$

$$Q^* \equiv \int_\Delta^\infty q \frac{E}{|\varepsilon|} \, dE = \int_\Delta^\infty q_Q \frac{E}{|\varepsilon|} \, dE \quad , \tag{7.31}$$

$$J^* \equiv \int_{\Delta}^{\infty} j \, dE, \qquad \text{cont'd (7.31)}$$

$$\text{and} \quad J \equiv \int_{\Delta}^{\infty} j \frac{E}{|\varepsilon|} \, dE = \int_{\Delta}^{\infty} j_Q \frac{E}{|\varepsilon|} \, dE \quad .$$

Before discussing the physical meaning and solving Eqs. (7.29) and (7.30), we note that they are not obtained without approximations. Indeed, we have used average values of τ_3 and τ_4 in these equations. We have set

$$\frac{1}{\ell_3} \equiv \frac{\int_{\Delta}^{\infty} \frac{1}{v_f \tau_3} q_Q \frac{E}{|\varepsilon|} \, dE}{\int_{\Delta}^{\infty} q_Q \frac{E}{|\varepsilon|} \, dE} \quad , \qquad (7.32)$$

and it was assumed that

$$\frac{\int_{\Delta}^{\infty} \frac{1}{v_f \tau_3} q \frac{E}{|\varepsilon|} \, dE}{\int_{\Delta}^{\infty} q \frac{E}{|\varepsilon|} \, dE} = \frac{1}{\ell_3} \quad , \qquad (7.33)$$

and similarly for ℓ_4. If τ_3 is independent of energy, Eqs. (7.32) and (7.33) follow directly from Eq. (7.26). In general, τ_3 is a strong function of E, and Eq. (7.33) does not necessarily hold.

In fact, Eq. (7.33) is only a good approximation near T_c. At any general value of temperature, Eq. (7.33) holds only at a distance away from the interface. Let us keep this in mind and proceed with the calculations, using Eqs. (7.32) and (7.33) as the approximate equations. We will discuss in more details the validity of this approximation in the later part of this section.

Within this scheme of approximation, we can see that Eq. (7.29) is just the equivalent of Ohm's law: Q*, as discussed in the previous sections, is equivalent to the electric potential. One calculates the normal electric current by multiplying the momentum of the quasiparticles, $m\, v_f$, by the density of states $N(0)\, E/|\varepsilon|$. Adding contributions from the two branches, we obtain the total electric current:

$$J_{qp} = eN(0)\, v_f \int_{\Delta}^{\infty} \frac{E}{|\varepsilon|} g_1\, dE + e\, N(0)\, v_f \int^{\infty} \frac{E}{|\varepsilon|}\, g_2 d\, E$$

$$= eN(0)\, v_f \int_{\Delta}^{\infty} \frac{E}{|\varepsilon|} (g_1 + g_2) dE = e\, N(0)\, v_f \int_{\Delta}^{\infty} \frac{E}{|\varepsilon|}\, j\, dE \qquad (7.34)$$

$$= eN(0)\, v_f\, J \quad .$$

Since the electrical conductivity σ is proportional to ℓ, the mean free path of the electrons, Eq. (7.29) is equivalent to Ohm's law

$$\vec{J} = \sigma \vec{E} \quad . \tag{7.35}$$

Equations (7.29) and (7.30) can be solved if one can write

$$\frac{Q}{Q^*} = \frac{J}{J^*} = \alpha^{-1} , \tag{7.36}$$

where α is a proportionality constant. When the quasiparticles are thermalized, α can be calculated as follows: At thermalization

$$q = q_Q = -Q^* \, f_o'(E)/f_o(\Delta) \qquad (f_o'(E) = d\, f_o(E)/dE),$$

$$j = j_Q = -J^* \, f_o'(E)/f_o(\Delta) \quad . \tag{7.37}$$

(These equalities were derived by Tinkham[40] with the assumption that the two excitation branches are in thermal equilibrium with each other but

are not in chemical equilibrium, i.e., they are characterized by different chemical potentials $\mu_>$ and $\mu_<$. In fact, Eq. (7.37) can be derived no matter what parameters specify the equilibrium situation of the quasiparticles: either their chemical potential or their effective temperature, as long as the deviation from thermal equilibrium f_0 is small. The proof is trivial and omitted here.) α can be expressed as:

$$\alpha^{-1} = \frac{\int_\Delta^\infty f_0' \ (E) \ (E/|\varepsilon|)dE}{\int_\Delta^\infty f_0' \ (E) \ dE} = - \left(1/f \ (\Delta)\right) \int_\Delta^\infty f_0' \ (E) \ \ E/|\varepsilon| dE \qquad (7.38)$$

In general, however, Eqs. (7.37) are not true when q and j are not thermalized. Immediately after the quasiparticles enter the superconductor, they are not thermalized, and α is spatially dependent. The temperature and spatial range in which Eq. (2.38) can be considered a good approximation will turn out to be the same range in which Eqs. (7.29) and (7.30) are applicable (i.e. Eq. (7.33) is a good approximation). We will see later why this is the case. For the moment, we will use these approximations and examine the solutions for Q* and J*.

The solutions are quite simple when we couple Eqs. (7.29) and (7.30) together to get a differential equation for Q*:

$$\frac{d^2Q^*}{d\chi^2} = \alpha^{-2} \frac{1}{\ell} \left(\frac{1}{\ell_3} + \frac{1}{\ell_4} \right) Q^*. \qquad (7.39)$$

Inside N, the right-hand side is zero, and we get

$$Q_N^* (x) = Q_N^* (0) + J_o \frac{1}{\ell} x \quad . \tag{7.40}$$

J_o is just the applied current. This solution may seem strange at first sight, because it says that Q* will increase (or decrease) linearly into N as a function of x. This is due to our choice of origin. We have chosen $\varepsilon_f - e\phi$ as the energy origin for the quasiparticles, and Eq. (7.39) simply means that the electric potential is a linear function of x in N.

Inside S, the solution of Eq. (7.38) is

$$Q_S^* (x) = Q_S^* (0) \exp (- \frac{x}{\lambda}) \quad , \tag{7.41}$$

where

$$\lambda = \alpha \left(\frac{1}{\ell} \left(\frac{1}{\ell_3} + \frac{1}{\ell_4} \right) \right)^{-1/2} \tag{7.42}$$

The complete solution for a SN boundary under Andreév transmission is shown in Fig. 18. Q^* is continuous across the boundary. (The reason for Q^* to be continuous will emerge when we discuss the boundary conditions later). The change in slope of Q^* at $x = 0$ occurs because not all the incident current from N is transmitted into S as normal current. The fraction that does is zero at low temperatures (Curve A in Fig. 18) and becomes unity near T_c (Curve C in Fig. 18). The value of $Q^*(0)$ is the excess boundary potential that one measures. The physical meaning of $Q^*(0)$ can be seen through its relation with $J_s(0)$: At $x = 0$, $J_s(0) = \ell(dQ^*/dx) - Q^*(0)\,\ell/\lambda$. We can define a fractional parameter F in Fig. 18, which is equal to the $dQ^*/dx|_{x=0^+} \Big/ dQ^*/dx|_{x=0^-}$. We then have $J_s(0) = F\,J_N(0)$. Since $J_N(0) = J_o$, the applied current, we can express $Q^*(0)$ as

$$Q^*(0) = -F\,J_o\,\lambda/\ell \quad , \tag{7.43}$$

The excess boundary resistance is proportional to $F\,\lambda/\ell$. Since $1/\ell$ is proportional to the resistivity of the superconductor in the normal state, the boundary resistance resulting from $Q^*(0)$ is equivalent to that obtained if a fraction F of the incident current enters the superconductor and proceeds dissipatively for a distance λ.

The above calculations are based on the assumption that Eqs. (7.29), (7.30), (7.33) and (7.39) are valid. The simple formulas we derived will turn out to agree satisfactorily with experimental results, and they certainly can be understood physically. One would like to do the whole

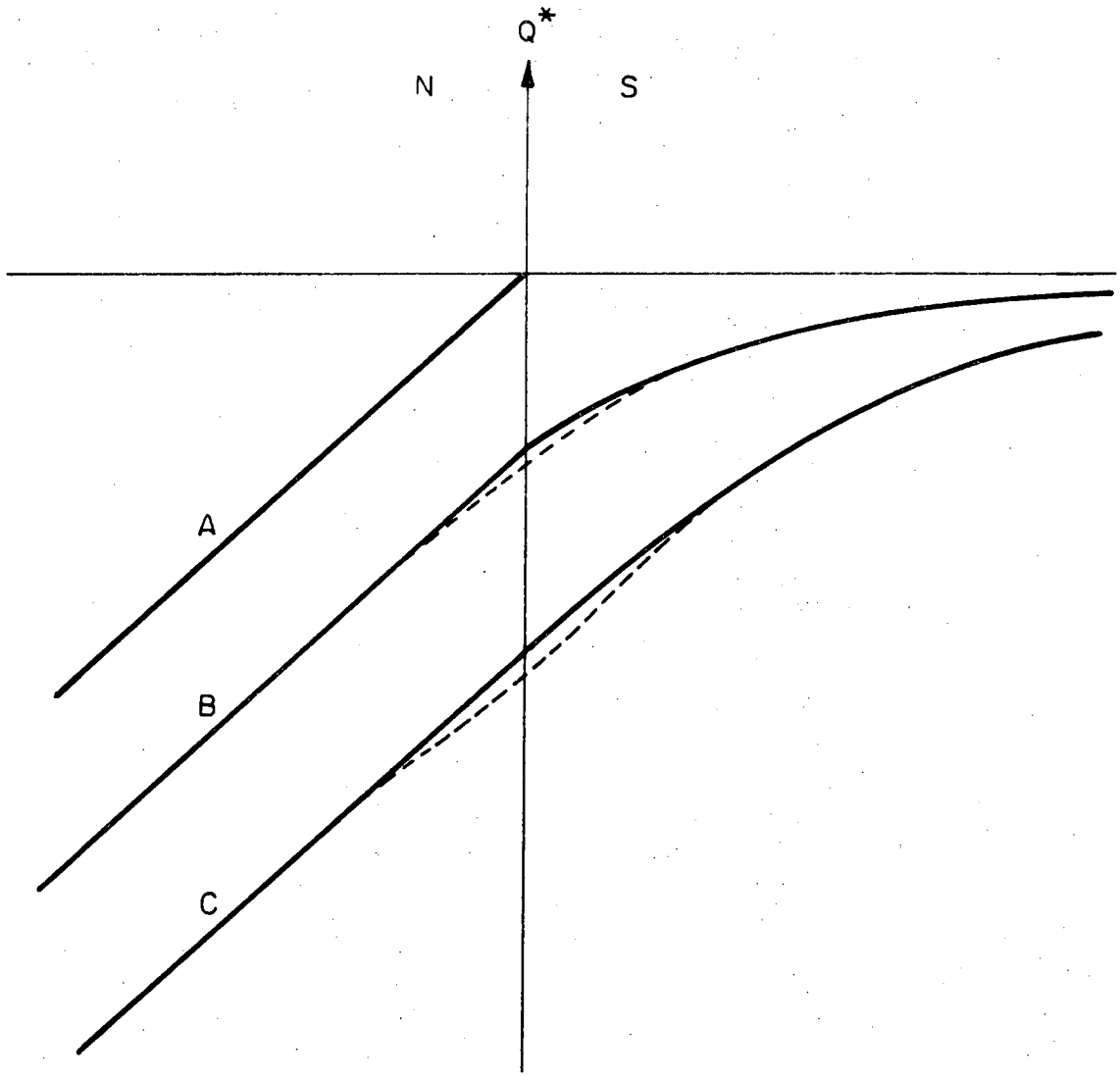

XBL777-5781

Fig. 18 Q* vs. x at three temperatures:

(A) $T \to 0$, (B) intermediate T,

(C) $T \to T_c$.

calculation without any approximations. But this calculation, which would require the q's and j's instead of the integrated quantities Q's and J's, is formidably difficult. The reason is that the physically meaningful quantities are all related to the Q's and J's, and it is very difficult to convert equations in q and j into these integrated quantities without some knowledge of the function forms of q's and j's, if all the energy-dependent parameters are to be treated exactly in the calculation.

We can use the following arguments to justify our approximation scheme in the temperature range where the boundary resistance is significant:

Let us first examine how q will relax to q_Q in the superconductor. This thermalization process is carried out through both the τ_2 and the τ_3 channels. The characteristic time for this relaxation is $(1/\tau_2 + 1/\tau_3)^{-1}$. As we will see in Section VII.E, τ_2 and τ_3 have the same order of magnitude in the intermediate temperature range $T/T_c \sim 0.8$, but near T_c, $\tau_3 \gg \tau_2$. Since the excess boundary resistance is more significant near T_c, it is reasonable to assume that in this temperature region, q will quickly relax to q_Q before the diminution through τ_3 - relaxation takes place. In Fig. 18, curve B and C are only approximate solutions to the problem, while the real solutions may look like the dotted lines shown near these curves. The overall solution is not far from our approximated results.

Another view of the situation is through examing the Andreév transmission coefficient T(E) defined in Eq. (7.21). Since the quasiparticles deep in N are thermalized where they start impinging upon the SN boundary,

the deviation of $q - q_Q$ from zero is due to the fact that $T(E)$ is not unity for all energies. The spread of nonzero $q = q_Q$ is then of an energy width $\sim\Delta$. The spread of q, however, is of an energy width kT from the Fermi factor. If Δ/kT is small, then Eq. (7.37) is a very good approximation, which is again true near T_c.

Granting our approximation to be correct, we can calculate the boundary conditions as in refs. 32 and 39. A most general boundary condition is

$$q_N = \gamma_{11}\, q_s + \gamma_{12}\, j_s \quad ,$$

and

$$j_N = \gamma_{21}\, q_s + \gamma_{22}\, j_s \quad . \qquad (x = 0) \qquad (7.44)$$

In the case of Andreév reflection, quasiparticles reverse their characters after reflection. The particle flux carried by g is $v_s N(E)\, g$. In N, $v_s = v_f$ and $N(E) = N(0)$, the density of states at the Fermi surface. In S, $v_s = v_f(\varepsilon/E)$, but $N(E) = N(0)(E/\varepsilon)$, and the extra coherence factors just cancel each other. On both sides the flux is proportional to g. The departing flux g_{1N} is equal to the sum of a reflected flux $(1 - T)$ g_{2N} and transmitted flux Tg_{1s}, and similarly for g_{2s}:

$$g_{1N} = (1 - T)\, g_{2N} + T\, g_{1s}$$

and (7.45)

$$g_{2s} = (1 - T)\, g_{1s} + T\, g_{2N}$$

when converted into the form of Eq. (7.44), we get

$$\gamma_{11} = 1 \quad ,$$

$$\gamma_{12} = 0 \quad ,$$

$$\gamma_{21} = -2\,\frac{1-T}{T} \quad , \tag{7.46}$$

$$\gamma_{22} = 1 \quad .$$

In ref. 32 and 39, these boundary conditions are integrated and converted into boundary conditions for Q and J. Later I will make a criticism on their mathematical approach. It should be noted that with our "nearly thermalized approximation", we cannot directly integrate Eqs. (7.44) and (7.46) to solve the problem and calculate the factor $F \equiv J_s/J_N$. The reason is that, to convert these equations, it is necessary to know the functional forms of the q's and j's. In other words, these equations match the dotted lines in Fig. 18. But within our approximation, we need to calculate the matching of the solid lines. Erroneous results would be obtained if we used the thermalized q's and j's in integrating Eq. (7.44).

We can, however, directly link J_N and J_s by the following method: Assume that, deep in N, quasiparticles on the k< branch start with a

thermalized distribution $g_{2N} = c\ f'(E)$, where C is a constant normalized to make J_N the applied current. Then, after boundary reflection, j_N and js would be, respectively,

$$j_N = g_{2N} + (1-T)\ g_{1N} \quad ,$$

and

$$j_S = T\ g_{2N} \quad .$$

Integrating these equations, we get

$$F^{-1} = \frac{J_N}{J_s} = \frac{\int_0^\infty f'(E)dE + \int_0^\infty (1-T(E))\ f'(E)dE}{\int_\Delta^\infty \frac{E}{|\varepsilon|}\ T(E)\ f'(E)\ dE} \tag{7.47}$$

For comparing with experimental data, we tabulated both F and α $\left(\equiv \frac{Q}{Q^*}\right)$ with a computer. αF is plotted vs. temperature in Fig. 19 and listed in Table 1. What we have done here is to take a thermalized beam of electrons and calculate how much of it will be converted into normal current in the superconductor, and set this amount to equal the normal

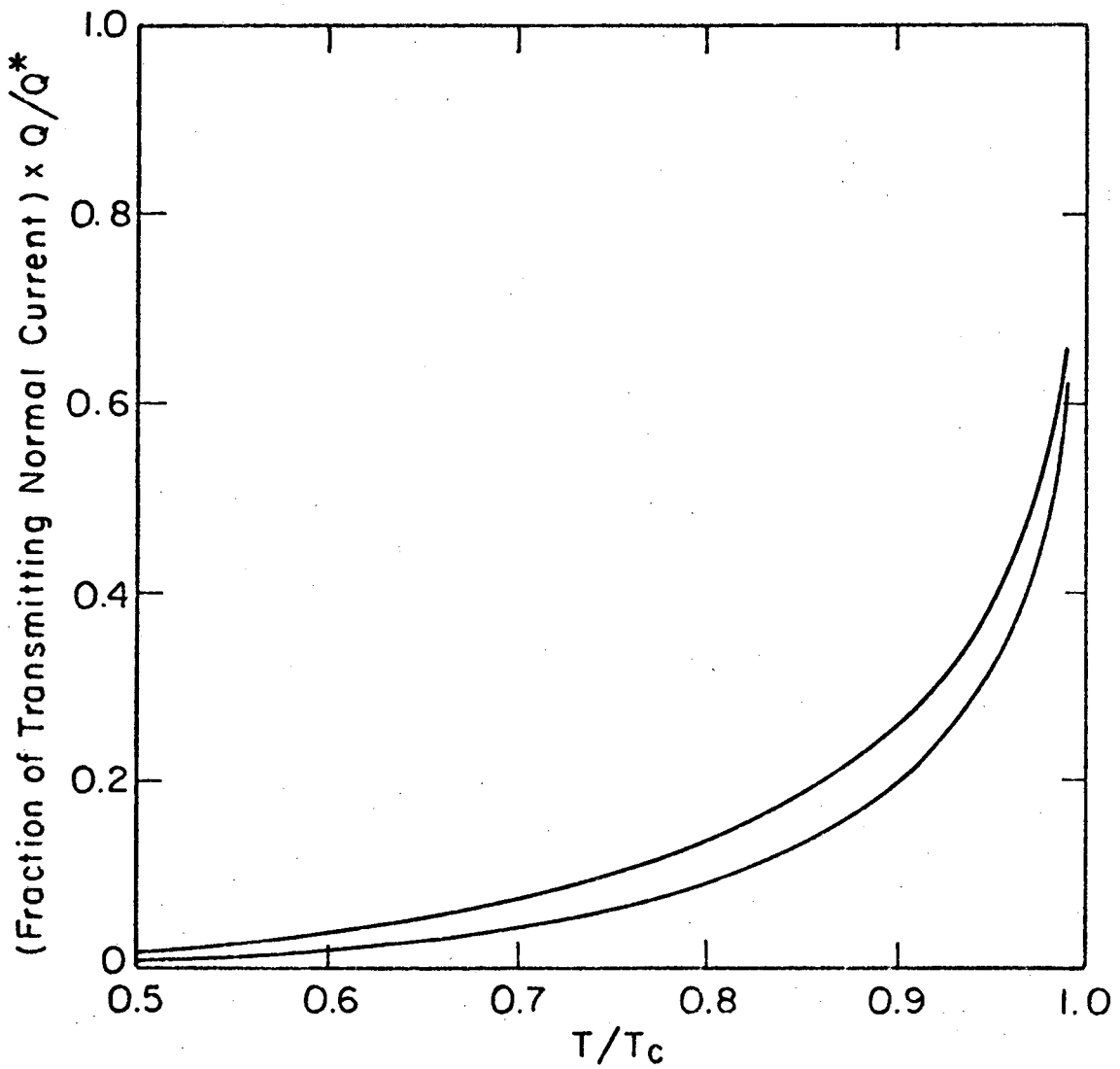

FIG. 19

XBL 7711-6411

TABLE I. VALUES OF αF AS DEFINED IN EQ. (7.48)

T/T_c	$\Delta(T)/\Delta(0)$	αF(Pb)	αF(Sn,In)	T/T_c	$\Delta(T)/\Delta(0)$	αF(Pb)	αF(Sn,In)
0.5	0.9569	0.0080	0.0180	0.78	0.7386	0.0784	0.1196
.52	.9488	.0098	.0213	.80	.7110	.0904	.1347
.54	.9399	.0120	.0250	.82	.6810	.1043	.1518
.56	.9299	.0144	.0292	.84	.6480	.1207	.1716
.58	.9190	.0172	.0339	.86	.6117	.1403	.1945
.6	.9070	.0204	.0390	.88	.5715	.1640	.2217
.62	.8939	.0231	.0447	.9	.5263	.1933	.2544
.64	.8796	.0282	.0499	.92	.4749	.2308	.2951
.66	.8640	.0329	.0580	.94	.4148	.2808	.3480
.68	.8471	.1382	.0657	.95	.3850	.3091	.3770
.7	.8288	.0489	.0743	.96	.3416	.3530	.4214
.72	.8089	.0512	.0830	.97	.2980	.4032	.4710
.74	.7874	.0591	.0944	.98	.2436	.4748	.5398
.76	.7640	.0681	.1063	.99	.1720	.5882	.6452

current after thermalization. Since $\int dE j_s\, E/|\varepsilon| = \int dE\, j_{sQ}\, E/|\varepsilon|$, as long as the normal current that is "lost" through the τ_3 and τ_4 channels in the thermalization region (the dotted region in Fig. 18) is negligibly small, Eq. (7.47) is a good approximation. This is again, within our scheme of approximation.

To compare our calculations with experimental results, we compute the boundary resistance from

$$R_{SNS} = R_N + 2\rho_s \frac{F\lambda}{A} \quad , \tag{7.48}$$

where R_N is the resistance of the normal region, ρ_s is the resistivity of the superconductor, and A is the cross-sectional area of the junction. λ is extended to 3-dimensional as

$$\lambda = \alpha \sqrt{\frac{1}{3}\, \ell \left(\frac{1}{\ell_3} + \frac{1}{\ell_4}\right)^{-1}} \quad , \tag{7.49}$$

where ℓ_3, apart from its dependence on temperature, is left as a fitting parameter.

D. Comments on Waldram's Formulation

In the previous section, we have solved the quasiparticle transport equations for the SNS sandwiches with the approximation that q and j in the significant temperature range are approximated by their thermalized

values q_Q and j_Q. Waldram[32] used a somewhat different approach and at first sight, it seems that he was able to handle the problem without any approximations. However, as we will see below, his formulation contains implicitly an assumption equivalent to ours; in addition, several errors were made in the calculations.

(1) Waldram started out with a pair of Boltzman equations similar to Eq. (7.25), except that the form of $(g_1 + g_{2Q})/\tau_3$ was used for the branch-crossing relaxation. In other words, he assumed that the τ_3 relaxation converts <u>all</u> g_1 excitations into g_2 and vice versa, rather than assuming that τ_3 relaxes g_1 and g_2 to equal numbers. His assumption was clearly incorrect on this point.

(2) The recombination process was not included in Waldram's equations. Therfore, not every kind of electron-phonon scattering was taken into account. Fortunately, as we will see in the next section. the τ_4 process does not contribute significantly in the SNS experiments.

(3) When the Boltzman equations were integrated, no distinction between Q and Q* was made. $\alpha \equiv Q/Q^*$ was taken to be unity. Also, the energy dependence of τ_3 and τ_4 was not considered, and the relaxation length ℓ_3 in Eqs. (7.32) and (7.33) was used <u>a priori</u>, while we saw in the last section, they can only be used in an approximate sense.

(4) Waldram proceeded to calculate the boundary resistance, recognizing that $q - q_Q$ and $j - j_Q$ relax in a length $(1/\ell_2 + 1/\ell_3)^{-1/2}\ \ell^{1/2}$. But in order to convert the equations of q and j to equations of Q and J, he assumed that

$$\int_\Delta^\infty (q - q_Q)dE = \int_\Delta^\infty (j-j_Q)dE = 0.$$

When we insert in $q_Q = Q^* \left(-f_0'(E)/f(\Delta)\right)$ and $j_Q = J^* \left(-f'(E)/f(\Delta)\right)$, we see that his assumption is equivalent to

$$\int_\Delta^\infty q \, dE = Q^*$$

and (7.50)

$$\int_\Delta^\infty j \, dE = J^* \quad .$$

However, conservation of quasiparticles will only give

$$\int_\Delta^\infty q \frac{E}{|\varepsilon|} \, dE = \int_\Delta^\infty q_Q \frac{E}{|\varepsilon|} \, dE = \alpha Q^* \tag{7.51}$$

and (7.50) does not hold.

The two implicit assumptions above, i.e., the use of ℓ_3 in the integration of the Boltzman equations and the assumed equalities in Eq. (7.50), are both correct in our approximation scheme. It is thus seen that Waldram's formulation should in essence be equivalent to ours. His final expression for the boundary resistance, however, contains ℓ_2 of both the superconductor and the normal metal. It can be seen that

this result is due to his relaxing the assumptions that were made at an earlier stage of his formulation. These assumptions, that q and j can be approximated by q_Q and j_Q will eliminate the ℓ_2 dependence of the resistance as shown in the last section.

(5) Finally, in matching the boundary resistance, he obtained a formula different from Eq. (7.46). He had chosen $v_s g$ as the particle flux to be matched at the boundary, while v_s N(E) g should be used as we have shown. In Andreév's original work, the square of the quasi-particle wave function $|\psi|^2$, multiplied by v_s was used as the particle flux as in ordinary quantum mechanics. Since $|\psi|^2$ is the number of the quasiparticles, $|\psi|^2$ = N(E) g.

E. The Relaxation Times

In this section, I will discuss the various relaxation times τ_i provided by theoretical calculations. In particular, we want to know their magnitudes and dependences on temperature. We want to know the relative contributions of τ_3 and τ_4 in the SNS resistance. We also want to compare the magnitudes of τ_2 and τ_3 near T_c and see whether the approximations outlined in Section VII-C are justified. These times will be discussed in order.

(1) The elastic collision time τ_i is practically equal to ℓ/v_f, where ℓ is the mean free path of electrons. ℓ can be determined from the resistivity ρ and the product $\rho\ell$ quoted in handbooks and other references.[53,60] v_f is the average Fermi velocity and can be calculated from the simple relation

$$v_f = \frac{\pi^2 k_B{}^2}{e^2 \gamma \rho \ell} ,$$

where γ is the coefficient of the linear term (electronic contribution) of the temperature dependence of the specific heat at low temperature.

All the other times involve electron-phonon interaction. Kaplan et al.[41] have used the Eliashberg formulation to calculate numerically the imaginary part of the quasiparticle energy, hence the quasiparticle lifetime, in terms of the famous electron-phonon coupling function $\alpha^2(E)$ $F(E)$. $\alpha(E)$ is the electron-phonon coupling strength and $F(E)$ is the phonon density of states. For most type I superconductors, this function is amply described by an E^2 dependence, with the exception of Pb and Hg. Their results are thus universally applicable apart from a scaling factor characteristic of the material. Other authors[40,43,43] have calculated the relaxation times using the Golden Rule. In several limits, their results agree with those of Kaplan et al. I will discuss the various relaxation times based on these calculations. No attempt will be made to outline their formulations. Instead, emphasis will be placed on the predicted numerical magnitudes and temperature dependences. The work of Kaplan et al. is probably the most useful one for this purpose, although we will encounter difficulties in directly applying their calculations, because they calculate the times as a function of both energy and temperature, while the useful quantities are the average

values over the quasiparticle distribution. Rough estimates based on plausible physical arguments will thus have to be made when necessary.

(2) The thermalization time τ_2 can be obtained from the electron-phonon scattering time $\tau_s(E,T)$ in ref. 41, and is similar to the "cooling time" t(T) in ref. 40. To estimate its magnitude, let us separate the discussion into two regimes. At low temperatures, near the SN boundary, there are few quasiparticles in S, and the current is carried mainly by the condensate. For the small number of quasiparticles, the average energy is close to gap energy Δ. τ_2 is then $\tau_s(\Delta, T \to o)$ and diverges as $(T/T_c)^{-7/2}$ due to the simple fact that there are few phonons at low temperature the electrons can scatter with. Close to T_c, Δ is small and normal electrons constitute most of the current flow. τ_2 should then be identified with τ_s $(kT, T \to T_c)$. $\tau_2(kT, T)$ converges to a finite value near T_c, and is $\sim 4 \times 10^{-10}$ sec for Sn and $\sim 8 \times 10^{-11}$ sec for Pb at T_c. Below T_c, τ_2 slowly increases to about twice as large at 0.9 T_c.

(3) The branch-crossing relaxation time τ_3 is identified with τ_Q in refs. 40 and 41. In both references, a thermally averaged value in the form of Eq. (7.32) was calculated. There are two components in τ_3: one due to inelastic scattering and involves $\alpha^2(E)F(E)$, and the other due to eleastic scattering in the presence of gap isotropy. The inelastic part diverges as $\tau_3(0)$ $(\Delta(T)/\Delta(o)^{-1}$ near T_c. It is this prefactor $\tau_3(0)$ that will later be used as an adjustable parameter in fitting the experimental data. Although τ_3 has complicated structures in its dependence on energy and temperature at low temperature, we need only consider its behaviour close to T_c since the SNS boundary resistance quickly converges to zero when the temperature is lowered below T_c

and any structure of τ_3 cannot be resolved. The values of $\tau_3(o)$ was calculated in ref. 41 to be 2.9×10^{-10} sec for Sn and 2.2×10^{-11} sec. for Pb, and in ref. 40 to be 4×10^{-10} sec for Sn and 4×10^{-12} sec. for Pb. The latter value of $\tau_3(o)$ for Pb is not reliable because that author used a simple E^2 dependence for $\alpha^2(E)F(E)$ in calculating electron-phonon interaction in Pb while it is well known that Pb has complicated structures in its $\alpha^2(E)F(E)$.

The elastic contribution to τ_3 was calculated in ref. 40. As stated in Section VII.C, the elastic contribution is zero in the absence of gap anisotropy. If one defines an average normalized gap anisotropy $\langle \alpha^2 \rangle$ by

$$\langle \alpha^2 \rangle \equiv \frac{\langle \delta\Delta^2 \rangle}{\langle \Delta \rangle^2} \tag{7.52}$$

With a simple calculation, one finds

$$\tau_3^{(e\ell.)} = \frac{\tau_1}{\langle \alpha^2 \rangle} \frac{k_B T}{\Delta} \left(1 + \frac{k_B T}{\Delta} \right) \tag{7.53}$$

Clarke and Paterson[35] found that a tolerable approximation of $\langle \alpha^2 \rangle$ in a dirty superconductor is given, in terms of the anisotropy of pure metal $\langle \alpha^2 \rangle_o$, by $\langle \alpha^2 \rangle / [1 + (\hbar/2\tau_1\Delta)^2]$. It can be verified[35] that in the case of SNS experiments, $\tau_3^{(e\ell)}$ is much larger than the inelastic part, and therefore negligible.

It should be mentioned at this point that Schmid and Schön[44] have also calculated the inelastic part of τ_3 (which they call τ_R) and found

$$\tau_3 = 0.73\ \tau_E \frac{\Delta(o)}{\Delta(T)} \left(1 + \frac{1}{4\ \tau_E^{\ 2}\ \Delta^2(T)}\right)^{1/2} \tag{7.54}$$

where τ_E is similar to τ_θ in ref. 40 and similar to τ_o in ref. 41. τ_E corresponds to the inelastic scattering time for electrons. The extra dependence on temperature of $\left(1 + \frac{1}{4\ \tau_E^{\ 2}\ \Delta^2(T)}\right)^{1/2}$ is the main difference between their results and those of the others. However, this factor becomes significant only at tempratures very close to T_c (for Sn, $T_c - T \leqslant 1\mu K$) and is difficult to verify experimentally. We shall therefore consider the main feature of the $1/\Delta(T)$ dependence in τ_3 in later analysis of the experimental data. I will discuss more of the Schmid and Schön results in the next section.

We now can see, our approximations in Section VII.C. are clearly valid when $T/T_c > 0.95$ where $\tau_3 >> \tau_2$ holds. Down to $T/T_c \simeq 0.8$, τ_3 and τ_2 become comparable and one has to know explicitly the functional forms of the quasiparticle distribution functions (g_i) in order to calculate the SN boundary resistance. The added effect that the deviation of the g_i's from the thermalization is small certainly helps to improve our approximation. However, for lack of anything better, we will cling to our approximated results. The Green function method used by Schmid and Schön, as will be discussed in the next section has perhaps paved the way for future theoretical calculations in a more exact way.

(4) The recombination time τ_4 has long been calculated. The earliest work by Rothwarf and Cohen[42] found τ_4 at low temperature to be proportional to $(\Delta/T)^{1/2}$ $\exp(-\Delta/kT)$. This result was confirmed by the calculations in ref. 41. The latter calculation also found that τ_4 approaches a constant value except for quasiparticles near the gap edge (in which case $E \sim 0$ and τ_4 diverges). τ_3 and τ_4 both derive from the electron-phonon interaction and thus should have the same order of magnitude at intermediate temperature range. However, as Rothwarf and Taylor[45] pointed out, phonons emitted in the recombination processes have energy greater than or equal to 2Δ and can break pairs. If the "pair breaking time" τ_B is comparable with or longer than the time τ_γ for a phonon to escape the system, one would then have an enhanced recombination time. Only τ_4 is affected by this enhancement process because pairs that are broken by the phonons will equally populate the two branches and hence τ_3 is not changed. Eisenmenger and Lassman[46] have used a phenomenological approach to find $\tau_\gamma \simeq 4d/\eta c_s$, where d is the thickness of the metal film, C_s is the average sound velocity, and η is the average interface phonon transmissivity. τ_B was calculated in ref. 41 to be $\sim 1 \times 10^{-10}$ sec for S_n and 3×10^{-11} sec for Pb. For the thermal phonons, τ_B is very weakly dependent on temperature. Taking a typical film thickness of $\sim$25 μm in the SNS experiments, and sound velocity of 10^5 cm sec^{-1}. We see the enhancement factor $(1 + \tau_r/\tau_B)$ for τ_4 can be larger than 10^3 even for $\eta = 1$. This justifies our neglecting τ_4^{-1} compared with τ_3^{-1}.

F. Time-Dependent — Ginzburg-Landau Theory

A different approach to the SN boundary problem uses time-dependent - Ginzburg-Landau theory (TDGL). The first people were Rieger, Scalapino, and Mercereau (RSM)[47]. They used a relaxation equation for the order parameter

$$\left(\frac{\partial}{\partial t} + 2\,\frac{i\mu}{\hbar}\right)\Psi = \frac{1}{\tau}\left[1 - \eta\,|\Psi|^2 + \xi^2\,(T)\left(\vec{\nabla} - \frac{2\,ie}{\hbar c}\vec{A}\right)^2\right]\Psi \qquad (7.55)$$

This equation was originally derived by Gorkov and Eiashberg from the BCS theory for a gapless system where the parameters τ, η, ξ all have definite meanings. While in the SN case, they are treated phenomenologically.

From Eq. (7.55) and a continuity equation for "space charge" in S, RSM derived an equation for the difference between the chemical potentials of the condensate μ_p and of the quasiparticles μ

$$\mu_p - \mu = \frac{m\xi^2(T)}{4|e|\tau}\,\frac{1}{|\Psi|^2}\,\vec{\nabla}\cdot\vec{j}_s \quad , \qquad (7.56)$$

where $\vec{j}s$ is the supercurrent in the superconductor. Since $\vec{\nabla}\cdot\vec{j}s = -\vec{\nabla}\cdot\vec{j}_N$ in the steady state, and, as we discussed in Section VII.C.

$\mu_p - \mu$ is just Q^*, we see that Eq. (7.56) is just the same as our approximated Eq. (7.39), if we make the identification of

$$\tau_3 = \frac{n}{|\Psi|^2} \frac{\xi^2(T)}{\ell^2} \frac{\tau_1}{\tau}^{2} \quad . \tag{7.57}$$

If we now use Eq. (7.56) as an empirical result, and use experimental data to determine $\xi^2(T)/\tau$, the theory would be essentially correct, even though these quantities cannot be physically interpreted directly through the theory. But if one chooses to define $\xi(T)$ as the Ginzburg-Landau coherence length and τ as the inelastic scattering time (in a gapless system, τ is the spin-flip time), we see that the correct temperature dependence of τ_3 would not be obtained as was clearly demonstrated by the experiments of Clarke and Paterson[35].

Yu and Mercereau[48] have used this theory to interpret their experiments on the potential measurement near a SN interface, and found reasonable agreement with experimental results, even though over a quite small temperature range. However, they found that they had to choose $\xi(T)$ much larger than the Ginzburg-Landau Coherence length. From the theory in previous sections, we know that they were actually measuring the quasiparticle decay length. Their experiments were done on extremely thin films and the decay length would involve both τ_3 and τ_4. I will not attempt to reinterpret their results using the theory in this thesis.

A much improved version of the TDGL theory was proposed by Schmid and Schön[44](SS); I will devote the rest of this section to discuss their theory. They have also calculated the SN boundary resistance. At the end of this section, we will see what were the assumptions and approximations used in their theory, to what extent it will apply, and how it is related to the theory in this paper.

SS used the equations of Gorkov and Eliashberg[49] in the form introduced by Eilenberger[50]. The Green's function form of these equations is essentially equivalent to the self-consistent BCS gap equations[33]. When a perturbation is applied, Δ will be changed to $\Delta + \delta\Delta_1 + \delta\Delta_2$, where $\delta\Delta_1$, the real part of $\delta\Delta$, is called the longitudinal mode and corresponds to a spatial variation of the magnitude of the order parameter, and $\delta\Delta_2$ is imaginary and is called the transverse mode and corresponds to the evolution of the phase of the order parameter. Physical perturbations of current and electric field are associated with the variation in $\delta\Delta_2$. The "retarded" and "advanced" Green's functions describe the response of the order parameter to the perturbations, while the "anomalous" Green's function describes the response of the quasiparticle distributions and their influence on the order parameter.

In the linearized theory, the equations of Gorkov and Eliashberg can be decoupled into a pair of a Boltzman equation, which describes the quasiparticles, and an equation for the order parameter similar to the Ginzburg-Landau equation. The imaginary part of the quasiparticle density of states solved from these equations then determines the lifetime of the quasiparticles.

When applied to the experiments of Clarke and Paterson[35], $\tau_3(\tau_R$ in SS) is,

$$\tau_3 = \frac{4kT}{\pi\Delta} \left(1 + \frac{1}{4\Delta^2\tau_E^{\,2}}\right)^{1/2} , \tag{7.58}$$

where τ_E is the electron-phonon scattering time (similar to τ_θ in ref. 40 and proportional to τ_o in ref. 41). This result is essentially the same as predicted by all other theorists.

For the SNS case, the boundary resistance (the existence of an electric potential) is shown by an extra energy-independent factor of the quasiparticle distribution, which was called η. This η is proportional to $e\phi$, and hence, Q^*. It was found that η obeys

$$\frac{1}{\tau_3} \eta = D \frac{d^2}{dx^2} \eta \tag{7.59}$$

where $D = \frac{1}{3} v_f \ell$ is the diffusion constant. We see that Eq. (7.59) is the same as our Eq. (7.39). As was discussed in Sec. VII.C, Eq. (7.59) is strictly valid only near T_c. This was also recognized by SS.

SS then proceeded to calculate the boundary resistance by using the electric field (due to the bias current) at the SN boundary as a

perturbation. In doing so, the Ginzburg Landau equation was used to obtain the variation in the order parameter:

$$\Delta(x) = \begin{cases} \Delta(T) \tanh (x/2^{1/2} \xi_{GL}) & x > 0 \quad \text{(S side)}, \\ 0 & x < 0 \quad \text{(N side)} \end{cases} . \tag{7.60}$$

This form of $\Delta(x)$ was substituted into Eq. (7.59) and the SN boundary resistivity was found to be

$$R/\rho_S = L\, \xi_{GL}(0)\, [(T_c - T)/T_c]^{-\rho} , \tag{7.61}$$

where L is 7.0 and 3.0, and ρ is 0.38 and 0.37 for Sn and Pb respectively. (In the original theory of Schmid and Schön, the left hand side of Eq. (7.61) was written as R/ρ_N because they assume the electric field is the same on the two sides of the SN boundary. Since in general $\rho_N \neq \rho_s$, the form of Eq. (7.61) is more correct.)

How good is this theory's predictions? We will make a comparison of the approximations used in their theory and our theory:

(1) In both cases, the quasiparticles that carry the current are assumed to be thermalized.

(2) In our theory, a step form of $\Delta(x)$ was used, while the form of $\Delta(x)$ in Eq. (7.60) was used in theirs. This is not a serious point

because the quasiparticle decay length is in general quite large compared with the Ginzburg-Landau coherence length. The form $\Delta(x)$ in Eq. (7.60) was obtained by assuming Δ vanishes continuously at the SN boundary, an assumption that is realistic only at T_c.

(3) The boundary matching due to Andreév transmission was taken into account in our theory (the F factor) while it was neglected in their theory. In fact, they assumed the electric field to continue across the boundary, which is strictly true only at very near T_c, and when $\rho_N = \rho_S$.

From these discussions, we conclude that while the two computations are complementary to each other, the neglecting of spatial variation of $\Delta(x)$ may not be serious, but the neglecting of Andreév transmission and boundary matching may cause significant weakening of the predicted temperature dependence of the boundary resistance, as can be seen in Eq. (7.61). It is possible that, based on the ground work of Schmid and Schön, an exact theory may be formulated. This author, however, will not offer to pursue the matter further.

VIII. EXPERIMENTAL PROCEDURES

A. The Preparation of Specimens

1. Materials Consideration

Two types of superconductor were used in the SNS experiments, lead and tin. It is essential to choose a normal metal which does not form intermetallic compounds with the superconductor and whose mutual solubility with the superconductors is small so that the diffusion of one material into the other is negligible.

Remarkably few materials satisfy these criteria. For lead, copper was chosen as the normal metal. The solid solubility of lead in copper is not higher than 0.29 wt% at 600°C and of lead in copper, less than 0.007 wt%.[51] The two materials do not form intermetallic compounds. For tin, iridium was used. Tin and iridium are not an ideal pair for SNS experiments, because although Ir is not soluble in Sn, Sn is slightly soluble in Ir and there are several stable intermetallic compounds between them.[51] This choice was partly for historical reasons. (M. L. Rappaport[52] has also measured Sn-Ir-Sn junctions). As will be discussed later, when preparing Sn-Ir specimens, the metals were always kept cool, and experimental results indicated that the interfacial diffusion and alloying were not noticeable.

It is advantageous, both experimentally and theoretically, to use materials with rather short mean free path. Experimentally, the effects of interdiffusion and boundary disorder are minimized and also the supercurrent through the junctions are suppressed[53]. Theoretically,

the short mean free path insures the validity of using the diffusion length of the quasiparticles as in Section VII.C. Also it will become apparent later that the thickness of the superconductor films has to be greater than the quasiparticle diffusion length, which is easier to achieve experimentally if the superconductor is sufficiently "dirtied". Too short a mean free path, however, will add in a complication of the "evanescent wave" of the subgap quasiparticles[54] which may undergo normal scattering (instead of the Andreév reflection). This will be further discussed in later sections.

Due to all these considerations, it was decided that $Pb_{0.99}$ $Bi_{0.01}$ $Cu_{0.97}$ $Al_{0.03}$, $Sn_{0.99}$ $In_{0.01}$ alloys would be used. All three were evaporated directly from boats without using the pellet-dropping techniques[53]. These alloys were formed and sliced prior to being placed in boats for evaporation. Separate experiments were performed to insure that the evaporated films were uniform. These experiments consist of evaporating several films in succession and measuring the resistivity of each film. It was found that Pb/Bi and Sn/In alloys did evaporate uniformly while the Cu/Al alloy, when evaporated from a Mo or Ta boat, would yield a Cu-rich film at first, with Al slowly increasing its contribution. This problem was solved by the use of a tungsten boat[55]. With a tungsten boat, the material evaporated from the Cu/Al crystal was initially Cu-rich; the material then quickly stabilized to possess a rather constant Al concentration until there was only a small amount of material left in the boat when the Al concentration became high. In preparing the junctions, the first fraction of material evaporated

was discarded. Up to the desired thickness of the Cu/Al film, the film was found to be uniform. New evaporant and boats were used each time.

Iridium was not an easily evaporable material. The sputter-evaporate[52] technique was then used, which will be described later. The iridum foils (99.98% pure) that was purchased[56] had mean free path and thickness that satisfied our requirements, and no extra "dirtying" was done.

2. The Pb-Cu-Pb Junctions

The Pb-Cu-Pb junctions were evaporated junctions in the configuration shown in Fig. 20. Three junctions were made each time on a 2.5 x 1.25 cm^2 glass slide. The two Pb/Bi strips were each roughly 200 μm wide, and the Cu/Al was a disc with a diameter = 0.32 cm. The junction area was then defined as the overlap of the two Pb/Bi strips. The stray conductance due to that part of the Cu/Al film which is not included in the junction contributes negligibly to the total junction conductance.[39,53] It should be noted that the correction due to the stray conductance only affects the absolute values of the resistance but not the shape of the temperature dependence. After the junction resistance measurement was completed, the glass slide was removed from the cryostat and the junction areas were determined under a microscope. The thickness of the films, as well as being monitored with a quartz crystal during the evaporation, were measured with a Dektak machine[57].

The glass slides were cleaned with Labtone, rinsed with tap water and distilled water, and degreased in isopranol vapor. Two slides were used each time, one of which had the junctions evaporated on it, the

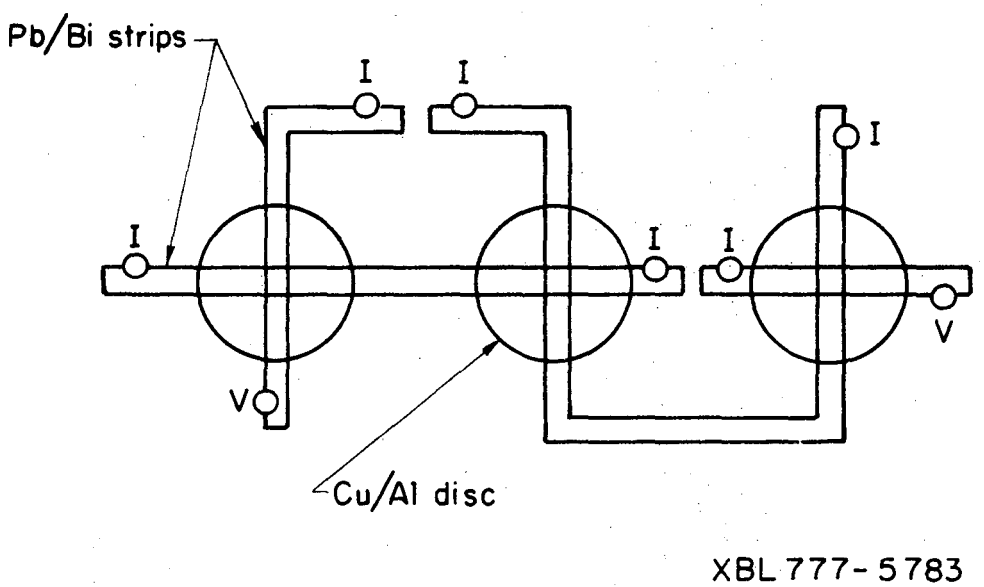

Fig. 20 Configuration of film junctions

other was coated with Pb/Bi simultaneously evaporated with the junction. This Pb/Bi coat was later scribed and used separately for the determination of the resistivity, the mean free path, and the transition temperature of the Pb/Bi.

The glass slides were mounted in a vacuum chamber that had the shape of a glass cross. One leg of the glass cross was connected to a LN_2 cooled cold trap and an oil diffusion pump. The other three legs were sealed with stainless steel plates onto the first of which were mounted the mask changer, the quartz crystal, the glass slide containers, and electrical and water (or LN_2) feedthroughs. On the second stainless steel plate were mounted the evaporation boats, water-cooled electrodes, and a magnetic feedthrough which was used to move the mask changer without breaking the vacuum. On the third plate was mounted a titanium sublimation pump with LN_2 cooled shields around it. The vacuum chamber and all parts were elaborately cleaned after each use to insure good vacuum in the next use.

After careful outgassing of the boats, we enclosed the vacuum chamber in an oven and baked it at 120°C for at least 24 hours. Other parts of the vacuum system such as the roughing valve, the gate valve, and the vacuum gauge tube, were baked with heater tapes. At the end of the bake-out, the chamber pressure was typically $\sim 10^{-8}$ torr. Pb/Bi, Cu/Al and Pb/Bi were evaporated in succession at very high evaporation rates ($\sim$1000 Å/sec for Pb/Bi and 100 Å/sec for Cu/Al). During the evaporation, the pressure of the chamber rose to $\sim 10^{-6}$ torr, a pressure which was believed to be due to metallic vapor because this pressure scaled roughly

with the evaporation rate and dropped quickly to low value once the evaporation was stopped. The interval between evaporations of different materials was made to be as short as possible to insure minimization of surface contamination. This interval was typically ~60 seconds, the time needed to change masks and bring the other boat to the evaporation temperature.

The success rate of making good junctions was remarkably low, usually about 10%. It turned out that making junctions with good interfacial cleanliness was not difficult (this was determined by measuring the junction resistance at low temperature: if interfacial dirt had existed, the junction resistance would have been higher than expected). The difficulties lay in making all films sufficiently thick, adherent to the substrate, and not cracked. It was essential that the films were thick enough: a thick Cu/Al film insured suppression of supercurrent through the junction and it was necessary that the Pb/Bi film was thicker than the quasiparticle diffusion length. Such films usually peeled off from the substrate, or cracked during evaporation. Various techniques were tried to improve the success rate in making these junctions: while heating the substrate or cooling it to LN_2 temperature aggravated the problem, seeding the substrate with a sputtered thin Au coat improved the adhesion of Cu/Al but worsened the adhesion of Pb/Bi. It was finally found that elaborate cleaning of the substrate and water-cooling it during evaporation was the only way to occasionally produce good junctions.

The precious few junctions that survived the frustrations were gratefully removed from the vacuum chamber and lead leads were attached with Pb/Bi eutectic solder (concentration of Bi = 56%, T_c = 8.4 K,

melting point = 126°C) which adhered excellently to glass. The lead leads were strengthened with indium pellets which anchored the leads to the substrate. The junctions were quickly mounted onto the cryostat and cooled down to LN_2 temperature. The total time between removing the junctions from the evaporator and cooling down was less than 15 minutes. Several junctions made with pure lead instead of Pb/Bi alloy were also prepared similarly.

3. The Sn-Ir-Sn Junctions

These junctions were made with iridium strips that were 76 μm thick. The iridium strips were purchased and annealed in low vacuum at ~400°C for 24 hours. It was hoped that the annealing would remove the anisotropy in the resistivity of iridium foil which was presumably hot-rolled. The iridium foils were cleaned in an ultrasonic cleaner with concentrated chloric acid, concentrated sulfuric acid, Labtone solution, and diluted aqua regia in succession. They were then rinsed with distilled water and degreased in isopranol vapor.

These strips and a mica sheet were clamped between two aluminum masks and mounted in the vacuum chamber. Different plates were used for the glass-cross vacuum chamber. The iridium strips were mounted on a plate that had a rotatable feedthrough, water-cooling line and electrical feedthrough[59]. The evaporator plate with water cooled electrode was used, except the magnetic feedthrough was used to drive a shutter. The third plate had the LN_2-cooled titanium sublimation pump as well as a needle valve which was connected to an Argon cylinder that supplied 99.999% pure Argon.

After the bake-out, the aluminum masks were used as the sputtering cathode. Argon was bled through the titanium sublimation pump. The iridium was then sputtered at 50 kV, 35 mA ($\sim$1mA/cm^2) in an argon pressure of 20 μm for 30 minutes. A small positive voltage was applied to other parts of the vacuum system to avoid bombarding them with Argon ion. After the sputtering, the iridium was rotated, and a tin or tin-indium disc of 0.29 cm diameter was evaporated on the iridium at a rate of $\sim$1000 Å/sec. The reverse side of the iridum was similarly sputtered and evaporated. Tin evaporated onto the mica sheet clamped between the masks alongside the iridium was used to determine the thickness of the tin and its resistivity and mean free path. Throughout the process, the iridium and its masks were cooled with water. Junctions made this way had a very high success rate. The only requirement was that the sputtering voltage be high enough and sputtering time be long enough to insure a clean interface. It was also found[52] that rubber "O" rings tended to be sputtered and would contaminate the junctions. Indium "O" rings were thus used for sealing the vacuum system. Electrical leads to the junctions were made with either lead or tin strips welded onto the Sn discs or soldered with In_2Bi (eutectic, Tc = 5.6K, melting point $\simeq$90°C). These leads were always found to be superconducting below the T_c of tin, to carry high supercurrent, to be very robust, and not to damage the tin discs except at the surface. Measured resistance of the junctions below T_c of Sn was not changed by using different kinds of electrical leads.

4. Determination of Mean Free Path

For each of the superconductor films evaporated, the film evaporated simultaneously (on glass for Pb, on mica for Sn) was scribed into a four terminal geometry so that its T_c and residual resistivity ρ could be measured. The mean free path ℓ was then determined by the relationship $(\rho\ell)^{-1} = 9.4 \times 10^{10}\ \Omega^{-1}\ cm^{-2}$ for Pb and $9.5 \times 10^{10}\ \Omega^{-1}\ cm^{-2}$ for Sn[60]. For all the films that we made (Pb/Bi, Sn, Sn/In), the resistivity was independent of temperature at low temperatures (below T_c). This was determined by applying a magnetic field to drive the films into the normal state below T_c.

B. The SQUID Voltmeter and Measurement Technique

1. The SQUID

Cylindrical Nb-NbOx-Pb dc SQUIDs were used in this experiment. These SQUIDs were rather easy to make and for the 20% which were usable, they survived a long time. The details of manufacturing and characteristics of these SQUIDs can be found elsewhere[61].

The SQUID was placed in a lead tube. A five turn coil was inserted in the middle of the SQUID for ac and dc modulation purposes. Another one-turn coil was wound around the SQUID, and used as the sensing coil for the null detector. The SQUID was modulated at 80 kH_z. An LC tank circuit with $Q \simeq 350$ was used to amplify the SQUID output signal and to match the SQUID impedance to a room temperature FET pre-amplifier. The SQUID and the tank circuit were immersed in liquid Helium. Typical noise for the SQUID was $\simeq 10^{-4}\ \phi_0\sqrt{H_z}$. The SQUID could be operated at any temperature below 4.2 K.

2. The SQUID Voltmeter

The voltmeter circuit is shown in Fig. 21. Three SNS junctions were connected in series. Biasing current was provided by an all-battery precision current supply. Because of the finite slewing rate of the SQUID, a ramp was used to drive the bias current from zero to the desired value. This ramp removed the tedium of having to turn the knob each time to increase or decrease the current, and also provided a convenient means to measure the I-V characteristics of the junctions.

The junctions were connected in series with the one turn coil on the SQUID and a standard resistor. Two standard resistors were used in this experiment, one with a Cu/Al rod of 0.4 cm diameter, 0.3 cm length, and 17.1 μΩ, the other one with a manganin plate of dimensions 1cm x 1 cm x 0.03 cm, and resistance 1.15 μΩ. The junctions, coil, and standard resistor formed a complete loop. When the bias current on the junction was increased, the current flowed through the sensing coil, the resulting 80 kH_z signal was then amplified by the tank circuit and the room temperature amplifiers and mixed with the reference signal. The output of the mixer was integrated and fed back as a current through the standard resistor. When the current through the sensing coil was zero, the voltages across the standard resistor and the junction were equal. Thus the amount of feedback current provided a direct measurement of the junction resistance. The open loop gain of this high impedence voltometer was $\sim 10^5$. In all cases, the sensitivity of the voltmeter was limited by the Johnson noise in the junctions and the standard resistor.

0 0 0 0 4 8 0 4 6 2 6

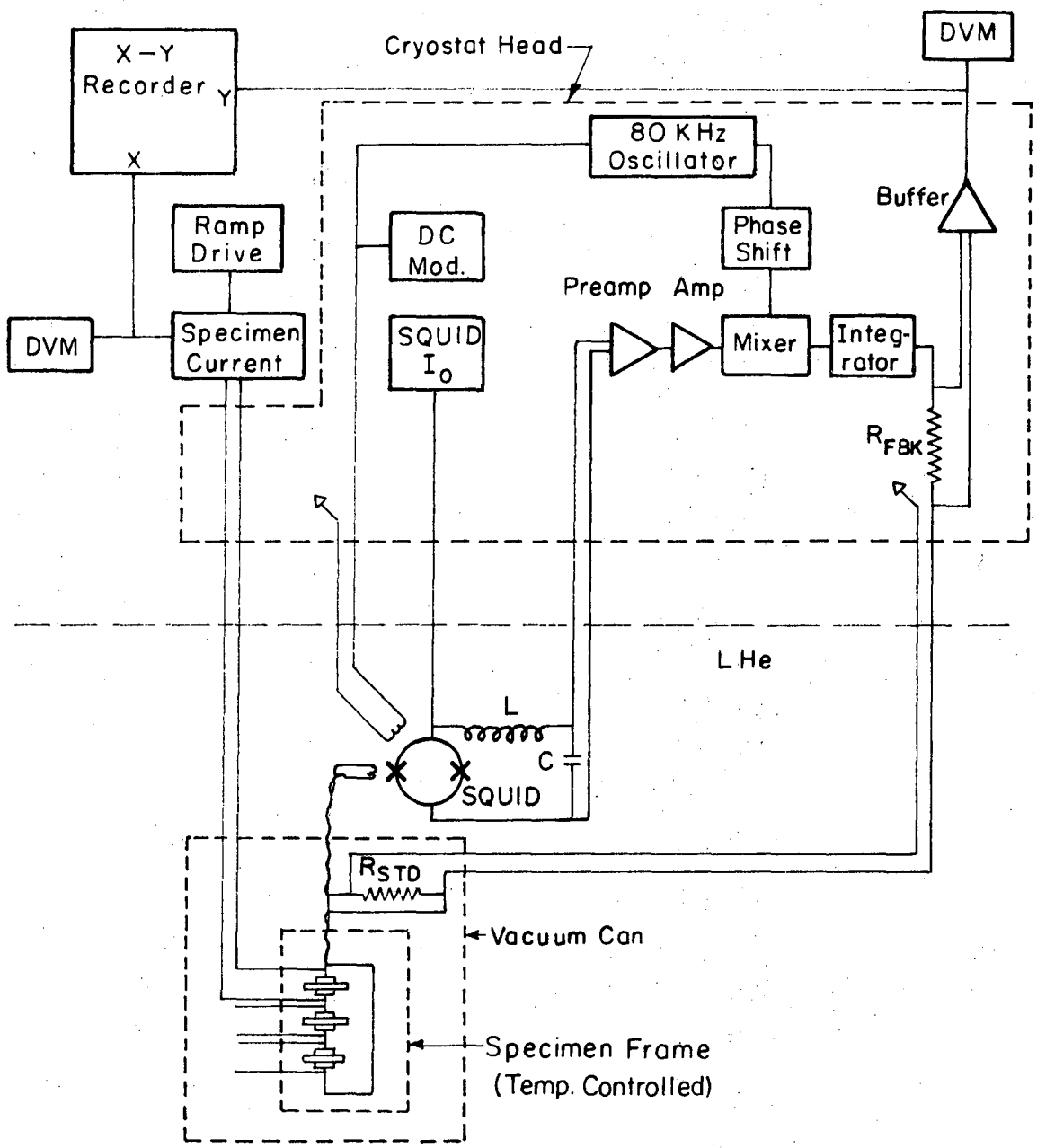

XBL777-5784

Fig. 21 SQUID voltmeter circuit

C. The Cryostat

1. The Dewar

The liquid helium dewar was a nominal 3-inch glass dewar designed by the author. It had an outer LN_2 bottle. The pump line for the vacuum space of the dewar was anchored to the dewar cart, and connected to the dewar through a bent metal hose which was easily deformable to release the tension due to the contraction of the dewar.

The dewar was connected to a pump through a mechanical manostat which controlled the pumping speed with a neoprene diaphram placed between a chamber that was connected to the dewar and a chamber that was connected to a gas tank that provided a reference pressure. Good stability of within 0.1 torr of pressure was achieved with this arrangement.

The dewar was shielded with two layers of μ-metal cylinders which reduced the ambient magnetic field to less than 10 mG.

2. The Liquid Helium Insert

The insert was designed to be used between 1.2 K and 8 K. A longitudinal section of the lower part of the insert is shown in Fig. 22.

A thin-walled stainless steel tube supported a SQUID mount and a vacuum can in the liquid helium. The SQUID was mounted on an aluminum frame outside the vacuum can. The SNS specimens were mounted on a copper plate inside the can. For the Pb-Cu-Pb junctions, the glass slide was attached to the copper plate with Apiezon N grease; for the Sn-Ir-Sn junctions, the ends of the iridium strips were clamped down with copper rods insulated with grease-soaked cigarette paper.

0 0 0 0 4 8 0 4 6 2 7

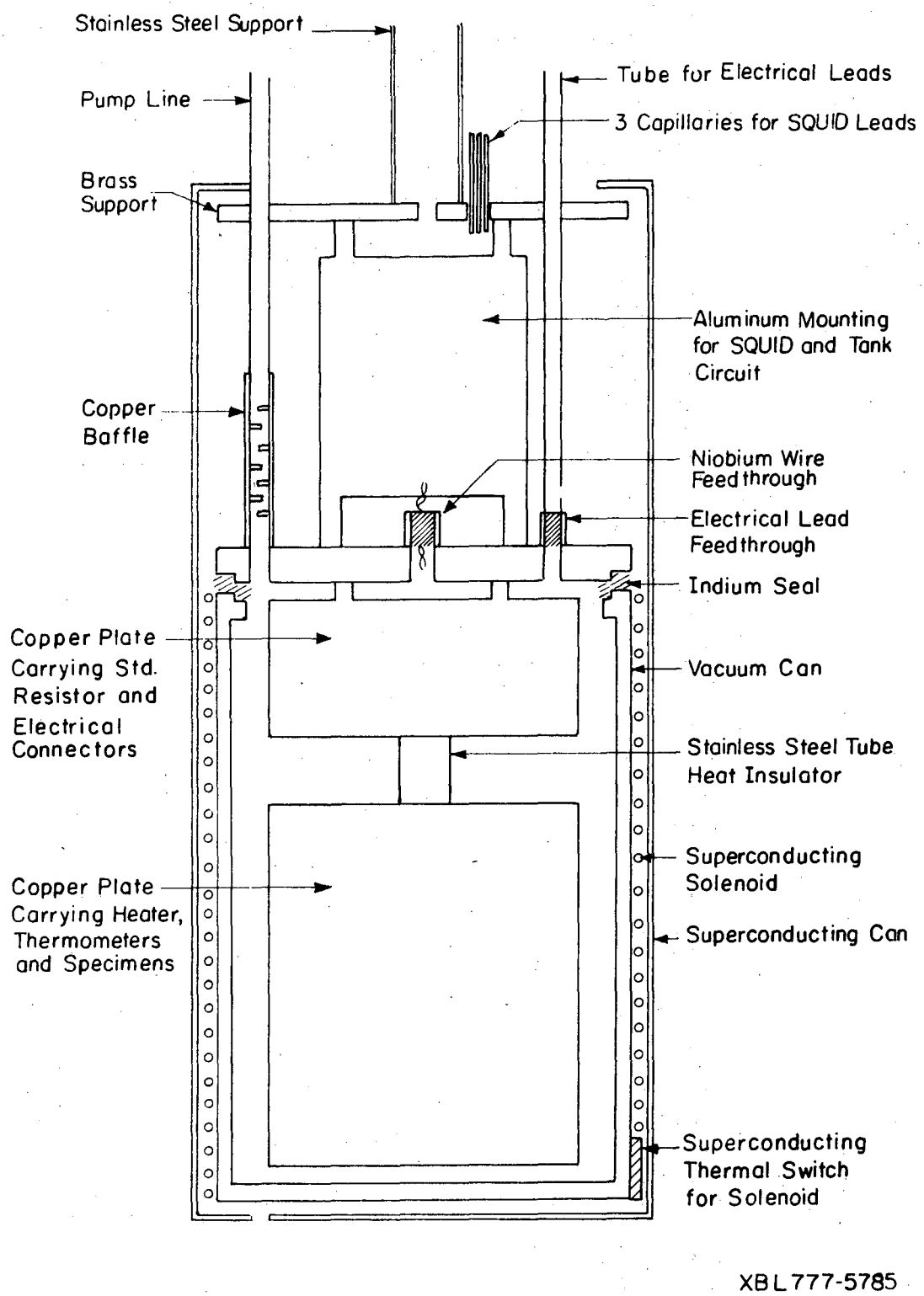

XBL 777-5785

Fig. 22 Lower portion of the cryostat.

Temperatures above 4.2 K were achieved by heat-insulating and applying heat to the specimen plate with a stainless steel tube that connected the plate to the vacuum can. An Allen-Bradley 56 Ω carbon resistor and a non-inductively wound manganin heater glued to the copper plate provided the sensor and heater that were used to stabilize the temperature of the plate. The stabilization was achieved with a Rochlin bridge circuit[62]. Electrical feedthroughs were made with an epoxy-sealed sleeve prepared with a standard procedure. These feedthroughs include the copper wire feedthroughs and a 0.002" Niobium wire feedthrough which connected the voltmeter circuit inside the vacuum can to the SQUID sensing coil. Three thin-walled stainless steel capillaries each with a twisted pair of copper wires were used for the SQUID. They were respectively used for the SQUID bias current, the tank circuit output, and the modulation currents.

A stainless steel pumping line connected to the vacuum can was interrupted with a copper tube blackened to provide a radiation baffle.

The actual temperature of the specimens was determined by a Germanium thermometer (Cryocal GE 989 resistor). A solenoid wound on the vacuum can enabled a persistent magnetic field to be applied to the specimens if needed.

One technique that is worth mentioning is the way to make superconducting connections between Pb (or Sn) and Nb. This was achieved by using a Nb-Pb/Sn union. The union was made by melting Pb-Sn 50-50 solder on a 0.002" thick Nb sheet in vacuum. One end of the union was welded to Nb wire, and the other was soldered to Pb(or Sn). These unions

provided high critical density and were superconducting above the transition temperature of Pb. (M. L. Rappaport[63] has made similar unions with Ta and Sn, but these could not be used above the T_c of Ta).

IX. EXPERIMENTAL RESULTS

A. Junction Properties

1. I (V) Characteristics

The typical I(V) characteristics are shown in Fig. 23, curve A. It is in general a straight line to the highest current used (~10 mA). The straight line extends to zero current as accurately as the experimental apparatus can determine. This purely resistive behaviour near zero current suggests that the proximity effect in the normal metal is not important: if the induced gap is significant, one would expect the resistance of the SNS junctions to be dependent on the current.[52,64] Some of the low energy quasiparticles incident on the SN boundary side from the N side would have been reflected before they reach the boundary. As the bias current is increased, the induced gap in the normal metal would be suppressed, and the threshold energy below which the quasiparticles would be reflected and the amount of reflected quasiparticles would both decrease. The resistance would then increase when the bias current is increased. Since this effect was not seen, one can conclude that the proximity effect in the normal metal is not significant within the temperature range that the data are important.

This is not the case for some junctions at very low temperatures. Figure 23 also shows a Pb-Cu-Pb junction at 1.4K. The junction I(V) shows a critical current and is non-linear at current slightly above this critical current. Fortunately, this non-linear I(V) behaviour does not show up above 0.5 T_c. In our analyzing the data to obtain the quasiparticle diffusion length, only data above 0.5 T_c are analyzed.

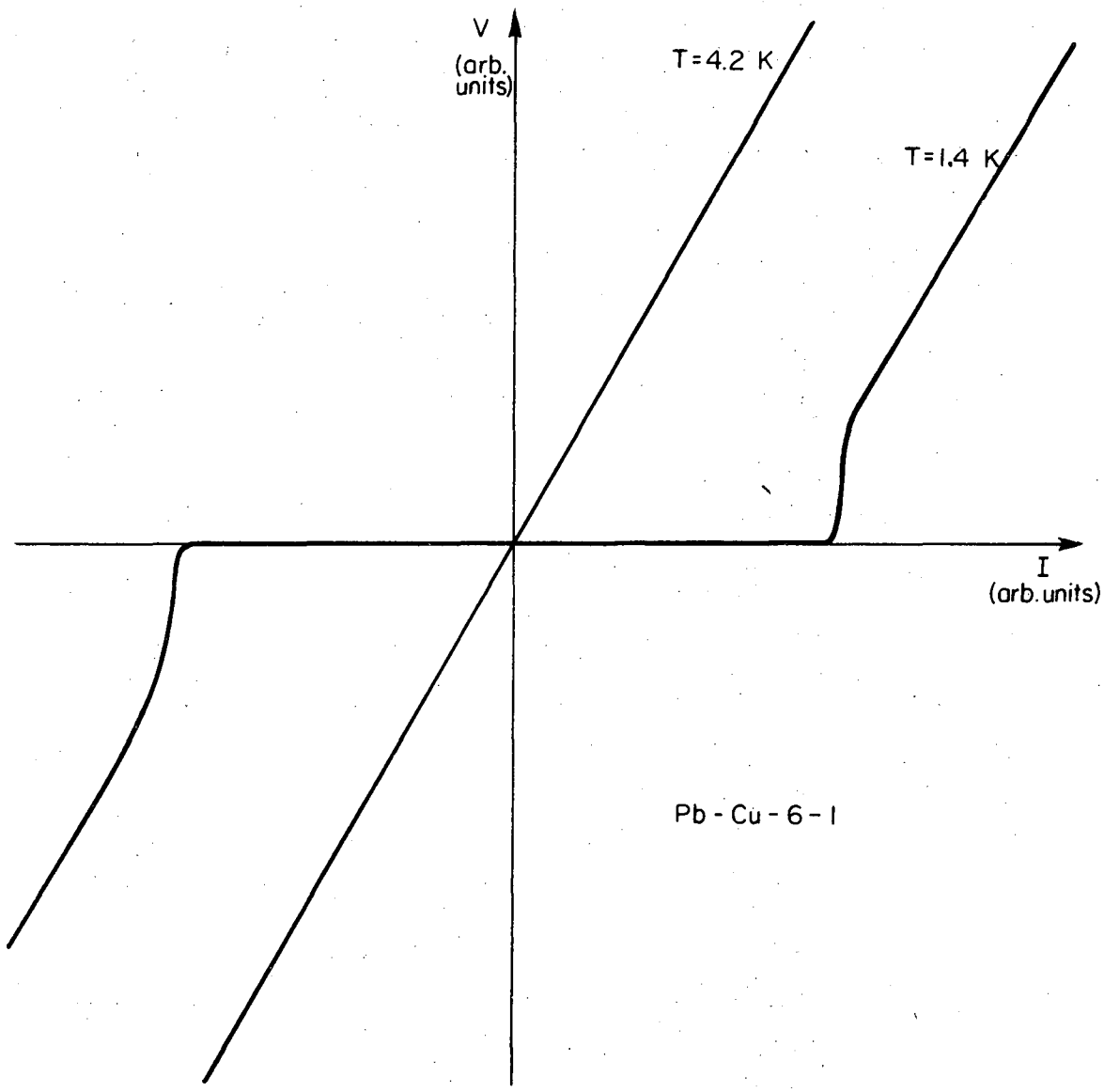

XBL 777-5786

Fig. 23 Current-voltage characteristics of a Pb/Bi-Cu/Aℓ-Pb/Bi junction at two temperatures.

The critical current through the SNS junctions actually provides a measure of the electron-phonon interaction strength in the normal metal[65]. Since this is not within the scope of this thesis and has been well-examined by other authors,[53,65] we will not go into any further detail of the behaviour of this critical current.

2. Resistivities and Mean Free Paths of the Materials

Several useful parameters are listed in Table II for the materials involved in this experiment.

The evaporated pure lead had a T^5 dependence in resistivity when the residual resistivity was subtracted out. This temperature-dependent part of the resistivity agrees with theoretical prediction[66] of the electron-phonon scattering contribution. The diffusion model for quasi-particles would then not be applicable for samples made with this pure lead. The 1% Bi alloy of Pb showed a decrease in T_c from bulk lead[58] while the 1% In alloy of Sn showed an increase in T_c. The nominal 3% Al alloy of Cu had a mean free path of 340 Å. This value is larger than other people have measured[35,65]. The reason for this discrepancy is probably that the other authors have used the pellet-dropping evaporation technique so that their Cu/Al reflected the true composition of the evaporant. In our experiments, Cu/Al was evaporated directly from the boat and the evaporated film, as a result, may have a composition determined by the relative vapor pressure of Cu and Al and the relative adhesion of the two materials to the tungsten boat.

TABLE II. PARAMETERS EXCEPT THAT FOR Pb ARE ALL FOR TEMPERATURE AT 4K

Parameter/Material	Pb	Pb/Bi	Sn	Sn/In	Cu/Al	Ir
v_f (10^8 cm-sec^{-1})	0.48	0.48	0.65	0.65		
$(\rho\ell)^{-1}$ (10^{10} Ω^{-1} cm^{-2})	9.4	9.4	9.5	9.5	15.4	
ρ ($\mu\Omega \cdot$ cm)	$.092 \times (1 + 7.152 \times 10^{-6}\ T^5)$	2.175	0.0297	.423	1.91	.396
ℓ (μm)	$1.46 \times (1 + 7.152 \times 10^{-6}\ T^5)$	0.066	3.367	.237	0.034	
T_c	7.20	7.16	3.73	3.74		

0 0 0 0 4 8 0 4 6 3 0

3. Sizes of the Junctions

The Cu/Al evaporated film was typically 1-3 μm thick. The Pb and Pb/Bi films were 15-25 μm thick. The Pb-Cu-Pb junctions all have an area between 2 to 4 x 10^{-4} cm^2. Their exact sizes will be quoted when each junction is separately considered in the next section.

The Sn-Ir junctions all have an area of 0.067 cm^2. The Sn films were made to be at least 75 μm thick and the Sn/In films were at least 30 μm thick. Ir was nominally 76 μm thick.

B. Junction Resistance and Quasiparticle Relaxation Time

In this section, the resistance vs. temperature of the junctions are plotted and discussed. The resistance is plotted between 0.5 T_c and T_c. When fitted to the theory, $\tau_3(0)$ is used as a fitting parameter. There are no other adjustable parameters. The T_c of the superconductor was determined from the resistive transition of the material and was measured for several different values of bias current applied to a strip of that material. The zero-bias T_c was then obtained by extrapolating to zero current. Because of the finite width of the resistive transition, the T_c measurement was only accurate to ± 5 mK. An independent T_c measurement was obtained directly from the SNS measurement: when the superconductor is at a temperature within its resistive transition, the SQUID voltmeter circuit becomes unstable.

With the help of a PDP-11 computer, a family of curves corresponding to the resistance of the junction calculated with a number of values of $\tau_3(0)$ were compared with the experimental data. A "best fit" to the

data was thus obtained. The emphasis of the "best fit" was always placed on the region near T_c.

The values of Δ/k_BT were obtained from Mühlschlegel[67] and $\Delta(0)/k_\beta T_c$ was taken as 2.15 for Pb and 1.76 for Sn. The best fit to the data was always with $\tau_3(T) = \tau_3(0) \times (\Delta(0)/\Delta(T))$. It was suggested to us[68] that a constant τ_3 might be the more appropriate time to be used. For several junctions, we tried to fit a constant τ_3 but the quality of the fit was always very poor. The comparison of the two fits will be presented at the appropriate place later.

The junctions will be discussed in order below. They are not listed in the chronological order in which they were made. At the end of this section, the data taken by M. L. Rappaport[52] will also be discussed and fitted to the theory. The measured $\tau_3(0)$ will be compared with theoretical predictions[40,41,44] in the next chapter.

1. Tin-Iridium

Two such junctions were measured. The expected low temperature resistance of the junction was calculated to be $4.49 \times 10^{-8}\ \Omega$. For both junctions, the measured low temperature resistance was within 10% of this expected value, implying the interface contamination between Sn and Ir was minimal. (In another run, the sputtering time on iridium was reduced to half, and the measured resistance at low temperature was $\sim 1.2 \times 10^{-7}\ \Omega$).

Figures 24 and 25 show the data for Sn-Ir-2 and Sn-Ir-3 along with the best fit with $\tau_3(T) = \tau_3(0)\ \ \Delta(0)/\Delta(T)$. Curves using $\tau_3(0)$ 20% larger or smaller than that of the "best fit" will make a clear difference

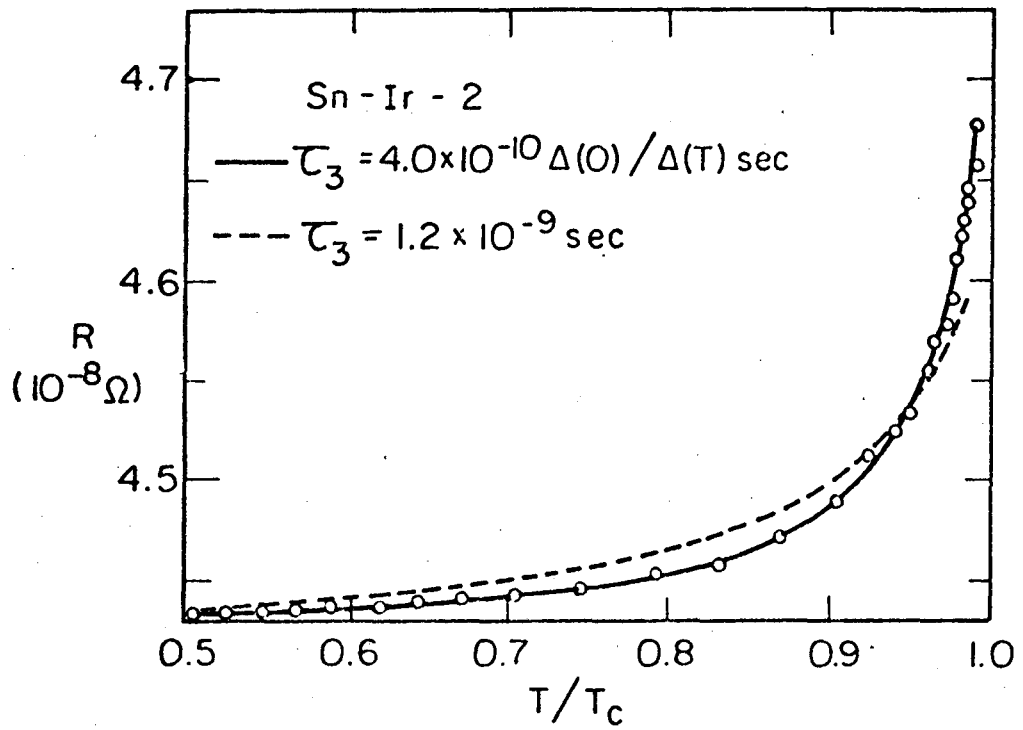

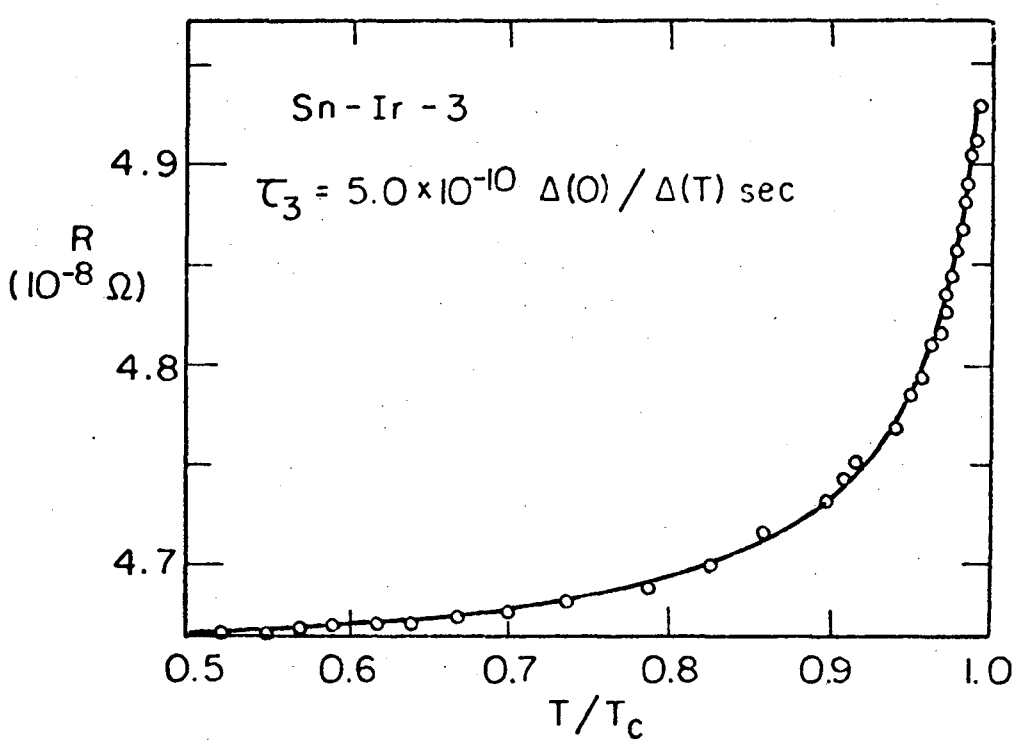

XBL 7711-6417

FIGs. 24 and 25

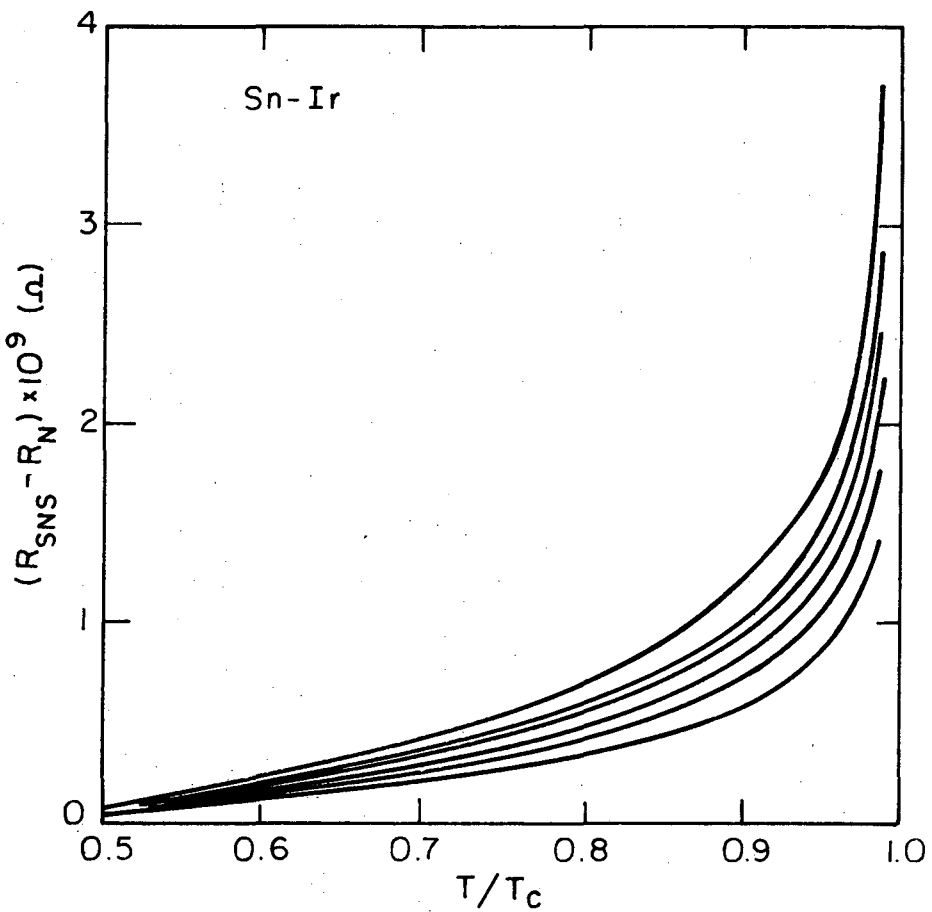

XBL 777-5789

Fig. 26 Family of curves used to fit the Sn-Ir junctions.

in the quality of the agreement to the experimental data. We therefore consider our $\tau_3(0)$ determined with the fitting process to be accurate within 20%. Figure 26 shows a family of curves that were used to fit the experimental data. The "best fits" were obtained with $\tau_3(0)$ = 4.0×10^{-10} sec. and 5.0×10^{-10} sec. for these two junctions.

Figure 24 also shows the calculated resistance of the junctions with τ_3 = constant. Clearly the fit is much worse than that with a $\tau_3(T)$ having a $1/\Delta$ dependence.

2. Tin/Indium - Iridium

Three junctions were measured. Their resistance and fitted curves are shown in Fig. 27. The value of $\tau_3(0)$ obtained from these junctions is 1.5×10^{-10} sec. These values are about a factor of 3 smaller than that for pure tin. The significance and possible explanation of the variation of $\tau_3(0)$ with impurity concentration will be discussed in the next chapter.

3. Lead/Bismuth - Copper/Aluminum

A large number of junctions of this type were made. Most of them had regions that peeled off from the substrate or had small cracks. This was probably due to the excessive heat applied to the surface of the substrate during the Cu/Al evaporation, even though the substrate was cooled with water. By making the Cu/Al thin, we could eliminate this problem easily. But such junctions would have large super current even at relatively high temperature ($\sim 0.7\ T_c$). We considered these junctions not acceptable. Several acceptable junctions were finally made.

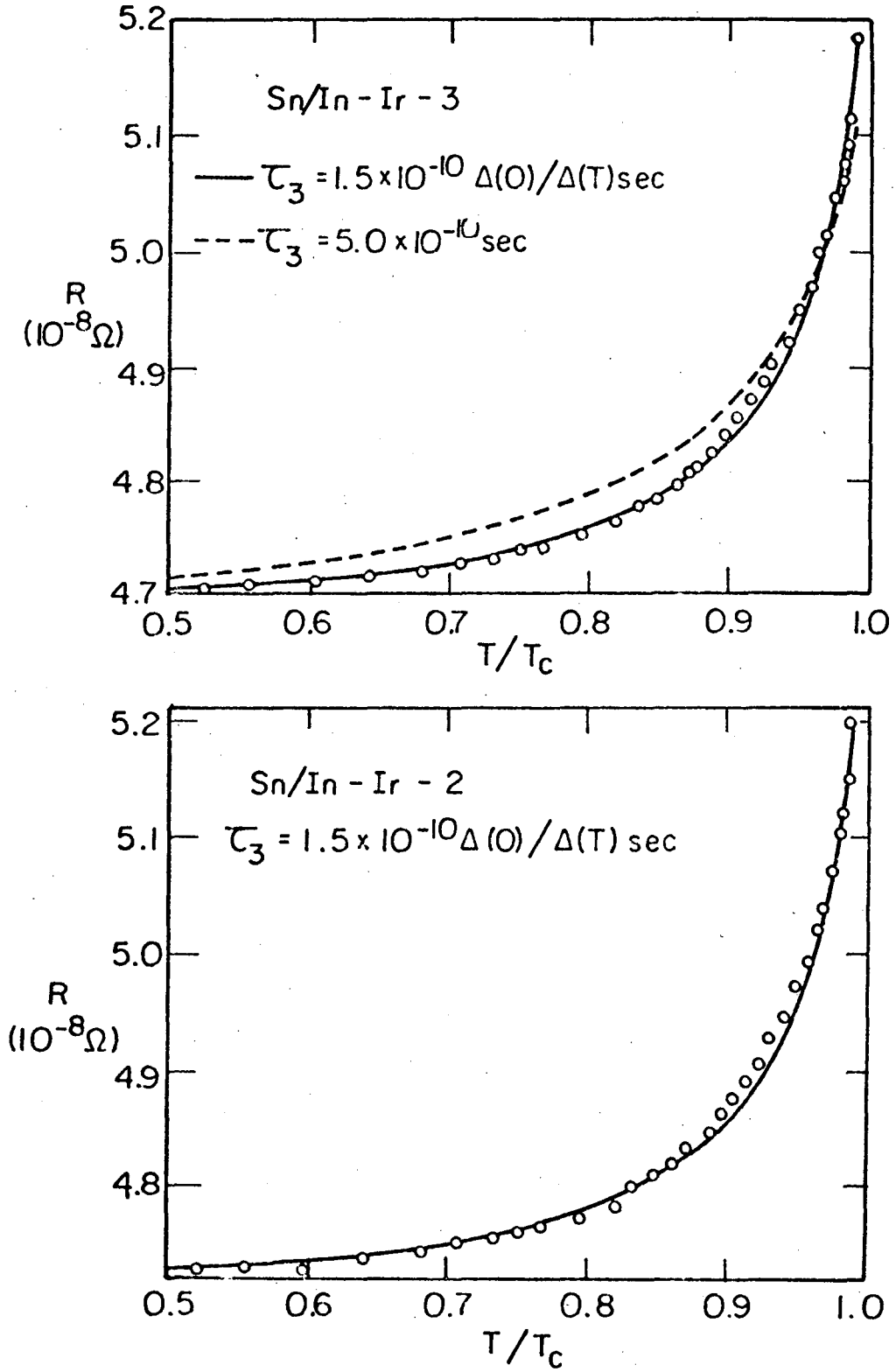

XBL 7711-6418

FIG. 27

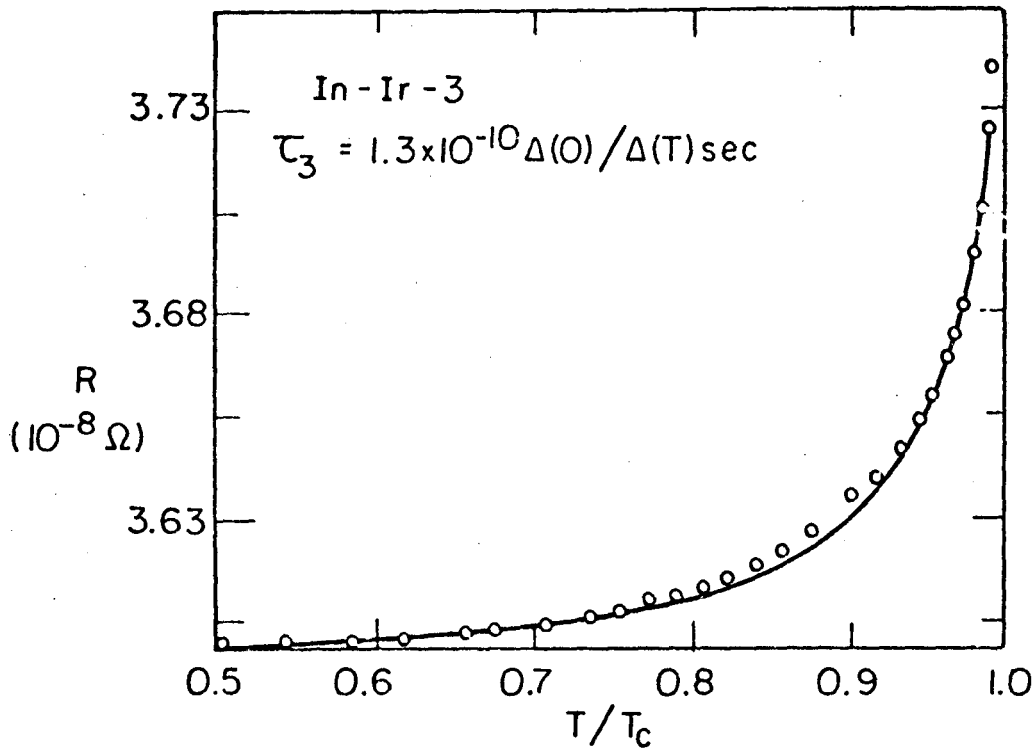

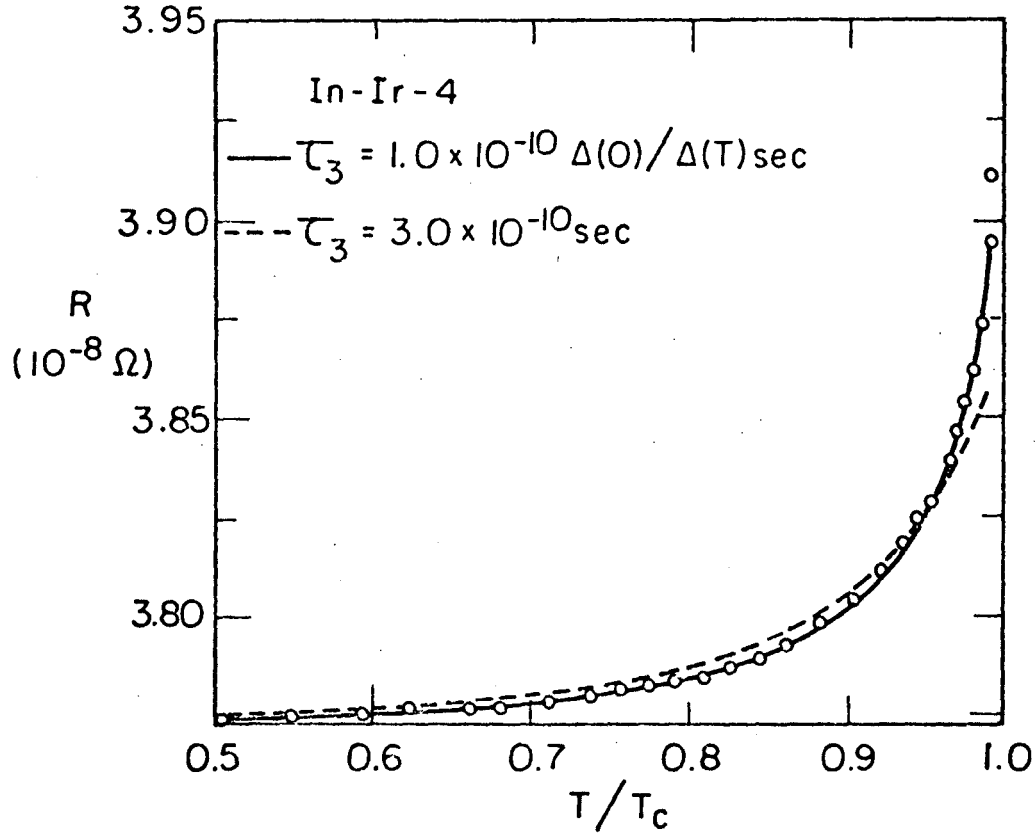

XBL 7711-6416

Fig. 28 In-Ir junctions (added in proof)

Figures 30 to 32 show the resistance of three of these junctions along with the best fit of $\tau_3 = \tau_3(0)\ \Delta(0)/\Delta(T)$. The dimensions of these junctions are 245 x 150 x 2.3 μm^3 for Pb-Cu-4-2, 160 x 120 x 1.6 μm^3 for Pb-Cu-6-1, and 185 x 188 x 2.4 μm^3 for Pb-Cu-7-1, with the third dimensions referring to the thickness of the Cu/Al film. The best fit to the experimental data were obtained with $\tau_3(0)$ between 1.0 and 1.5×10^{-11} sec. In Fig. 30 we also show the fit to the data with τ_3 = constant, the fit is clearly far worse.

4. Tin - Copper/Aluminum

Some Sn - Cu/Al-Sn film junctions were made in a similar way to the Pb/Bi-Cu/Al-Pb/Bi junctions. These junctions showed considerable interfacial diffusion (and/or alloying) between Sn and Cu. The low temperature resistance was always much larger than expected from the contribution of the Cu/Al alone. A typical example is shown in Fig. 33. The size of this junction was 172 x 142 x 1.6 μm^3 and should have a resistance of 1.26 $\mu\Omega$ at low temperature.

Besides the excessive low temperature resistance, an added difficulty in interpreting the experimental results of these junctions is the fact that the superconductor film was not thick enough. It is important that the thickness of the superconductor film be larger than the quasiparticle relaxation length. Otherwise, the normal current would be diverted into the direction along the superconductor film (along the superconductor strips crossing the junctions in Fig. 20). The normal current would then see a much smaller cross-section than that of the junction, and cause the measured resistance to be larger than the resistance obtained if the

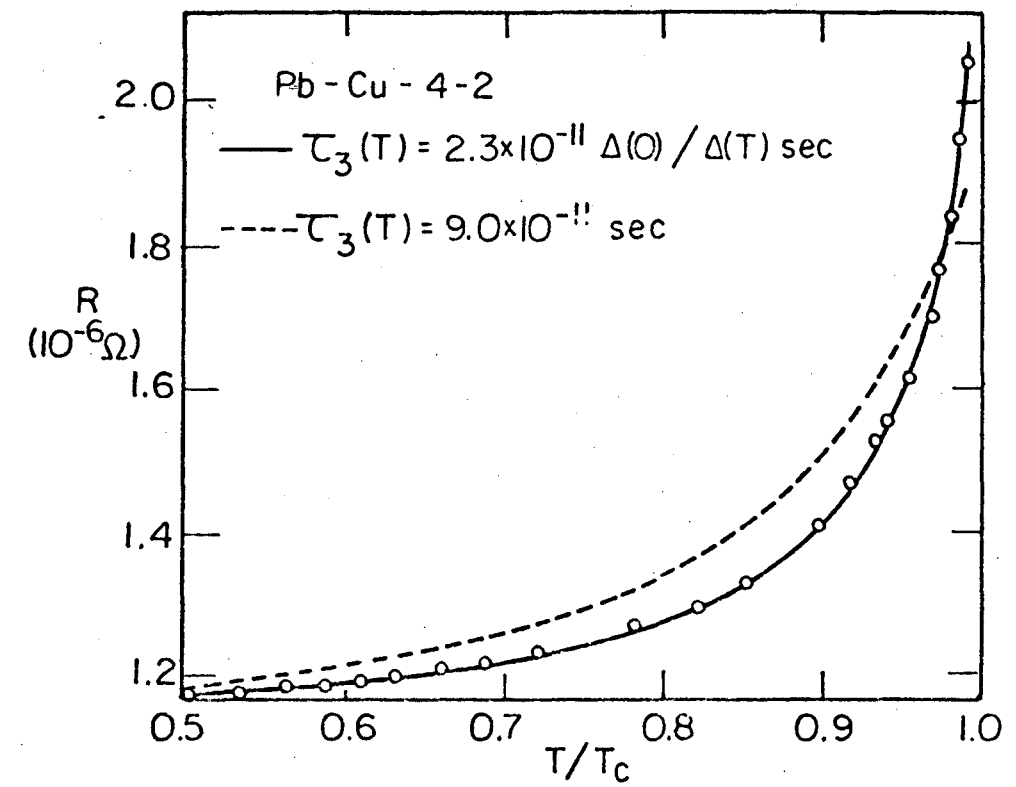

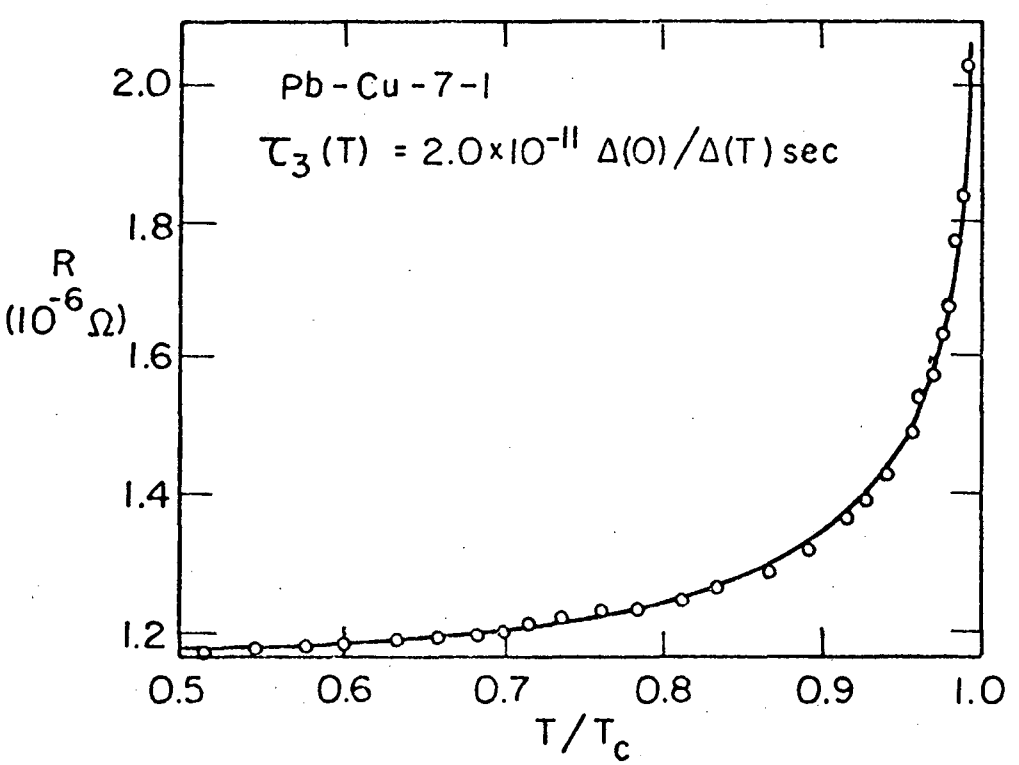

XBL 7711-6415

Figs. 30 and 31

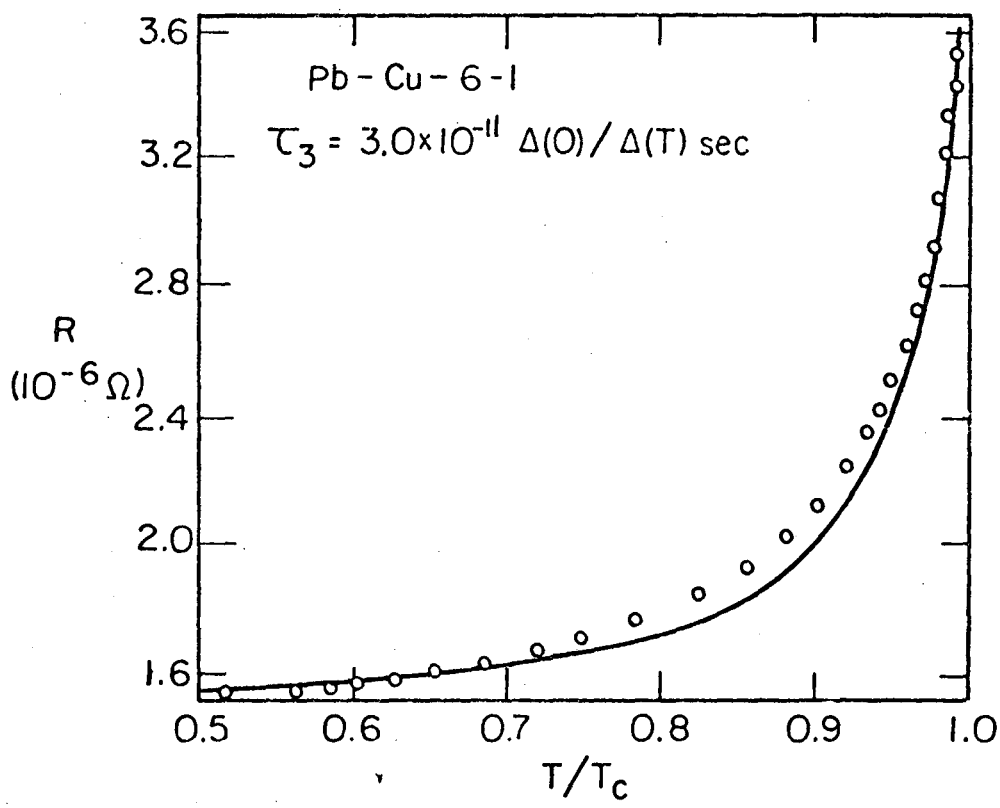

XBL 7711-6412

FIG. 32

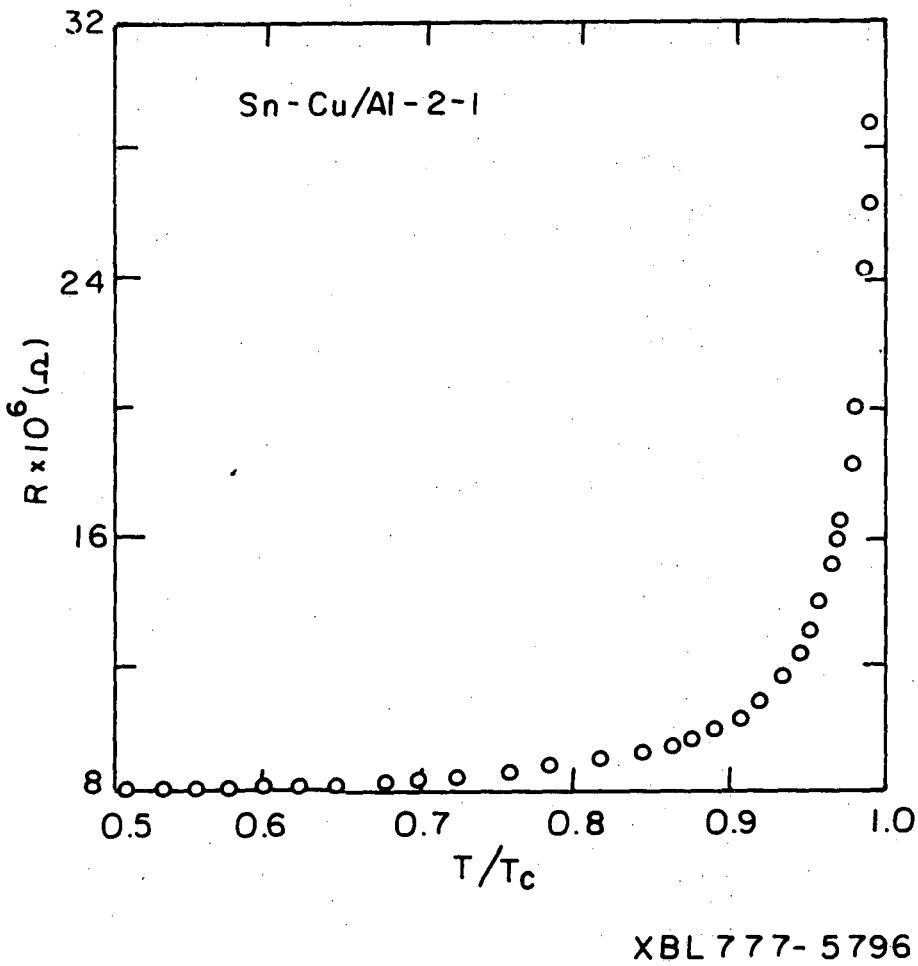

Fig. 33 R(T) for junction Sn-Cu/Aℓ-2-1.

current flows only perpendicularly to the junction. This effect causes the rapid rise of junction resistance near T_c shown in Fig. 33.

5. Lead - Copper/Aluminum

Junctions made with pure lead instread of the Pb/Bi alloy were also measured. A typical example is shown in Fig. 34. The resistance of these junctions at low temperature had reasonable values, implying that the interfacial alloying and diffusion were not important. However, they also show a much too rapid rise in resistance near T_c. This is due to the same effect discussed in previous paragraph: the thickness of the superconductor film was not great enough. The data in Fig. 34 were fitted to the calculated resistance. The functional forms of the data and calculated values as functions of temperature were quite different, and to bring the calculated resistance close to the measured values, we had to use $\tau_3(0)$ as large as 1×10^{-8} sec.

C. Rappaport's Data

M. L. Rappaport[52] has measured resistance of SNS junctions made with the sputter-evaporate technique. He used pure tin and lead as the superconductor, and a variety of normal metals (Ir, Cu, Au, Ag, Pt, Mg, Rh, and Ni). A discussion of his results will be given in this section.

With Sn as superconductor only two Sn-Ir-Sn junctions were made. The resistivity and mean free path for this evaporated tin were 1.05×10^{-7} Ω-cm and 0.98 μm respectively. The data for these two junctions as shown in Fig. 35 along with fitted curve using $\tau_3 \propto \Delta(0)/\Delta(T)$

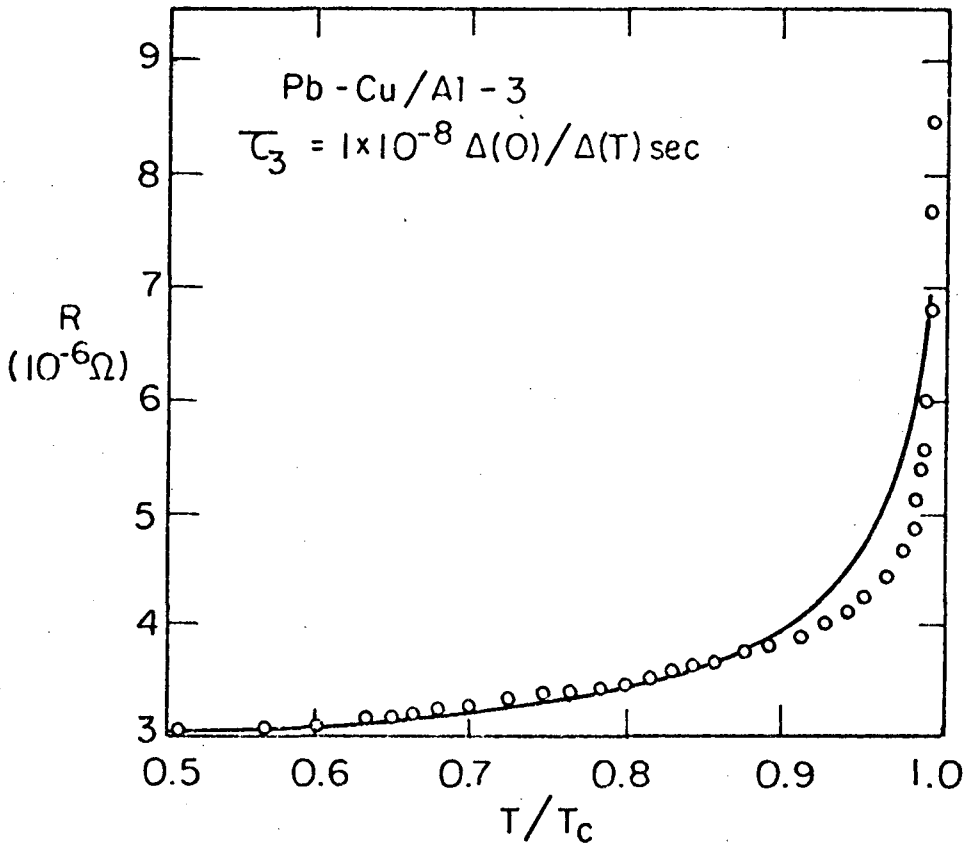

XBL 7711-6414

Fig. 34

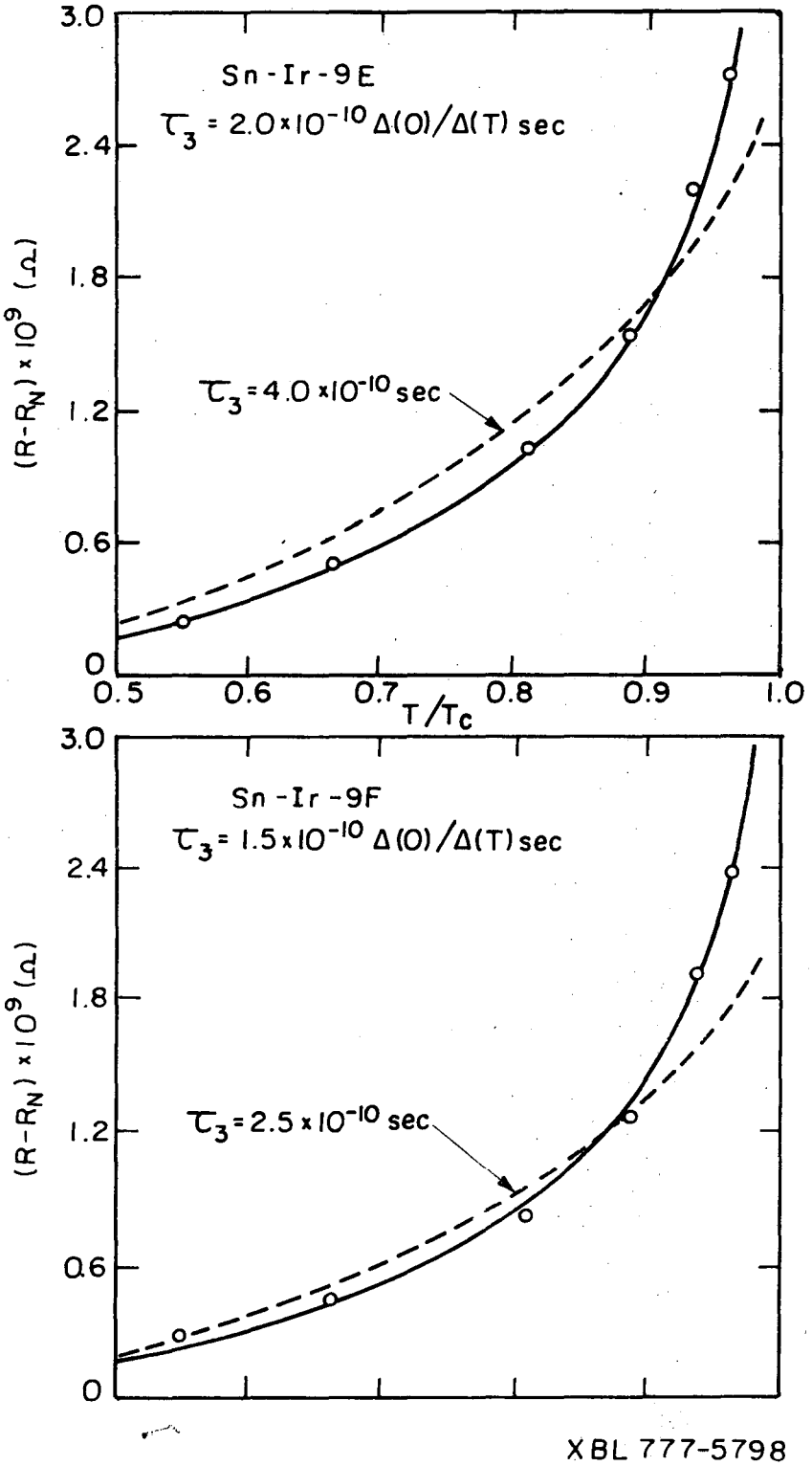

Fig. 35 R(T) for Rappaport's Sn-Ir junctions.

and $\tau_3 \propto$ constant. We see that the best fit is obtained $\tau_3 = \tau_3(0)$ $\Delta(0)/\Delta(T)$. $\tau_3(0)$ determined from these data was slightly smaller than our value (see last section). It should also be noted that the mean free path for Sn is smaller in Rappaport's junctions.

Most of his junctions made with Pb showed a minimum of resistance at ~5 K except those made with platinum as the normal metal. This feature was not seen in any of our Pb junctions made with evaporated films. Harding, Pippard and Tomlinson (HPT)[54] had suggested that this feature was caused by interfacial dirt at the SN boundary. However, their suggestion cannot explain why this resistance minimum does not occur in Pb-Pt-Pb junctions. The resistance of these SNS junctions at low temperature also came out to be very close to the expected value that one calculates from the geometry and resistivity of the normal metal. We will therefore choose not to apply the HPT suggestion to reinterpret Rappaport's results, but rather leave this puzzle for future investigation.

An example of the resistance of a Pb-Cu-Pb junction is shown in Fig. 36. The calculated resistance with $\tau_3 = 1.0 \times 10^{-11}$ $\Delta(0)/\Delta(T)$ sec is also shown. The agreement between experimental data and the calculation is reasonably good above 0.9 T_c. But the rising tail of resistance toward low temperature (although at very low temperature, this trail tapers off again) clearly deviates from the calculated value much more drastically than for any of our junctions.

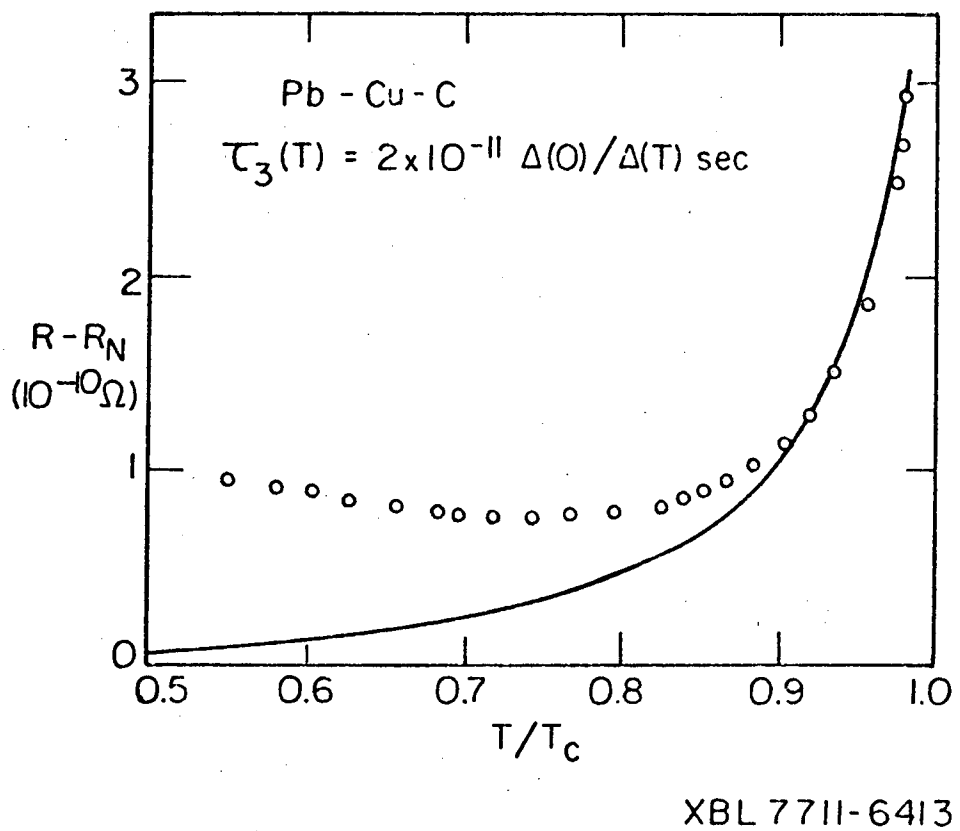

XBL 7711-6413

FIG. 36

X. DISCUSSIONS AND CONCLUSIONS

A. Comparison of the Experimental Data with Waldram's Theory

Judging from the good agreement between experimental data and the theoretical prediction, we consider our model outlined in Chapter VII to be a good description for the SNS boundary problem. The model, which includes several approximations, works especially well near the T_c of the superconductor. Waldram's model, which did not include an explicit approximation for the quasiparticle distributions, has also been discussed in Chapter VII. As we have pointed out, the implicit approximations in Waldram's formulation were actually similar to ours. These approximations were relaxed at a later point in his calculation. In this section, we will see how well Waldram's calculations do agree with the experimental data.

One junction, Pb-Cu-4-2 (Fig. 30), has been used to test Waldram's theory. To apply his theory, one needs to know all the τ_i's for both S and N. τ_1 can be obtained from the mean free path measurement (Table I). τ_2 can be obtained from the temperature coefficient of the room temperature resistivity of the metal.[70] The formula for τ_2 is simply

$$\tau_2 = \frac{\tau_\Theta}{8.4} \quad \frac{\Theta}{T}^{3} \tag{10.1}$$

where τ_Θ is the electron-phonon scattering time at Debye energy, and Θ is the Debye temperature.

For copper, this leads to

$$\tau_{2N} = 1.24 \times 10^{-10} \left(\frac{T_c}{T}\right)^3 \text{ sec} , \tag{10.2}$$

whereas for lead, τ_2 was left as a fitting parameter. τ_2 is related to τ_3 by the relation[40]

$$\tau_3 = 0.068 \ \tau_\Theta \left(\frac{\Theta}{T_c}\right)^3 \frac{\Delta(0)}{\Delta(T)} . \tag{10.3}$$

Thus, when $\tau_3(0)$ is increased, so is τ_{2s}.

Waldrams's results for the SNS resistance was calculated with a computer. The following parameters were used: (I will not derive or specify the meaning of these terms, the reader is referred to Waldram's original paper.)

$\gamma_{11} = \nu = \frac{|\varepsilon|}{E}$, $\gamma_{12} = 0$, (for Andreév reflection)

$\gamma_{21} = -\alpha\nu$, $\gamma_{22} = \nu$;

$A = -\nu$, $\alpha = 2R/(1-R)$,

$B = (\ell_o/\lambda_2)^2 + \alpha\nu$,

$C = -\nu$,

$D = (\ell_o/\lambda_2)^N \ A - B = -(\ell_o/\lambda_2)^N \nu - (\ell_o/\lambda_2)^s \nu - \alpha\nu$,

$\Delta = \nu^2$;

$$U_1 = A/D = \frac{1}{(\ell_o/\lambda_2)^N + (\ell_o/\lambda_2)^s + \alpha} ,$$

$$U_2 = -1/D = \frac{1}{\nu[(\ell_o/\lambda_2)^N + (\ell_o/\lambda_2)^s + \alpha]}$$

$$U_3 = C/D = U_1 ,$$

$$U_4 = \nu U_1 ;$$

$$W_i = \int_{\Delta}^{\infty} - f_o'(E)\, U_i \left[\left(\frac{\ell_o}{\lambda_2}\right)^N + \left(\frac{\ell_o}{\lambda_2}\right)^s\right] dE/f_o(\Delta) ,$$

$$Z = \frac{(\ell_o/\lambda_3)^s - (\ell_o/\lambda_2)^s}{(\ell_o/\lambda_2)^N + (\ell_o/\lambda_2)^s} (W_2 W_4 - W_1 W_3) ;$$

and $$h = E\, \ell_o^N \frac{W_1 - Z}{(\ell_o/\lambda_3)^s W_3 + (\ell_o/\lambda_2)^s (1 - W_3) + (\ell_o/\lambda_2)^N (1 - W_1 + Z)}.$$

h is the "excess boundary potential" which is equal to $Q_s^*(0)$. The boundary resistance is thus

$$R_{SNS} - R_N = 2\, \rho^N \frac{h}{E} \frac{1}{A} , \qquad (10.5)$$

where A is the cross-sectional area of the junction.

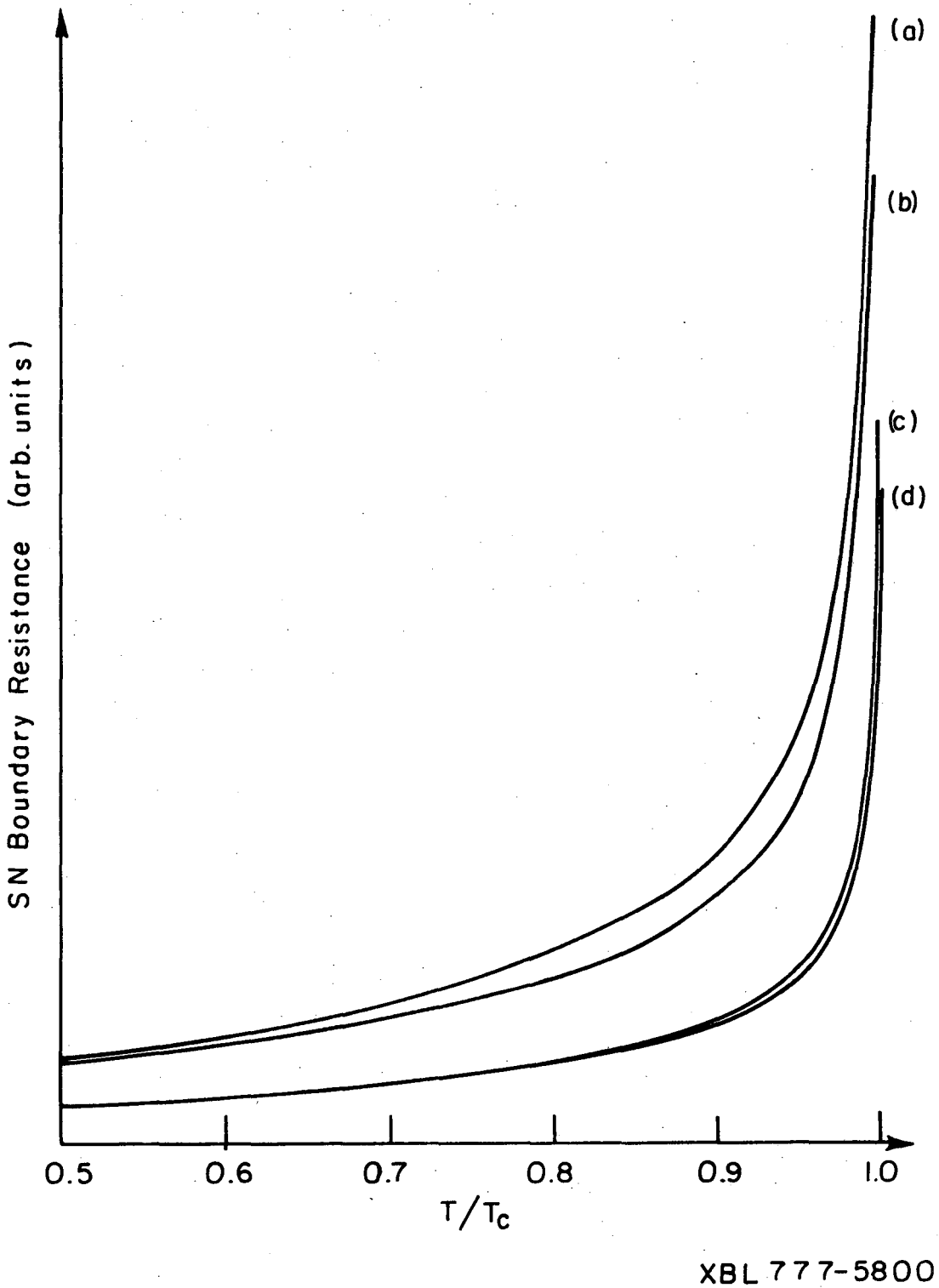

Fig. 37 R(T) calculated with Waldram's theory: (a) dirty S, dirty N; (b) dirty S, clean N; (c) clean S, dirty N; (d) clean S, clean N.

A few typical results are shown in Fig. 37. Curve (b) has all the same τ_i's as curve (a) except that the normal metal is assumed to have τ_1 100 times larger than that of curve (a). Similarly, curve (d) is calculated for τ_1^N 100 times larger than that of curve (c). Curves (c) and (d) are calculated with τ_1^S 10 times larger than that of (a) and (b), i.e., the latter two are 10 times "dirtier". We see that the resistance calculated from Waldram's theory is much more strongly dependent on the mean free parth of the superconductor, while almost independent of the mean free path of the normal metal. This is an expected result, although one cannot easily see this from the complicated formula for the boundary resistance.

The best fit to the experimental data for Pb-Cu-4-2 is shown in Fig. 38 with $\tau_3 = 5.5 \times 10^{-11}\ \Delta(0)/\Delta(T)$ sec. (the solid line). In the same figure, the best fit with the theory in this paper ($\tau_3 = 2.3 \times 10^{-11}\ \Delta(0)/\Delta(T)$ sec.) is also shown (the dashed line). It is seen that the fit with experimental data is clearly better with our calculation.

It might be argued that here we are using the pure Andreév boundary conditions for the calculation of boundary resistance, while in reality, interfacial dirt or boundary mismatch may modify the boundary conditions significantly and could result in a better fit to the experimental data with Waldram's calculation. We have used the following boundary conditions to calculate the SN resistance in the presence of "normal" boundary reflection. Assume a fraction β of the incident electron on the boundary is reflected as "electrons" while the rest undergo Andreév reflection (or transmission), the γ- factors in Eq. (10.4) are modified to be

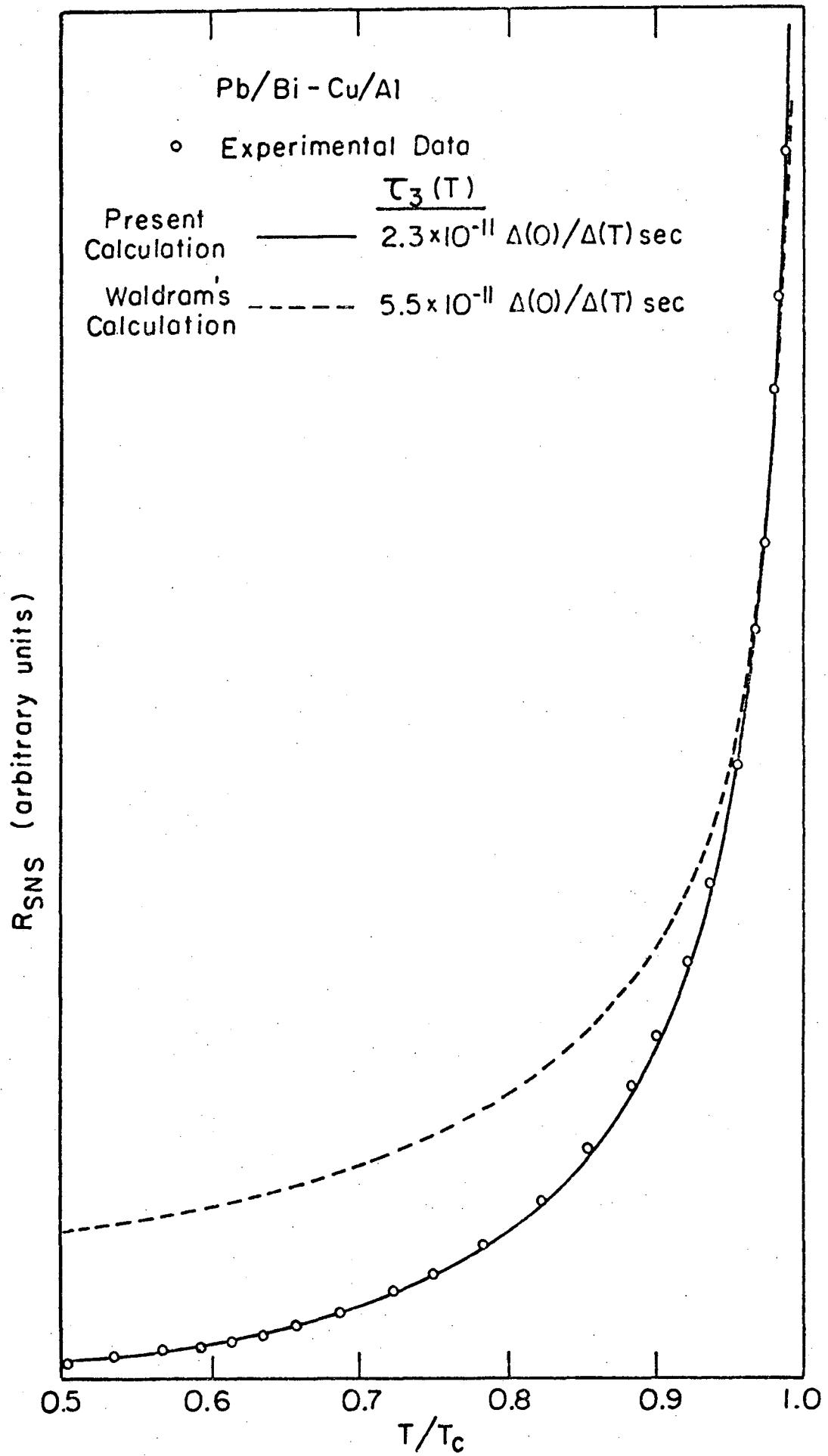

FIG. 38

XBL7711-6410

$$
\begin{aligned}
\gamma_{11} &= \nu\,(T + 2\beta - 2\beta T)/T \quad , \\
\gamma_{12} &= 2\nu\beta\,(\beta\,T - \beta - T)/[T(1-\beta)] \quad , \\
\gamma_{21} &= 2\nu\,(1-\beta)\,(T-1)/T \quad , \\
\gamma_{22} &= \gamma_{11} \quad , \quad T \equiv 1 - R \quad .
\end{aligned}
\tag{10.6}
$$

When the corresponding changes of the other parameters in Eq. (10.4) are made, one obtain a family of curves as shown in Fig. 39. When compared with Fig. 38, it is seen that by adding "normal reflection" at the boundary, the fit to the experimental data with Waldram's calculation can only be made worse.

B. Related Experiments by Other Authors

1. SNS Junction Experiments

Besides those of M. L. Rappaport, two pieces of work by Pippard, Shepherd, and Tindall, (PST) and Harding, Pippard and Tomlinson (HPT) can be found in the literature that are related to the experiments described in this thesis. The PST experiments were done on three types of SNS systems: the evaporated junctions similar to our Pb-Cu junctions, a normal metal sheet with superconductors applied to both sides with a soldering iron, and a superconductor driven with magnetic field into an intermediate state with a multiple SN layered structure. HPT used a sputter-evaporate technique similar to ours as described in Chapter VIII.

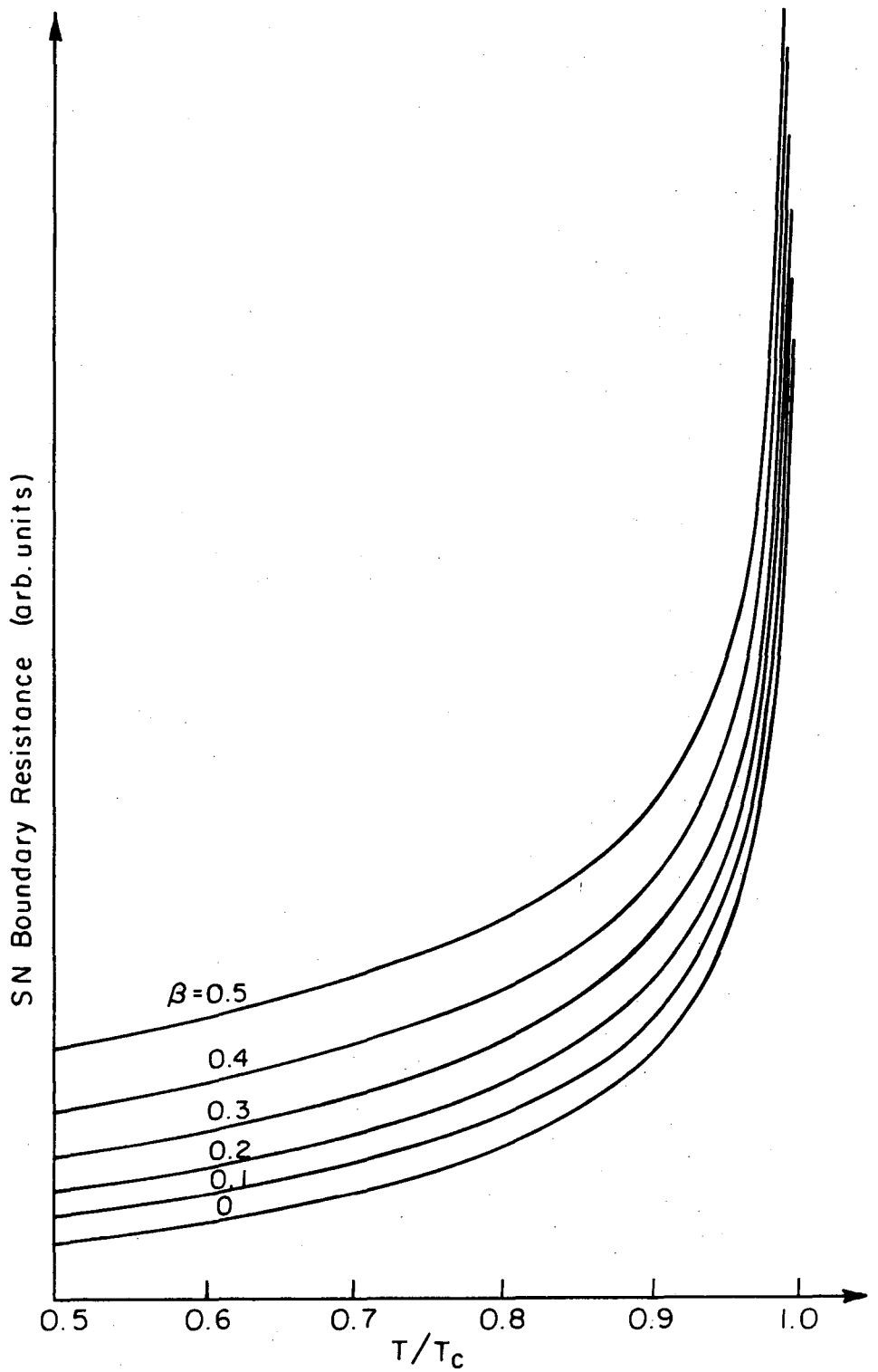

XBL777-5802

Fig. 39 R(T) calculated from Waldram's theory assuming a fraction β of the incident quasiparticles are "normally" reflected.

Except for the experiments on the superconductor in the intermediate state, there are two major differences between their experimental results and ours:

i) They have found a low temperature resistance of the junctions rather larger than the expected resistance of the normal metal alone. Because this effect was also seen in our Sn-Ir-Sn junction if the iridium was not sputtered adequately, we suspect what they have seen is a severe interfacial contamination problem. This effect was not seen in their experiment on the superconductor in the intermediate state.

ii) Because they interpreted the SN boundary resistance as a potential discontinuity at the SN interface, they did not take special caution to make the superconductor thick enough. As discussed in the previous chapter, this will result in a sharp rise of the SNS resistance near T_c. Indeed their data, except on the junctions with S heavily alloyed, showed this behaviour.

HPT have also seen a resistive minimum similar to that described in Section IX.C, except that the minimum was to a higher degree and did not appear at a fixed temperature. HPT attributed this to a "partial contamination" of the SN interface. In other words, one has a parallel electrical path of an SN joint and a superconductor-insulator-normal metal (SIN) junction. Since the resistance of the SIN junction increases with decreasing temperature while the resistance of the SN decreases toward low temperatures, the parallel of the two would possess a resistive minimum.

Whether this explanation is true or not, it still fails to explain point (i) above. HPT went on to explain that the excessive low temperature resistance was due to the "evanescent wave" of the incident electron. The idea was that, for electrons with energy less than the energy gap, the electrons will be Andreév-reflected, but at the same time an exponentially decaying wave will proceed in the superconductor. This "evanescent wave" will undergo scattering inside the superconductor and will contribute to an excess resistance even at low temperature.

While I will not venture into saying whether this theory is correct or not, I should point out that the effect of "evanescent wave" was certainly not discernible in our experiments. One expects the "evanescent wave" to contribute when the mean free path ℓ of the superconductor becomes comparable with the decay length $2\pi/k = h/\sqrt{2mE}$ of the "evanescent wave". In our experiments, for both Pb and Sn, $2\pi/k$ is on the order of a few tens of Angstroms (for $E \sim 0$), and is much smaller than the mean free path of the superconductor.

HPT supported their theory of "evanescent wave" by the experimental observation that the SN boundary resistance did not depend on the resistivity ρ of the superconductor through the simple relation of $\rho^{1/2}$ which one expects if the boundary resistance is derived from the quasiparticle relaxation alone. While we have also observed this effect, we believe it is due to another reason, namely the modification of electron-phonon interaction strength at the presence of impurity scattering. We will come back to discuss more on this effect in a later section.

2. The Microbridge Experiments

Several authors[71] have measured resistance of microbridges made of various materials. A microbridge is a superconductor with a very small cross-sectional area. When a current is passed through the bridge, "phase slip" centers will be generated, and one obtains a local SNS region. It has been consistently found that the measured resistance of these bridges was larger than expected from the known resistivity and the geometry of the phase strip center. This is clearly due to the extra decay of the quasiparticles. However, a quantitative description of the quasiparticle decay and an identification of the relaxation length is quite difficult: The microbridge is a dynamically varying system, and the order parameter (hence the normal region) varies quickly with time. What one measures is an average result of this variation in time. Also, because of the smallness of the cross-section of the bridges and the relatively large current density applied to these bridges, the recombination time τ_4 may play a more important role in the quasiparticle relaxation process. Recently, Dolan and Jackel[72] have made measurements on microbridges with many pairs of small and closely-spaced S and N probes near the phase slip region. They found that the voltages measured by the S probes on one side of the phase slip center were essentially constant, but the voltages measured by the N probes varied with the distance away from the phase center according to a simple diffusion relation (i.e., in an exponential form with a decay length of $\sqrt{v_f \tau \ell/3}$). At large distances from the phase-slip region the voltages measured by the S and N probes were the same. This was to be expected

from the theory in Chapter VII: the S probes measured μ, the electrochemical potential, which is constant inside the superconductor, while the N probes measured $e\phi$, or equivalently, Q^*, which varies with spacial distance. The success of the diffusion model points to the fact that our approximated solution (Eq. (7.39) for the Boltzman equation is probably quite adequate in describing the decay of Q^* in the microbridges.

C. Comparison of the Values of $\tau_3(0)$ Obtained by Theory and Other Experiments, and the Effect of Impurity

In Table III, we list the values of $\tau_3(0)$ theoretically and experimentally determined by other authors with those obtained in our work. There is an order-of-magnitude agreement among the results, although detailed numerical discrepancy still exists.

One interesting effect in the experimentally measured $\tau_3(0)$ for tin is that this time decreased by about a factor of 3 with the addition of 1% impurity. A. Schmid[73,74] has predicted such an effect. His theory is qualitatively as follows: In a pure metal with spherical Fermi surface, electrons can only interact with longitudinal phonons because of momentum conservation. When impurity is added, however, the translational symmetry of the elctron wave function is lost, and the electrons can couple with transverse phonons. The electron-phonon scattering rate is thus increased, and $\tau_3(0)$ should decrease. Schmid has numerically calculated the increase in τ^{-1} for aluminum as a function of $p_F\ell$, the product of Fermi momentum and mean free path. The part of his calculation of the enhancement factor due to electron-phonon scattering is quite

TABLE III. $\tau_3(0)$ (sec.)

	Calculated		Experimentally measured	
	Tinkham[a]	Kaplan *et al.*[b]	SIN[c]	SNS
Sn	2×10^{-10}	2.9×10^{-10}	1×10^{-10}	4.0×10^{-10}
Sn (1% In)	- - -	- - -	- - -	1.5×10^{-10}
Pb	4×10^{-12}	2.1×10^{-11}	3×10^{-12}	- - -
Pb (1% Bi)	- - -	- - -	- - -	2.4×10^{-11}
Pb (10% Bi)	- - -	4.7×10^{-12}	- - -	- - -
In	- - -	1.0×10^{-10}	- - -	1.2×10^{-10}[e]
Ta	1.4×10^{-10}[d]	2.2×10^{-10}	- - -	6.5×10^{-11}[d]

[a] Ref. 20

[b] Ref. 19

[c] Ref. 11

[d] Ref. 27

[e] Added in proof.

universally applicable to materials having a simple E^2 dependence in their electron-phonon interaction function (i.e., $\alpha^2(E)\ F(E)$). This is apparent from Eq. (III.9) in reference 74. (It is noted that his calculation also includes the enhancement due to electron-electron interaction which varies in strength among materials. This part of his calculation on aluminum will certainly not apply to other materials). If we use $p_F\ell = 1.9 \times 10^4\ \hbar$ and $1.33 \times 10^3\ \hbar$ for our Sn and Sn/In respectively, we see that his calculation would predict a decrease in $\tau_3(0)$ by a factor of ~3.4 due to the addition of the 1% impurity.

It is not certain whether we were seeing the effect predicted by Schmid. We note that the addition of impurity will change the phonon structure of the material, as is evident from the change in T_c. This could also have an effect on changing the value of $\tau_3(0)$.

D. Conclusions

The experimental results that we obtained from the measurement on the resistance of the SNS junctions provided a way to measure the branch-crossing relaxation time of electrons in a superconductor. Our calculations, based on a detailed account for the electron relaxations through the Boltzmann equations, agreed very well with experimental results. The experimentally determined $\tau_3(0)$ was in reasonable agreement with theoretical calculations and other experiments, although the value of $\tau_3(0)$ depends on whether one uses Waldram's or our formulation.

The importance of a knowledge on the value of $\tau_3(0)$ lies in the fact that $\tau_3(0)$ is related to the basic electron-phonon interaction strength. Many other authors have measured the recombination times (τ_4)

of superconductors, but in their experiments, τ_4 was always enhanced by the phonon trapping mechanism.[75] However τ_3 is not enhanced. The values of $\tau_3(0)$ should then provide a means for estimating the phonon enhancement factor in the measurements of the relaxation times.

One drawback in using the SNS technique to measure τ_3 is that the SN boundary resistance is very small at low temperatures, so that any structure in $\tau_3(T)$ at low temperature would not be seen.

Although we did not change the concentration of impurity in the superconductor over a wide range, we did see a decrease of $\tau_3(0)$ in tin when 1% impurity of indium was added. This result may be due to the impurity-aided electron-transverse phonon coupling.[76]

Another experiment that is related to our SNS experiments is the "thermal electric effect" in superconductors[77]. Heat current in superconductors is carried by the normal electrons and phonons rather than by the condensate. The electron thermal current also corresponds to a shift in the Fermi surface, and a calculation similar to that in Chapter VII would show that there is a finite Q* inside the superconductor when the heat current is applied. However, in doing this calculation, one has to be careful in applying the symmetry of the quasiparticle distribution functions at $+ k_F$ and $- k_F$ on the Fermi surface. For electric current, the $+ k_F$ and $- k_F$ quasiparticles contribute similarly to generating electric field in the superconductor (Section VII.C), while for thermal currents, $+ k_F$ electrons and $- k_F$ holes have equal parts in carrying the thermal current, but they contribute oppositely to the electric field in the superconductor. The net Q* generated by the thermal current is thus due to the asymmetry of the excitation spectrum for the $k_{F>}$ and

$k_{F<}$ quasiparticles (Fig. 14), and/or the asymmetry of the gap parameter Δ on the two branches. This thermal electric effect should be an interesting follow-up experiment for the present SNS experiments.

0 0 0 0 4 8 0 4 6 4 7

ACKNOWLEDGEMENT

It is with great pleasure that I acknowledge the guidance and support from my research adviser, Professor John Clarke. I am especially indebted to his patience with my many stumblings, both over theory and experiment. Special thanks go to Dr. Michael L. Rappaport for his generosity in sharing his time and expertise in laboratory work on uncountable occasions. And to Dr. Marc J. Feldman for his many critical suggestions at times when the experiments in this thesis seemed to face insurmountable difficulties. My other colleagues in the Clarke group are also gratefully acknowledged for innumerable discussions and ideas which have helped make my four and a half years of research work at Berkeley stimulating, productive and enjoyable.

None of this work could have been successful without the skills and cooperation of the professional shops and staff of both the Physics Department and the Lawrence Berkeley Laboratory. Their good spirit and unlimited patience will always be warmly remembered. I should especially thank Antoinette Czerwinski and Gloria C. Pelatowsky for their careful preparation of this thesis.

Foremost I am indebted to my wife, Shi-ling, for her encouragement throughout this work, for her understanding and tolerance of the many evenings and weekends that she had to be by herself while I worked in the lab, and for her sharing the many moments of frustration and happiness of my graduate carrer in the comfortable home she provided.

This work was performed under the auspices of the U.S. Energy Research and Development Administration.

REFERENCES

1. John Clarke and Richard F. Voss, Phys. Rev. Lett. 33, 24 (1974).
2. Richard F. Voss and John Clarke, Phys. Rev. B13, 556 (1976).
3. J. M. Richardson, Bell Syst. Tech. J. 29, 11, (1950).
4. M. K. Maul, M. W. P. Strandberg and R. L. Kyhl, Phys. Rev. 182, 522 (1969).
5. R. M. Katz and K. Rose, Proc. IEEE 61, 55 (1973).
6. G. J. van Gurp, Phys. Rev. 178, 650 (1969).
7. G. J. van Gurp, Philips Res. Rep. Suppl. No. 5 (1969).
8. J. M. Smith and M. W. P. Strandberg, J. Appl. Phys. 44, 2365 (1973).
9. D. J. van Ooijen and W. F. Druyvesteyn, Phys. Lett. 6, 30 (1963).
10. G. J. van Gurp, Phy. Rev. 166, 436 (1968).
11. C. Heiden, Proc. Conference on Fluctuations in Superconductors, Pacific Grove, Calif., 1968, (ed. W. S. Gorce and F. Chilton), p. 231.
12. R. P. Huebener and D. E. Gallus, Phys. Rev. B7, 4089 (1973).
13. S. W. Shen and A. van der Ziel, Physica 64, 587 (1973).
14. J. B. Kruger and C. Heiden, Proc. 12th International Conference on Low Temperature Physics, Kyoto, Japan, 1970 (ed. E. Kanda), p. 415.
15. J. Thompson and W. D. H. Joiner, Solid State Comm. 16, 849 (1975).
16. For a review, see M. Tinkham, Introduction to Superconductivity, (McGraw-Hill, New York, 1975).
17. K. M. van Vliet and E. R. Chennete [Physics 31, 985 (1965)] have tackled the problem of realistic boundary conditions using a Green's function technique.

0 0 0 0 4 8 0 4 6 4 8

18. S. Chandrasekhar, Rev. Mod. Phys. 15, 1 (1943).

19. M. Strongin, O. F. Kammerer, and A. Paskin, Phys. Rev. Lett. 23, 949 (1965).

20. M. K. Maul and M. W. P. Strandberg, J. Appl. Phys. 40, 2822 (1969).

21. R. C. Williams and R. C. Backus, J. Appl. Phys. 20, 98 (1949).

22. L. Holland, Properties of Glass Surfaces, Chap. 8 (Chapman and Hall, London, 1964).

23. J. A. Pask and R. M. Fulrath, J. of Am. Ceramics Soc. 45, 592 (1965).

24. R. Y. Chiao et al., Rev. de Phys. App. 9, 183 (1974).

25. W. H. Parker, private communication.

26. Properties of Materials at Low Temperature, (ed. V. J. Johnson, Pergamon Press, 1961).

27. C. Kittel, Introduction to Solid State Physics, 4th ed. p. 263 (John Wiley and Sons, New York, 1971).

28. D. N. Langenberg, Proc. 14th International Conference on Low Temperature Physics, Otaniemi, Finland, 1975 Vol. 5, p. 223.

29. J. Clarke, G. I. Hoffer, P. L. Richards, N. H. Yeh, Proc. 14th International Conference on Low Temperature Physics, Otaniemi, Finland, 1975, Vol. 4, p. 226. A detailed account of this work will be published in the Journal of Applied Physics.

30. S. H. Liu, to be published.

31. M. B. Ketchen, thesis, University of California, 1977. An account of this work will be published.

32. J. R. Waldram, Proc. Roy. Soc. Lond. A 345, 231 (1975).

33. J. Bardeen, L. N. Cooper, and J. R. Schrieffer, Phys. Rev. 108, 1175 (1957).

34. V. L. Ginzburg and L. D. Landau, Zh. eksp. teor. Fiz. 20, 1064 (1950).

35. J. Clarke, Phys. Rev. Lett. 28, 1363 (1972); J. Clarke and J. L. Paterson, J. Low Temp. Phys. 15, 491 (1974).

36. A. F. Andreév, Zh. eksp. teor. Fiz. 46, 182 (1964). (Soviet Physics JETP 19, 1228).

37. J. Bar-Sagi, to be published.

38. L. D. Landau and E. M. Lifshitz, Quantum Mechanics, § 23. (Addison-Wesley, 1970).

39. A. B. Pippard, J. G. Shepherd, and D. A. Tindall, Proc. Roy. Soc. Lond. A 324, 17 (1970).

40. M. Tinkham, Phys. Rev. B6, 1747 (1972).

41. S. B. Kaplan, C. C. Chi, D. N. Langenberg, J. J. Chang, S. Jafarey, and D. J. Scalapino, Phys. Rev. B14, 4854 (1976).

42. A. Rothwarf and M. Cohen, Phys. Rev. 130, 1401 (1963).

43. L. Tewordt, Phys. Rev. 127, 371 (1962); 128, 12 (1962); J. R. Schrieffer and M. M. Ginsberg, Phys. Rev. Lett. 8, 207 (1962); V. G. Baryakhtar, V. F. Klepikov, and V. P. Seminozhenko, Fiz. Tverd. Tela. 15, 1213 (1973). (Soviet Phys. - Solid State 15, 817).

44. A. Schmid and G. Schön, J. Low Temp. Phys. 20, 207 (1975).

45. A. Rothwarf and B. N. Taylor, Phys. Rev. Lett. 19, 27 (1967).

46. W. Eisenmenger, K. Lassmann, H. J. Trumpp, and R. Kauss, Appl. Phys. 11, 307 (1976).

47. T. J. Rieger, D. J. Scalapino, and J. E. Mercereau, Phys. Rev. Lett. 27, 1787 (1971).

48. M. L. Yu and J. E. Mercereau, Phys. Rev. Lett 28, 1117 (1972).

49. G. M. Eliasberg, Zh. Eksp. Teor. Fiz. 61, 12 4 (1971) (Soviet Physics - JETP 34, 668); 39, 1437 (1971) (JETP 12, 1000).

50. G. Eilenberger, Z. Phys. 214, 195 (1968).

51. M. Hansen, Constitution of Binary Alloys, (McGraw-Hill, New York, 1958).

52. M. L. Rappaport, Thesis, University of California, 1975; Report of Lawrence Berkeley Laboratory, LBL-5473 (1975).

53. J. Clarke, Thesis, University of Cambridge, 1967.

54. G. L. Harding, A. B. Pippard, and J. R. Tomlinson, Proc. Roy. Soc. Lond. A 340, 1 (1974).

55. Ordered from R. D. Mathis and Co., Los Angeles. Special Order No. TH-350.

56. Ordered from Engelhard Minerals and Chemicals Co., Murray Hill, New Jersey.

57. Dektak, Sloan Instruments, Santa Barbara, Calif.

58. J. G. Adler and S. C. Ng, Can. J. Phys. 43, 594 (1965).

59. M. L. Rappaport, Preprint, for publication in Rev. Sci. Instru.

60. R. G. Chambers, Proc. Roy. Soc. 215, 481 (1952).

61. J. Clarke, W. M. Goubau, and M. B. Ketchen, J. Low Temp. Phys. 25, 99 (1976).

62. G. I. Rochlin, Rev. Sci. Instr. 41, 73 (1970).

63. M. L. Rappaport, Lawrence Berkeley Laboratory Report, LBL-3513.

64. J. Clarke, S. M. Freake, M. L. Rappaport, and T. L. Thorp, Solid State Comm. 11, 689 (1972).

65. J. Clarke, Proc. Roy. Soc. A308, 447 (1969)

66. J. M. Ziman, Principles of the Theory of Solids, Chapt. 7, (Cambridge University, 1964).

67. B. Mühlschlegel, Z. Phys. 155, 313 (1959).

68. M. Tinkham, private communication. Also see ref. 71.

69. For a review and comprehensive references, see G. Duetscher and P. G. de Gennes, in Superconductivity, edited by R. D. Parks (Dekker, New York, 1969).

70. J. M. Ziman, Electrons and Phonons, Chapt. 9, (Oxford University Press, London, 1968). Also see ref. 40.

71. W. J. Scolopol, M. R. Beasley and M. Tinkham, J. Low Temp. Phys. 16, 145 (1974); T. M. Klapwijk and J. E. Moiij, Physics Letters 57A, 97 (1976).

72. G. J. Dolan and L. D. Jackel, Bull. Am. Phys. Soc. 22, 375 (1977). A more detailed account of this work is to be published.

73. A. Schmid, Z. Phys. 271, 251 (1974).

74. A. Schmid, Z. Phys. 259, 421 (1973).

75. W. Eisenmenger, K. Lassmann, H. J. Trump, and R. Krauss, Appl. Phys. 12, 163 (1977).

76. K. E. Gray and I. Schuller (to be published) have observed similar effect due to impurity on the electron-phonon scattering time in aluminum.

77. C. M. Falco has reported experimental work similar to the idea described here. See Bull. Am. Phys. Soc. 22, 373 (1977).

This report was done with support from the Department of Energy. Any conclusions or opinions expressed in this report represent solely those of the author(s) and not necessarily those of The Regents of the University of California, the Lawrence Berkeley Laboratory or the Department of Energy.

TECHNICAL INFORMATION DEPARTMENT
LAWRENCE BERKELEY LABORATORY
UNIVERSITY OF CALIFORNIA
BERKELEY, CALIFORNIA 94720